ELECTROANALYTICAL TECHNIQUES FOR PROBING NEUROCHEMICAL MECHANISMS

Justin Michael Kita

A dissertation submitted to the faculty of the University of North Carolina at Chapel Hill in partial fulfillment for the degree of Doctor of Philosophy in the Department of Chemistry

Chapel Hill
2008

Approved by:

Dr. R. Mark Wightman

Dr. Mark Schoenfisch

Dr. Royce Murray

Dr. Robert Rosenberg

Dr. Christopher Fecko

ABSTRACT

Justin M. Kita: Electroanalytical techniques for probing neurochemical mechanisms
(Under the direction of Dr. R. Mark Wightman)

Behavioral, as with all, functions of the brain are governed by biochemical processes in and between brain cells. Neurotransmitters are particularly important in these processes because they are responsible for relaying information between the brain cells. The neurotransmitter dopamine is believed to be directly involved in the neuronal circuitry of pleasure and reward, and hence is an important contributor to behavior. Extensive research into understanding mechanisms involved in dopamine release and regulation may allow us to develop potential pharmacological solutions to eliminate negative behaviors such as drug addiction. Detection of dopamine was performed electrochemically, placing microelectrodes into regions of the brain that were abundant in dopamine release and receptor sites. With a stimulating electrode, artificial action potentials were generated that mimicked biological conditions conducive to dopamine release. The dopamine release was then analyzed under various pharmacological conditions to determine which biological mechanisms were responsible for regulating the amount of dopamine released per stimulation. Additional experiments were performed to determine which other neurotransmitters might be involved in reward mechanisms. A microsensor capable of selectively detecting the neuromodulator nitric oxide was developed to measure changes of nitric oxide *in vitro*. My thesis has focused primarily on developing detection methods that allow for an understanding of the factors and mechanisms that regulate extracellular concentrations of neurotransmitters.

To Chia.

ACKNOWLEDGEMENTS

I have worked with many people throughout the course of my researching career. I would like to thank Dr. John DiCesare for inspiring me to obtain a PhD. For assistance in conducting my research, I would like to thank, in no particular order, Chia Li who has been a huge help both in editing my thesis and helping with experimentation. For personal support and research assistance, I would like to thank Paul Walsh and Charlie Miller. Additionally, I would like to thank all members of the Wightman lab for helpful discussion.

None of this research would have been possible without the multiple funding agencies that supported me throughout my five years. I would like to thank NSF, GAANN, Eastman, and NIH for personal remuneration as well as funding my research.

Table of Contents

List of Tables

List of Figures

List of Abbreviations

17FTMS	(heptadecafluoro-1,1,2,2,-tetrahydrodecyl)trimethoxysilane
5-HT	5-hydroxytryptamine
aCSF	artificial cerebrospinal fluid
ANOVA	analysis of variance
AP	anterior-posterior
BSA	bovine serum albumin
CP	caudate-putamen
CS +/-	conditioned stimulus
CV	cyclic voltammetry
DA	dopamine
DC	direct current
DV	dorsal-ventral
EDTA	ethylenediaminetetraacetic acid
fMRI	functional magnetic resonance imaging
FSCV	fast-scan cyclic voltammetry
G-protein	guanine nucleotide-ginding protein
HEPES	4-(2-hydroxyethyl)-1-piperazineethanesulfonic acid
HPLC	high performance liquid chromatography
HQ	hydroquinone
ICSS	intracranial self-stimulation
iMLF	interstitial medial longitudinal fasciculus
LH	lateral hypothalamus

L-NAME	n-nitro-l-arginie methyl ester
LTD	long-term depression
LTP	long-term potentiation
MFB	medial forebrain bundle
ML	medial-lateral
MTMOS	methyltrimethoxysilane
NAcc	nucleus accumbens
NMDA	n-methyl d-aspartate
NO	nitric oxide
NT	neurotransmitter
PBS	phosphate buffered saline
RN	red nucleus
SCM	scanning confocal microscope
SEM	scanning electron microscope
SEM	standard error of mean
SSRI	selective serotonin reuptake inhibitor
TH	tyrosine hydroxylase
TRIS	tris(hydroxymethyl)aminomethane
TTX	tetrodotoxin
UV	ultra-violet
VTA	ventral tagmental area

CHAPTER 1 - Microelectrodes for studying neurobiology

INTRODUCTION

Microelectrodes have been used to elucidate a number of neurobiological questions, including investigation into the basics of vesicular release at the cellular level using a technique known as constant potential amperometry (Mosharov and Sulzer 2005). More recently, however, fast-scan cyclic voltammetry (FSCV) has emerged as one of the primary alternatives to microdialysis for studying neurobiology due to its less invasive implantation and enhanced temporal resolution (Peters et al. 2004). Both techniques have proven critical for furthering our understanding of brain chemistry and its role in behavioral neurobiology.

The structure of the neuron has been well established, and for the comprehension of neuronal communication, it is important to understand the role of each neuronal component. The branch-like structures of the neuron, the dendrites, are responsible for receiving input from surrounding neurons and converting these inputs into electrical signals known as action potentials (Fig. 1.1). The soma, or cell body, of the neuron contains typical cellular machinery present in other cells, including the mitochondria and nucleus, and is also responsible for neurotransmitter synthesis. Once the action potential has been generated and passed through the soma, it traverses the axon and enters the terminal region. The terminals act as the primary outputs of the neuron and transduce the electrical signal into a chemical signal in the form of a neurotransmitter. Once released, these neurotransmitters enter the synapse and diffuse to neighboring neurons, where they initiate neuronal communication.

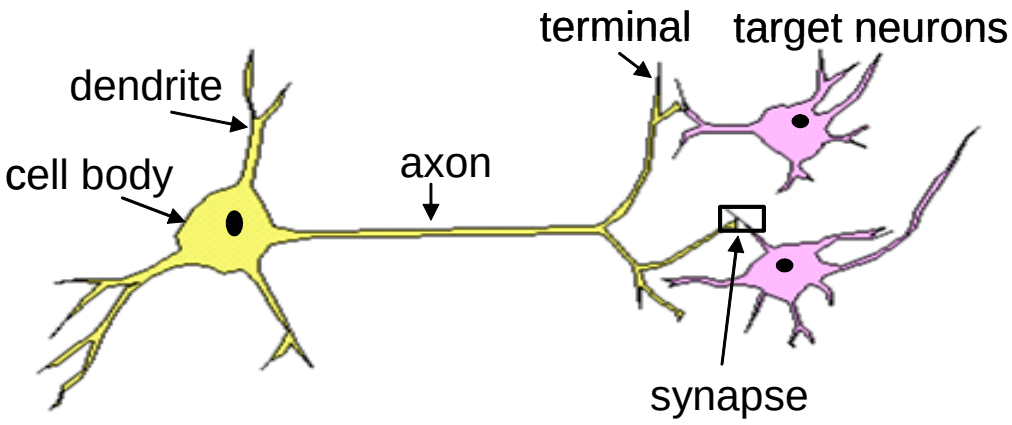

Figure 1.1 Anatomical structure of the neuron. The dendrites are the neuronal inputs and receive signals from neighboring neurons. These inputs create action potentials, which can summate at the cell body and ultimately pass through the axon to the neuronal terminals, which transduce the electrical signal into a neurochemical signal, termed a neurotransmitter. The released neurotransmitter can then interact with neighboring neurons to initiate neuronal communication.

Measurement of the release of small quantities of neurotransmitter in the extracellular space requires a sensor that is both small and rapid. Microelectrodes are thus ideal for this type of application since they possess dimensions in the micron range (Wightman 2006). Microelectrodes can be fabricated in a variety of ways, either through insulation of a carbon fiber with a glass capillary (Figure 1.2), or utilization of carbon fiber nanoelectrodes (Wu et al. 2005). The small size of the carbon fiber electrode minimizes the double-layer capacitance, thus making it possible to make recordings on the sub-second time scale (Amatore and Maisonhaute 2005). Microelectrodes are not inherently selective; however, the selectivity of the microelectrode can be enhanced either through application of techniques such as FSCV or chemical modification of the electrode surface.

Electrochemical detection utilizing microelectrodes requires that the detected species be electroactive. Several neurochemical transmitters can be electrochemically detected, such as dopamine and serotonin and many other molecules derived from the amino acids tyrosine and tryptophan. Additionally, there are other processes, such as transient changes in physiological pH, which can be detected electrochemically using FSCV. Microelectrodes are also capable of measuring changes in concentration of several biologically relevant gases such as nitric oxide (Shin et al. 2005), oxygen (Venton et al. 2003), and carbon monoxide (Lee and Kim 2007). In the case of FSCV, multiple analytes can be detected simultaneously, and when combined with sophisticated data analysis procedures, the individual concentrations can be accurately measured as a function of time (Heien et al. 2005).

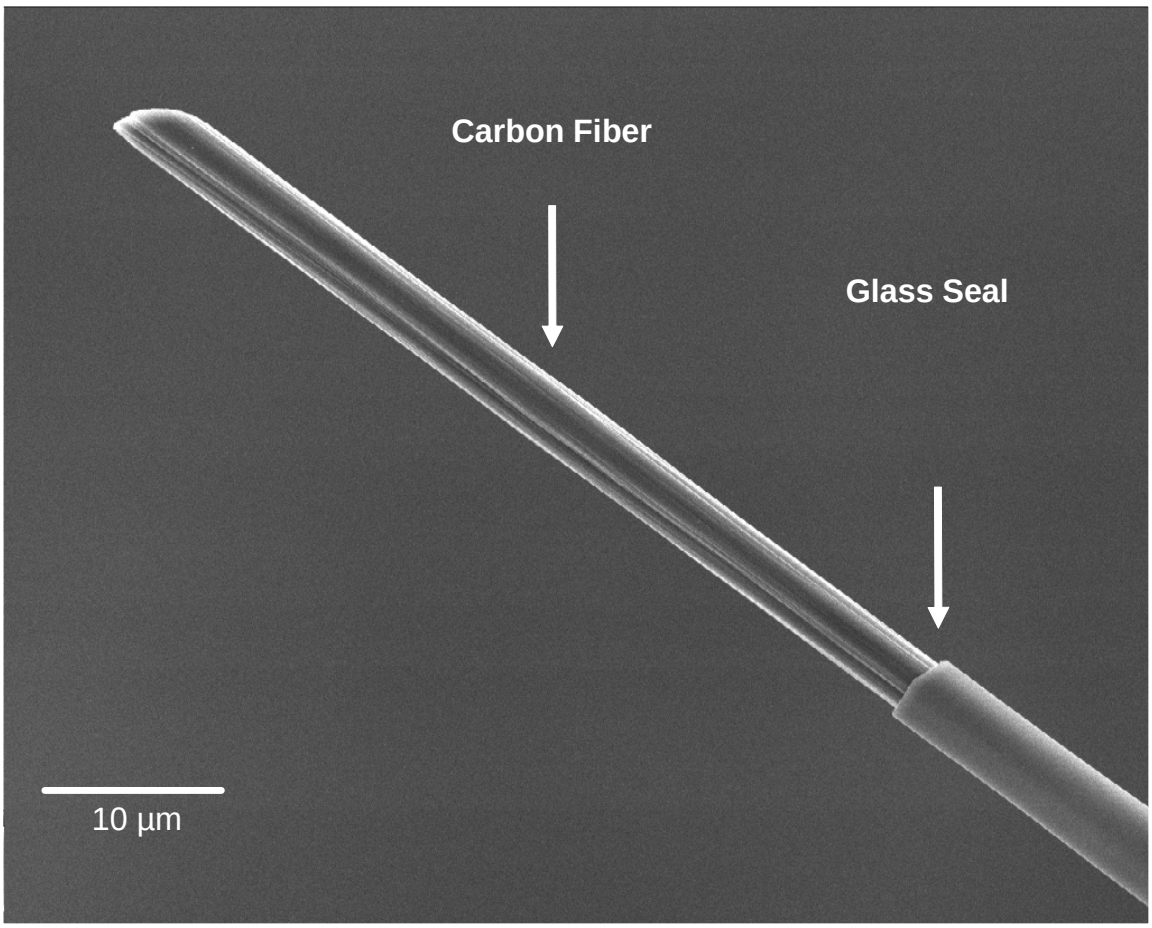

Figure 1.2 SEM image of a carbon fiber microelectrode. Scanning electron microscope image of a pulled glass capillary carbon fiber microelectrode. The diameter of the carbon fiber is 6 µm and the length is approximately 50-100 µmm (Kawagoe et al. 1993).

Many biological changes, particularly at the protein level, occur on the order of minutes; however, many biological changes also occur on the order of milliseconds, termed phasic changes. Early neurobiological techniques such as microdialysis were limited to measuring tonic changes, or changes that occur over several minutes. This limitation prevented further study of neurobiological mechanisms, which can alter chemical communication within a matter of a few milliseconds. These changes can be monitored with microelectrodes either through amperometry or voltammetry (John and Jones 2007).

Microelectrodes are now widely used in numerous biological preparations, ranging from single cell to awake, behaving animals. This versatility permits neuroscientists to probe a variety of neurobiological mechanisms such as exocytosis, neuron receptor functionality, and chemical changes that occur in addiction to drugs of abuse. This thesis will provide specific examples of how microelectrodes can be used to measure rapid biological and chemical changes.

APPLICATIONS

Investigating exocytosis using amperometry

Neurons communicate with each other chemically through a process known as exocytosis, where one cell is electrically stimulated to elicit the release of neurotransmitters which can then diffuse to neighboring cells to initiate a biological action. Microelectrodes have significantly advanced our understanding of the exocytotic process (Westerink and Ewing 2008). Measuring the released neurotransmitters requires a detection method that is both rapid and sensitive enough to measure zeptomole quantities. FSCV lacks the required temporal resolution; however, constant potential amperometry can achieve microsecond resolution by holding a microelectrode at a constant potential that is sufficient to cause electrooxidation of any nearby molecules. The current can be measured and the number of electroactive molecules contacting the microelectrode can be quantitated (Borges et al. 2008). Amperometry, can be used at the cellular level to determine a variety of neurobiological parameters, such as vesicular neurotransmitter content, frequency and kinetics of neurotransmitter release, and exocytotic release mechanisms (Amatore et al. 2007; Mosharov 2008). Because of the dimensions of the microelectrode, it can be placed sufficiently close to the cell to ensure complete oxidation of the extruded molecules. This allows the exact amount of neurotransmitter contained within each vesicle to be determined (Mosharov et al. 2003), as well as to measure the frequency of firing under different conditions (Miranda-Ferreira et al. 2008). Amperometry has been used to determine the role of various ion channels in the exocytotic process. By measuring the frequency and kinetics of individual release events, the role of the Ca^{2+} channel was found to have separate effects on fusion pore binding and dilation (Wang et al. 2006).

Information on the organization of the internal structure of the neuron is typically provided by other common neurobiological techniques such as electron and

fluorescence spectroscopy. In particular these techniques have been used to determine the compartmentalization of neuronal vesicles into three distinct subpopulations: readily releasable, recycling, and reserve pools (Duncan et al. 2003; Rizzoli and Betz 2005). Microelectrodes have been used to confirm these results by individually accessing each of the compartments and measuring the resulting neurotransmitter release from the reserve pool (Villanueva et al. 2006). Further amperometric studies have investigated the proteins implicated in the exocytotic machinery. Genetic silencing of one of these proteins, synaptotagmin I, led to a decreased amount of fractional release of both dopamine and norepinephrine (Moore et al. 2006). Further work with the protein synapsin demonstrated that deletion of synapsin ultimately led to an increased number of catecholamine release events, and that overexpression of synapsin led to a decreased number of release events (Villanueva et al. 2006). These amperometric measurements suggest that synapsin acts as an endogenous negative regulator of catecholamine release. Amperometry provides a reliable means of verifying the results obtained through other preparations.

As these examples show, amperometry is a valuable technique that is useful for studying fundamental systems such as cellular preparations. The sub-second temporal resolution of amperometry makes it an ideal technique for measuring the kinetics of exocytotic events, and the small size of microelectrodes makes measuring the quantal size of neurotransmitter vesicles possible. Through direct measurement of released neurotransmitters, amperometry provides a complementary means of studying the effects of cellular proteins on exocytosis.

Investigating full neuronal circuitry using voltammetry

Where microelectrodes truly excel is when they are coupled with FSCV to detect electroactive neurotransmitters directly. This technique takes full advantage of the

microelectrode's inherent superior spatial and temporal resolution in addition to the selectivity provided by cyclic voltammetry. By locating the potentials at which the maximum cathodic and anodic currents occur, one can distinguish many different neurotransmitters (Heien et al. 2004). FSCV coupled with microelectrodes can be used to monitor sub-second changes in neurotransmitter concentration as a result of pharmacological or behavioral manipulations. This unique setup allows for measurements in anesthetized (Greco et al. 2006) and behaving animals (Heien et al. 2005) to probe the correlation between behavior and neurotransmission.

Of particular interest is the study of phasic and tonic changes in neurotransmitter concentration. Previously, phasic and tonic changes were measured using electrophysiology (Tobler et al. 2005; Schultz 2007), which is a technique that measures the electrical signals generated during neuronal communication. Unfortunately these signals cannot be accurately correlated with the type of neurotransmitter it employs (Ungless et al. 2004; Margolis et al. 2006), thus requiring an alternate approach to measure the neurotransmitter directly. It has also been suggested that neurons undergoing phasic or burst firing do not have sufficient strength to modify surrounding neuronal circuits (Goto et al. 2007); however, it seems likely that phasic firing of dopamine neurons and subsequent release of dopamine has a significant role in learning and memory (Day et al. 2007). For the molecule dopamine, there has been a significant amount of study into understanding the rapid changes that the dopaminergic system undergoes upon repeated stimulation (Montague et al. 2004). In these studies, cyclic voltammetry was coupled with microelectrodes to determine the mechanism by which neurons are able to regulate these transient increases and decreases in dopamine release, ultimately determined to be dependent on the dopamine D2 autoreceptor (Kita et al. 2007).

As a direct result of measuring neurotransmitter release, much can be learned about both natural rewards and drugs of abuse and their effects on neuronal circuitry. Drugs such as cocaine are known to cause increased extracellular concentrations of dopamine over a period of 30 minutes to 1 hour; however, there are additional effects of cocaine that occur on the timescale of a few seconds (Stuber et al. 2005). Upon administration of cocaine to a behaving rat, both tonic and phasic levels of dopamine increase significantly which can be measured using FSCV (Stuber et al. 2005). Drugs can also be used to explore the kinetics of neuronal receptor function. The dopamine D2 autoreceptor is responsible for regulating the amount of dopamine released from the neuron. Once dopamine has been released into the synapse, it can bind to the D2 autoreceptor, thereby inhibiting further dopamine release. The kinetics of activation was studied using FSCV by varying the amount of time in between subsequent release events and comparing the amplitude of the first and the second release event (Phillips et al. 2002). Studying the kinetics of both drugs and receptors can be easily accomplished by directly measuring the concentration of released neurotransmitter (Exley and Cragg 2008).

Not all neurotransmitters are released via exocytosis. Adenosine is a molecule produced during metabolism that acts as a chemical messenger. FSCV has been used to measure changes in adenosine concentration as a result of electrical stimulation of the neuron (Cechova and Venton 2008). Other signals that have been detected using FSCV that are not exocytotic include changes in oxygen concentration and changes in physiological pH (Venton et al. 2003). Both of these changes have been implicated in blood flow, along with nitric oxide (Amatore et al. 2006; Rancillac et al. 2006). Microelectrodes are now allowing the study of biological phenomena that were previously only accessible through functional magnetic resonance imaging (fMRI) and other less spatially resolved techniques.

THESIS OVERVIEW

Neuronal regulation mechanisms

The neuron is a highly plastic cell with an extensive network of inputs and outputs that are modulated by neighboring neurons, as well as its own internal regulatory mechanisms. Many of these internal regulatory processes occur at the neuron terminal, the site of neurotransmitter release and synthesis, while neighboring neurons primarily exert their effects at the dendrites. This thesis will focus on investigating how these processes regulate neuronal activity.

Within dopaminergic neurons, tyrosine is converted to dopamine by tyrosine hydroxylase (TH), which is the rate-limiting enzyme in dopamine synthesis (Fig. 1.3). Once synthesized, dopamine is packaged into vesicles by the vesicular monoamine transporter (VMAT). When an action potential propagates through the axon and into the terminal, Ca^{2+} channels in the terminal open, leading to the fusion of dopamine containing vesicles with the neuron membrane. This vesicular fusion leads to the exocytotic release of dopamine. Upon release from the terminals, a neurotransmitter may interact with postsynaptic cells as well as with proteins on the presynaptic neuron (Fig. 1.3). Two regulatory proteins on the presynaptic neuron that are investigated within the thesis are the D2 autoreceptor (D2) and the dopamine transporter (DAT) (Fig. 1.3). The D2 autoreceptor, which was investigated in Chapter 2, is responsible for self-regulating the synthesis and release of dopamine. Upon activation of the autoreceptor by dopamine, a protein cascade occurs which inhibits both the synthesis and release of dopamine. Any molecule which activates the receptor in this fashion is termed an agonist, while a molecule that blocks the receptor and prevents its natural function is termed an antagonist. The DAT is responsible for binding extracellular dopamine and returning it to the inside of the neuron for recycling. Certain molecules, termed uptake inhibitors, can bind to the transporter and block the re-uptake of neurotransmitters. The

kinetics and pharmacology of both of these presynaptic proteins were investigated using FSCV coupled with microelectrodes.

In Chapters 2-4, FSCV was used to investigate the release of neurotransmitters in the nigrostriatal and mesolimbic pathways of the anesthetized rat. The nigrostriatal pathway has been associated with Parkinson's disease, which is a disease that significantly affects motor function. The nigrostriatal pathway originates in the substantia nigra (SN) and projects along the medial forebrain bundle (MFB) to the caudate putamen (CP) (Fig. 1.4). The mesolimbic pathway is the system which has been implicated in reward-related behavior and consists of projections originating in the ventral tegmental area (VTA) and extending through the MFB toward the nucleus accumbens (NAcc) (Fig. 1.4). Both pathways are primarily dopaminergic and release dopamine at the terminals. However, based on data in Chapters 3-4, it appears that there are other projections which extend from the MFB to regions in the midbrain adjacent to the VTA and SN. Both the red nucleus (RN) and the interstitial medial longitudinal fasciculus (iMLF), situated dorsally to the VTA, demonstrated the presence of releasable neurotransmitters in the midbrain (Fig. 1.5).

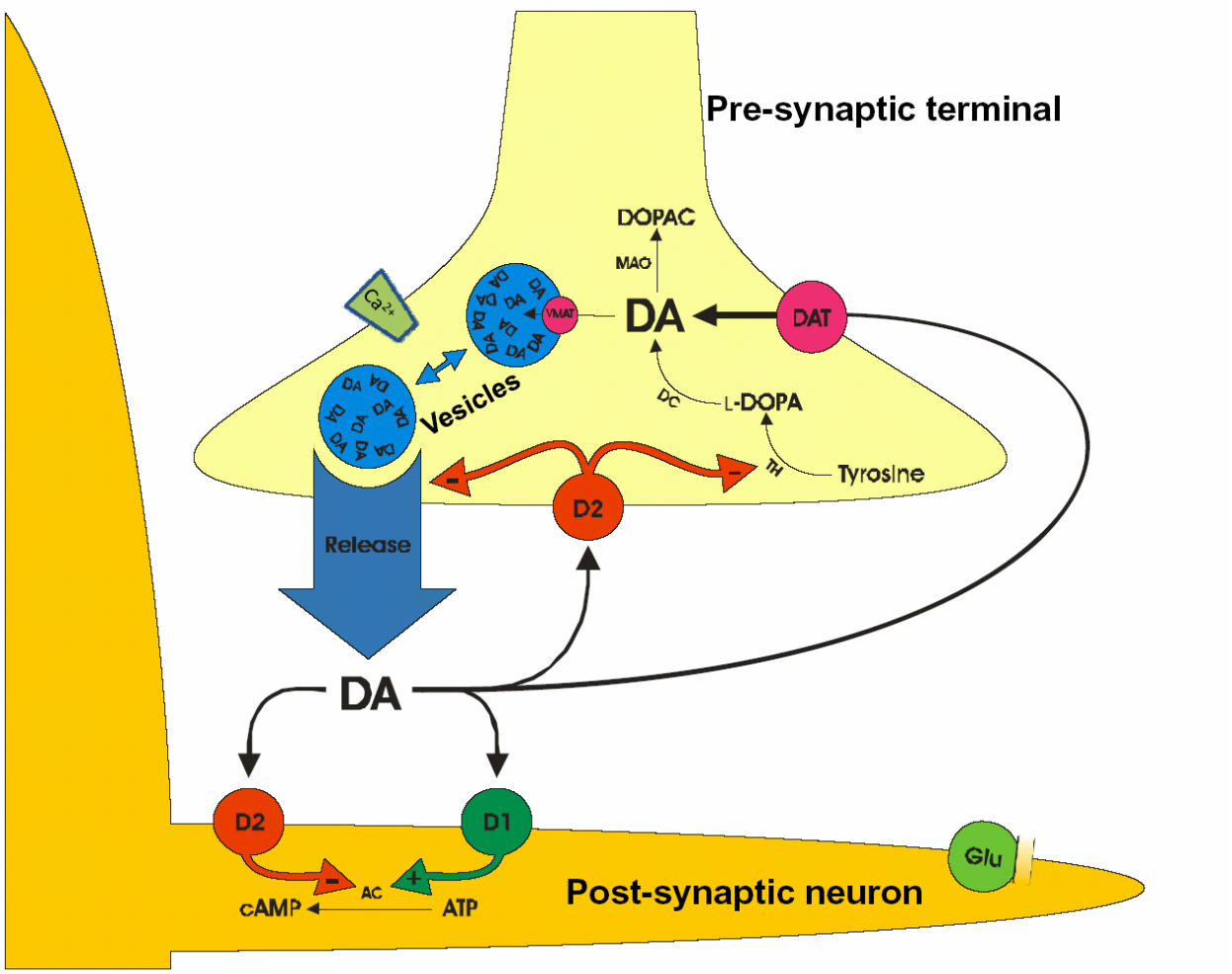

Figure 1.3. Schematic of synaptic machinery. The image represents a diagram of the presynaptic neuron forming a synape on a postsynaptic neuron. Dopamine is synthesized from tyrosine via tyrosine hydroxylase (TH) and packaged into vesicles. Action potentials which reach the neuron terminals cause an influx in Ca^{2+} and the subsequent release of dopamine into the extracellular space. Once in the extracellular space, dopamine may either bind to postsynaptic receptors, presynaptic receptors, or be returned to the inside of the cell via the DAT.

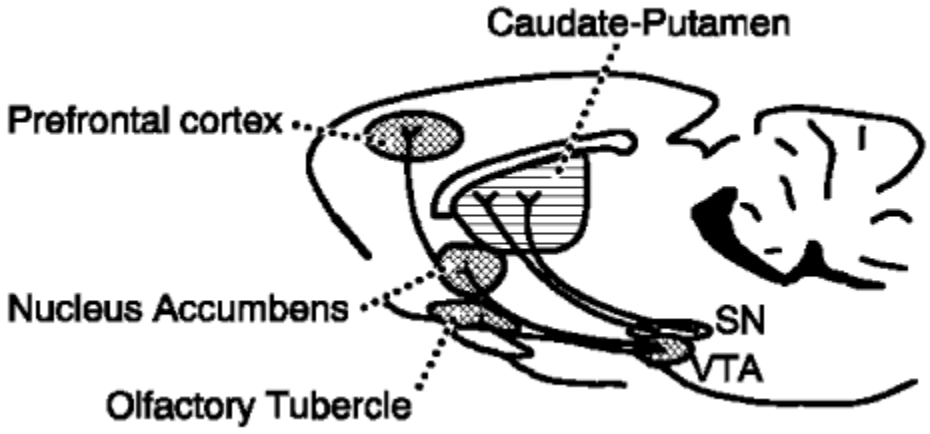

Figure 1.4. Dopaminergic pathways in the rat brain. The diagram demonstrates the two primary dopaminergic pathways in the rat brain. The nigrostriatal pathway extends from the SN to the CP, while the mesolimbic pathway projects from the VTA to the NAcc. (http://www.cellscience.com/CCA_files/image003.gif)

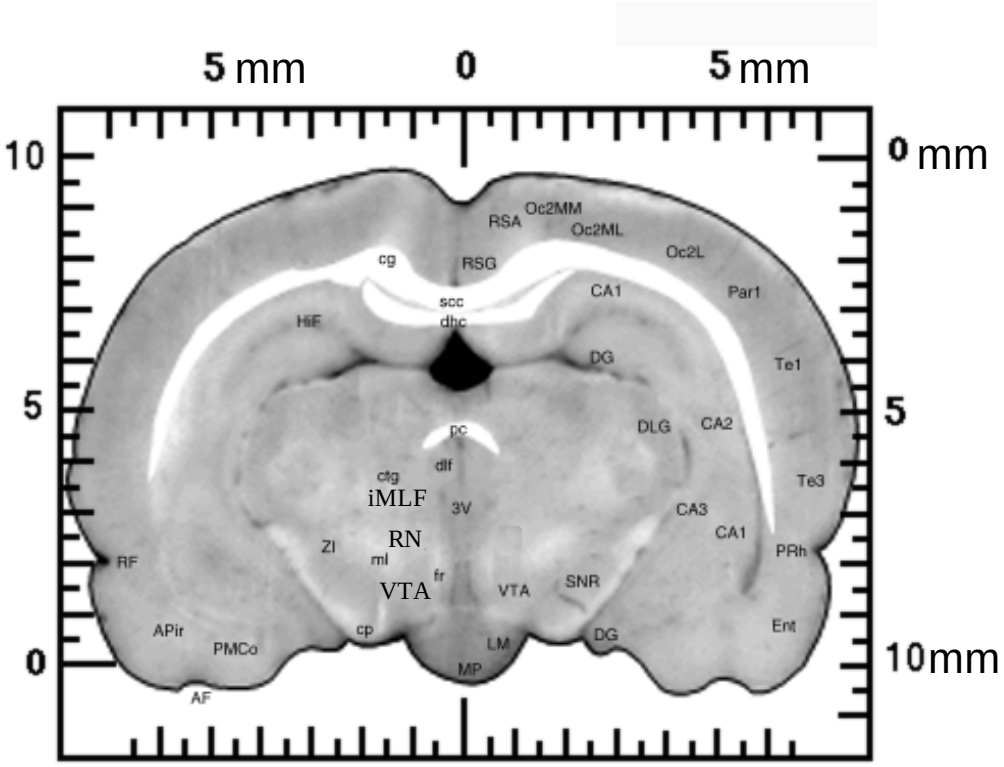

Figure 1.5. Coronal slice of the rat midbrain. This coronal slice is obtained -5.0 mm posterior from bregma and represents the neuronal structures present in the midbrain of the rat. The midbrain region is investigated in Chapters 3 and 4. The VTA extends along the MFB to the NAcc, while the iMLF and RN project from the MFB to the midbrain. (http://www.loni.ucla.edu/Research/Atlases/Data/rat/RatAtlasViewer.shtml)

Electrochemical measurements

A goal of *in vivo* electrochemical measurements of neurotransmitters is to understand the factors that regulate their extracellular concentrations within the intact brain. Amperometry has insufficient chemical selectivity for this application; therefore, to obtain sufficient chemical and temporal resolution to study these regulatory mechanisms, FSCV was used to measure sub-second changes in extracellular neurotransmitter concentration. FSCV is performed by controlling the potential of the carbon-fiber electrode versus a reference electrode (Bath et al. 2000). The potential of the working electrode is held at -0.4 V vs Ag/AgCl between scans and is ramped to +1.0 V at 300 V/s and repeated at a frequency of 50 Hz (Fig. 1.6a). When not in the presence of measurable dopamine, the rapid voltage ramp generates a large background current (1.6b). However, in the presence of dopamine, adsorption to the electrode surface occurs at the holding potential of -0.4 V. During the forward scan, dopamine is oxidized in a two electron process to dopamine-o-quinone, and subsequently re-reduced to dopamine in a two electron process on the reverse scan (Fig. 1.6c). This electrochemical process causes a minor change in the background current (Fig. 1.6d, blue trace). Because the background current (Fig. 1.6b) is relatively stable over the time course of the experiment, it can be background subtracted from the dopamine containing background to yield a cyclic voltammogram (CV) with characteristic peaks for dopamine (Fig. 1.6e).

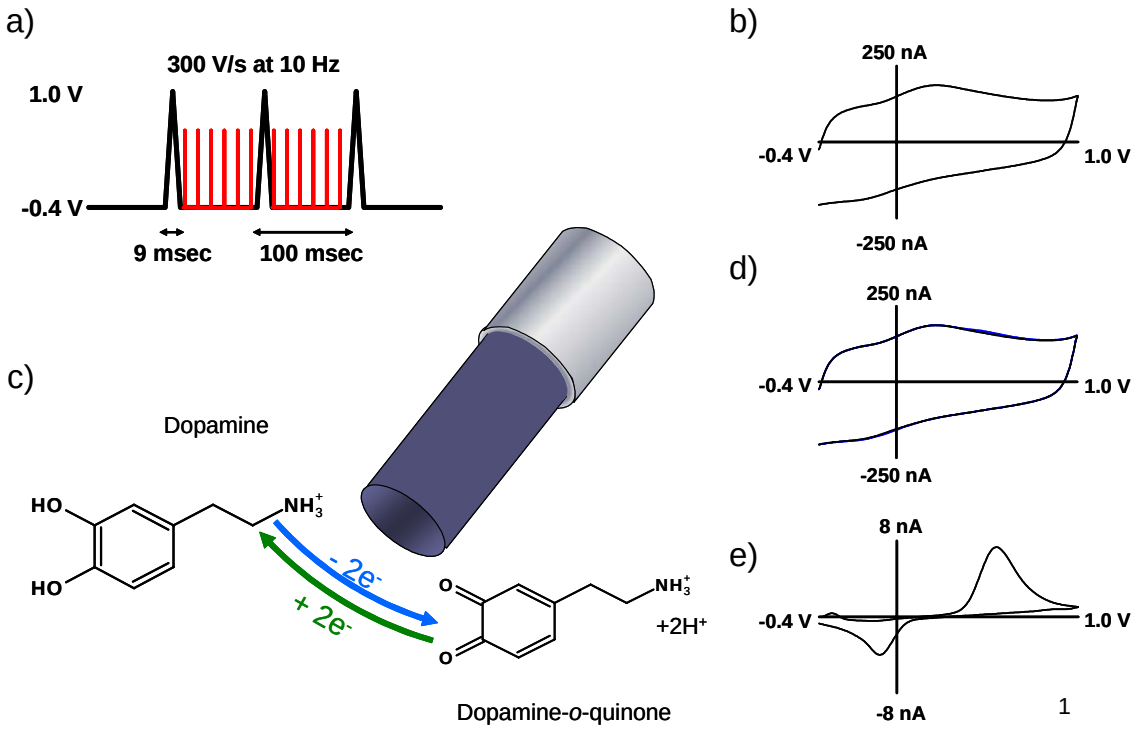

Figure 1.6. Fast-scan cyclic voltammetry. (a) Waveform applied to the carbon fiber electrode. (b) Background current in response to the voltage ramp. (c) Resulting electrochemical reaction of dopamine in response to the applied voltage ramp. (d) Resulting current due to the presence of dopamine at the carbon fiber electrode. (e) Background subtracted cyclic voltammogram for dopamine.

Project overviews

Dopamine D2 receptors modulate facilitation of release

Chapter 2 focuses on understanding the role that D2 autoreceptors play in modulating the release of dopamine. Initially, it was believed that each action potential elicited an identical concentration of neurotransmitter release. Recent work, however, has suggested that the concentration of action potential-mediated release of dopamine is not a constant value per stimulus pulse, but instead is dependent on the stimulation history of the neuron (Montague et al. 2004). To evaluate this claim, the dynamic changes in dopamine release were captured by a mathematical model composed of three factors and their associated time constant: a short-term facilitation factor, a short-term depression factor, and a long-term depression factor. The aim of this project is to investigate the role that the D2 autoreceptor plays in this dynamic modulation and identify the biological mechanisms that are responsible for each of the three mathematical factors.

Somatodendritic release of dopamine in the VTA

While Chapter 2 demonstrates how dopamine release at the terminals influences neurons; Chapter 3 focuses on dopamine release at the dendrites and its potential role as a neuromodulator. Somatodendritic dopamine release has been widely studied in whole animals through microdialysis studies, but electrically evoked release had yet to be measured on a sub-second time scale. Release was evoked via a bipolar stimulating electrode implanted in the MFB, and signals were recorded in the VTA. The occurrences of action potentials, which extend from the axon backward to the cell body, implicate the VTA in a more complex circuit that was previously believed. Typical regulation of the mesolimbic dopaminergic pathway occurs via inhibition or excitation from neighboring neurons; however, this work demonstrated that the pathway is capable

of providing its own self-regulation. To verify the somatodendritic release of dopamine, four different methods were employed: electrochemistry, physiology, independent chemical analysis, and pharmacology. The aim of this project is to determine if dendrites possess self-regulation mechanisms, such as dopamine release, and what role they play in typical neuronal function.

Neurobiological survey of the midbrain

Chapter 4 again focuses on the mesolimbic dopamine pathway; however, the emphasis is on two neighboring regions in the midbrain, the RN and iMLF. These two novel neurotransmitter releasing regions were discovered by combining immunohistochemical labeling of the midbrain with traditional FSCV measurements. Electrical stimulation of the MFB led to electrochemical signals in each of these two regions, while immunohistochemical labeling provided a clearer picture of the neurotransmitters present in each region. The implications of this work are far reaching due to the fact that each of these regions is quite small which has prevented extensive neurochemical analysis. The goal of this project is to determine which neurotransmitters are present in each region and determine a possible role for their release.

Fabrication and characterization of a nitric oxide sensor

Chapter 5 revolves around the development of a sensor capable of selectively measuring nitric oxide. As cerebral blood flow is crucial to the natural function of the brain, the development of a sensor capable of detecting the neuromodulator nitric oxide is critical in understanding how neuronal activity modulates blood flow. As mentioned previously, released neurotransmitter can bind to post-synaptic receptors on neighboring neurons. In some cases, this post-synaptic receptor activation leads to the generation of a retrograde messenger, which can then cross the synapse and modulate pre-synaptic

neuronal activity. Requirements for a nitric oxide sensor include the ability to distinguish nitric oxide from other neurotransmitters and to record neuronal fluctuations on a sub-second scale.

Summary

Each chapter alludes to a different aspect of neuronal regulation. Chapters 2 and 5 investigate regulatory mechanisms which occur at dopaminergic terminals, while Chapters 3 and 4 investigate neuromodulation at the cell bodies. The spatial resolution afforded by microelectrodes allowed investigation of these regionally specific mechanisms, while the temporal resolution of the electrochemical techniques was sufficiently rapid to evaluate the time course of each process. In this way, electrochemistry can be used to probe the neurochemical mechanisms which are responsible for regulating neuronal activity.

REFERENCES

Amatore C. and Maisonhaute E. (2005) When voltammetry reaches nanoseconds. *Analytical chemistry* **77,** 303A-311A.

Amatore C., Arbault S., Bonifas I., Guille M., Lemaitre F. and Verchier Y. (2007) Relationship between amperometric pre-spike feet and secretion granule composition in chromaffin cells: an overview. *Biophys Chem* **129,** 181-189.

Amatore C., Arbault S., Bouret Y., Cauli B., Guille M., Rancillac A. and Rossier J. (2006) Nitric oxide release during evoked neuronal activity in cerebellum slices: detection with platinized carbon-fiber microelectrodes. *Chemphyschem* **7,** 181-187.

Bath B. D., Michael B. J., Trafton B. J., Joseph J. D., Runnels P. L. and Wightman R. M. (2000) Subsecond adsorption and desorption of dopamine at carbon-fiber microelectrodes. *Analytical Chemistry* **72,** 5994-6002.

Borges R., Camacho M. and Gillis K. D. (2008) Measuring secretion in chromaffin cells using electrophysiological and electrochemical methods. *Acta physiologica (Oxford, England)* **192,** 173-184.

Cechova S. and Venton B. J. (2008) Transient adenosine efflux in the rat caudate-putamen. *Journal of neurochemistry*.

Day J. J., Roitman M. F., Wightman R. M. and Carelli R. M. (2007) Associative learning mediates dynamic shifts in dopamine signaling in the nucleus accumbens. *Nat Neurosci* **10,** 1020-1028.

Duncan R. R., Greaves J., Wiegand U. K., Matskevich I., Bodammer G., Apps D. K., Shipston M. J. and Chow R. H. (2003) Functional and spatial segregation of secretory vesicle pools according to vesicle age. *Nature* **422,** 176-180.

Exley R. and Cragg S. J. (2008) Presynaptic nicotinic receptors: a dynamic and diverse cholinergic filter of striatal dopamine neurotransmission. *British journal of pharmacology* **153 Suppl 1,** S283-297.

Goto Y., Otani S. and Grace A. A. (2007) The Yin and Yang of dopamine release: a new perspective. *Neuropharmacology* **53,** 583-587.

Greco P. G., Meisel R. L., Heidenreich B. A. and Garris P. A. (2006) Voltammetric measurement of electrically evoked dopamine levels in the striatum of the anesthetized Syrian hamster. *Journal of neuroscience methods* **152,** 55-64.

Heien M. L., Johnson M. A. and Wightman R. M. (2004) Resolving neurotransmitters detected by fast-scan cyclic voltammetry. *Analytical chemistry* **76,** 5697-5704.

Heien M. L., Khan A. S., Ariansen J. L., Cheer J. F., Phillips P. E., Wassum K. M. and Wightman R. M. (2005) Real-time measurement of dopamine fluctuations after cocaine in the brain of behaving rats. *Proc Natl Acad Sci U S A* **102,** 10023-10028.

John C. E. and Jones S. R. (2007) Voltammetric characterization of the effect of monoamine uptake inhibitors and releasers on dopamine and serotonin uptake in mouse caudate-putamen and substantia nigra slices. *Neuropharmacology* **52,** 1596-1605.

Kawagoe K. T., Zimmerman J. B. and Wightman R. M. (1993) Principles of voltammetry and microelectrode surface states. *Journal of neuroscience methods* **48,** 225-240.

Kita J. M., Parker L. E., Phillips P. E., Garris P. A. and Wightman R. M. (2007) Paradoxical modulation of short-term facilitation of dopamine release by dopamine autoreceptors. *Journal of neurochemistry* **102,** 1115-1124.

Lee Y. and Kim J. (2007) Simultaneous electrochemical detection of nitric oxide and carbon monoxide generated from mouse kidney organ tissues. *Analytical chemistry* **79,** 7669-7675.

Margolis E. B., Lock H., Hjelmstad G. O. and Fields H. L. (2006) The ventral tegmental area revisited: is there an electrophysiological marker for dopaminergic neurons? *J Physiol* **577,** 907-924.

Miranda-Ferreira R., de Pascual R., de Diego A. M., Caricati-Neto A., Gandia L., Jurkiewicz A. and Garcia A. G. (2008) Single-vesicle catecholamine release has greater quantal content and faster kinetics in chromaffin cells from hypertensive, as compared with normotensive, rats. *The Journal of pharmacology and experimental therapeutics* **324,** 685-693.

Montague P. R., McClure S. M., Baldwin P. R., Phillips P. E., Budygin E. A., Stuber G. D., Kilpatrick M. R. and Wightman R. M. (2004) Dynamic gain control of dopamine delivery in freely moving animals. *J Neurosci* **24,** 1754-1759.

Moore J. M., Papke J. B., Cahill A. L. and Harkins A. B. (2006) Stable gene silencing of synaptotagmin I in rat PC12 cells inhibits Ca2+-evoked release of catecholamine. *Am J Physiol Cell Physiol* **291,** C270-281.

Mosharov E. V. (2008) Analysis of single-vesicle exocytotic events recorded by amperometry. *Methods Mol Biol* **440,** 315-327.

Mosharov E. V. and Sulzer D. (2005) Analysis of exocytotic events recorded by amperometry. *Nat Methods* **2,** 651-658.

Mosharov E. V., Gong L. W., Khanna B., Sulzer D. and Lindau M. (2003) Intracellular patch electrochemistry: regulation of cytosolic catecholamines in chromaffin cells. *J Neurosci* **23,** 5835-5845.

Peters J. L., Miner L. H., Michael A. C. and Sesack S. R. (2004) Ultrastructure at carbon fiber microelectrode implantation sites after acute voltammetric measurements in the striatum of anesthetized rats. *Journal of neuroscience methods* **137,** 9-23.

Phillips P. E., Hancock P. J. and Stamford J. A. (2002) Time window of autoreceptor-mediated inhibition of limbic and striatal dopamine release. *Synapse* **44,** 15-22.

Rancillac A., Rossier J., Guille M., Tong X. K., Geoffroy H., Amatore C., Arbault S., Hamel E. and Cauli B. (2006) Glutamatergic Control of Microvascular Tone by Distinct GABA Neurons in the Cerebellum. *J Neurosci* **26,** 6997-7006.

Rizzoli S. O. and Betz W. J. (2005) Synaptic vesicle pools. *Nature reviews* **6,** 57-69.

Schultz W. (2007) Behavioral dopamine signals. *Trends in neurosciences* **30,** 203-210.

Shin J. H., Weinman S. W. and Schoenfisch M. H. (2005) Sol-Gel Derived Amperometric Nitric Oxide Microsensor. *Anal. Chem.* **77,** 3494-3501.

Stuber G. D., Wightman R. M. and Carelli R. M. (2005) Extinction of cocaine self-administration reveals functionally and temporally distinct dopaminergic signals in the nucleus accumbens. *Neuron* **46,** 661-669.

Tobler P. N., Fiorillo C. D. and Schultz W. (2005) Adaptive coding of reward value by dopamine neurons. *Science* **307,** 1642-1645.

Ungless M. A., Magill P. J. and Bolam J. P. (2004) Uniform inhibition of dopamine neurons in the ventral tegmental area by aversive stimuli. *Science* **303,** 2040-2042.

Venton B. J., Michael D. J. and Wightman R. M. (2003) Correlation of local changes in extracellular oxygen and pH that accompany dopaminergic terminal activity in the rat caudate-putamen. *J Neurochem* **84,** 373-381.

Villanueva M., Thornley K., Augustine G. J. and Wightman R. M. (2006) Synapsin II negatively regulates catecholamine release. *Brain cell biology* **35,** 125-136.

Wang C. T., Bai J., Chang P. Y., Chapman E. R. and Jackson M. B. (2006) Synaptotagmin-Ca(2+) triggers two sequential steps in regulated exocytosis in rat PC12 cells: fusion pore opening and fusion pore dilation. *J Physiol* **570,** 295-307.

Westerink R. H. and Ewing A. G. (2008) The PC12 cell as model for neurosecretion. *Acta physiologica (Oxford, England)* **192,** 273-285.

Wightman R. M. (2006) Detection technologies. Probing cellular chemistry in biological systems with microelectrodes. *Science* **311,** 1570-1574.

Wu W. Z., Huang W. H., Wang W., Wang Z. L., Cheng J. K., Xu T., Zhang R. Y., Chen Y. and Liu J. (2005) Monitoring dopamine release from single living vesicles with nanoelectrodes. *J Am Chem Soc* **127,** 8914-8915.

CHAPTER 2 - Dopamine D2 receptors modulate facilitation of release

INTRODUCTION

Measurements in both alert primates (Waelti et al. 2001; Tobler et al. 2005) and rats (Pan et al. 2005) have shown that dopaminergic neurons exhibit phasic activity during reward related tasks that follows the pattern of a prediction error, one of the basic tenets of learning theory (Schultz et al. 1997; Schultz and Dickinson 2000). Transient firing of dopaminergic neurons leads to release in terminal regions that has the form of a transient increase in extracellular dopamine that is subsequently returned to baseline as a consequence of clearance by the dopamine transporter (Chergui et al. 1994; Wightman and Robinson 2002). This release and uptake can be directly measured with rapid voltammetric techniques. Initial modeling of dopamine release evoked by burst firing suggested that the concentration released by each impulse was constant (Wightman et al. 1988), but subsequent studies showed that the concentration of released dopamine fluctuates, exhibiting both facilitation and depression based on stimulation history (Garris et al. 1999; Yavich and MacDonald 2000; Cragg 2003; Montague et al. 2004).

Early voltammetric measurements showed that a long-term (minutes) depression of dopamine release occurred with prolonged stimulation (Ewing et al. 1983; Michael et al. 1987) or rapidly repeated trains (Yavich 1996; Yavich and MacDonald 2000). This depression was shown to depend on the capacity of the newly synthesized, readily releasable pool and the ability of a reserve pool of dopamine to restore the releasable compartment. Recent work suggests the reserve pool is maintained by synapsin, a protein that interacts with the surface of synaptic vesicles (Venton et al. 2006). Another critical control point that influences the relationship between impulse flow and dopamine release is the D2-like dopamine autoreceptor. Inhibition of the dopamine autoreceptor potentiates release of dopamine (Gonon and Buda 1985; Yavich 1996) because activation of the autoreceptor causes inhibition of dopamine synthesis and a lowering of

the release probability (Sibley 1999). Activation of the autoreceptor inhibits dopamine release rapidly, operating on a second time scale (Phillips et al. 2002).

We have recently investigated dynamic changes in dopamine release using a mathematical model that incorporates both facilitatory and depressive components (Montague et al. 2004). Using stimulation conditions similar to those imposed during intracranial self-stimulation of dopamine cell bodies (Wise 2004), dopamine release was found to be modulated by a short-term facilitation component, a short-term depression component, and a long-term depression component (Montague et al. 2004). Thus, the model enabled us to quantify the previously described facilitation and depression of dopamine release. Here we consider the neurobiological correlates of these components. The long-term depression has been attributed to the slow refilling of the releasable pool. Mechanisms underlying the short-term facilitation and depression terms have not been assigned although an autoreceptor mechanism seems likely for the short-term depression component. In this work we directly probe the role of the D2 autoreceptor by administering exogenous D2 antagonist and agonist and examining electrically stimulated release. We find that activation of the D2 receptor not only causes depression of dopamine release but that the same treatment also augments the short-term facilitation. In contrast, blockade of the D2 receptor removes both short-term components leaving only a long-term depression factor that regulates dopamine release. These findings indicate that the plasticity of short-term changes in dopamine release is a direct consequence of D2-dopamine autoreceptor activation.

MATERIALS AND METHODS

Animals and surgery

Male Sprague-Dawley rats (225-350g; Charles River, Wilmington, MA) were anesthetized with urethane (1.5 g/kg, i.p.) and placed in a stereotaxic frame (Kopf, Tujunga, CA). A heating pad (Harvard Apparatus, Holliston, MA) maintained a constant body temperature of 37°C. Holes were drilled in the skull for the working, reference, and stimulation electrodes at coordinates selected from the atlas of Paxinos and Watson (Paxinos and Watson, 1986). The carbon-fiber microelectrode was placed in the striatum (AP +1.2, ML +2.0, and DV -4.5). The stimulating electrode was placed in the substantia nigra (AP -5.2, ML +1.0, and DV -7.5). Both the carbon-fiber and stimulating electrodes were adjusted in the dorsal-ventral coordinate while stimulating to achieve maximal dopamine release. An Ag/AgCl reference was inserted in the contralateral side.

Electrical stimulation

An untwisted bipolar stimulating electrode (Plastics One, Roanoke, VA) was used to stimulate dopaminergic neurons. The stimulus was provided by an analog stimulus isolator (A-M Systems, Sequim, WA). The stimulation train consisted of biphasic pulses (± 300 μA, 2 ms/phase unless otherwise noted). The frequency and number of pulses per train were varied as noted in the text. Stimulations used were designed to mimic those for which an animal will lever-press during ICSS. The pulses were generated by a computer and applied between the cyclic voltammograms to avoid electrical interference.

Electrochemistry

Cylindrical carbon fiber microelectrodes were prepared using T650 carbon fibers (3 μm radius, Amoco) and encased in glass capillaries (A-M Systems, Sequim, WA) and

pulled with a micropipette puller (Narashige, East Meadow, NY). The protruding fiber was then cut to a length of 50-100 μm. On the day of use, the electrode was soaked for 10 minutes in isopropanol purified with activated carbon (Bath et al. 2000). To make contact with the carbon fiber, a wire coated with silver paint was inserted into the open end of the capillary and twisted to ensure solid contact with the fiber. The wire was then secured using epoxy. The reference electrode was chloridized by placing a silver wire in an HCl solution and applying 5V.

Fast-scan cyclic voltammetry was used in all experiments (Bath et al. 2000). The instrumentation controlled the potential of the carbon-fiber electrode while the reference electrode was held at ground potential. The potential of the working electrode was held at -0.4 V vs Ag/AgCl between scans and was ramped to +1.0 V at 300 V/s and repeated at a frequency of 10 Hz. After the experiment the working electrode was calibrated *in vitro* using dopamine solutions of known concentration.

Data analysis

Data were analyzed in Graph Pad Prism (Graph Pad Software, San Diego, CA) and are expressed as mean ± SEM. Statistical significance was determined using a two-way ANOVA, and posthoc comparisons were performed using the method of least squares with a Bonferroni correction.

Peak amplitude for each stimulation train was calculated by subtracting the difference between the concentration at the base and the apex of the response. This minimizes the effect produced by the inhibition of uptake which slows the return to baseline. For experiments involving five stimulation trains (Figures 2.4-5), three post drug files were collected and averaged to fully capture the effect of the drug. Each post-drug train was then normalized to its corresponding pre-drug train to compare the overall facilitation and depression at each train in the pattern.

Simulations of the data were performed on the basis of the dynamic model described previously (Montague et al. 2004). The model was developed to predict dopamine release when the neuron is exposed to a complex series of stimulations such as what occurs during ICSS. During a stimulation train, the amount of dopamine released per stimulus pulse $[DA]_p$ can be defined by the following equation:

$$[DA]_p = a_0 * f * d_1 * d_2 \quad (1)$$

where a_0 is the initial concentration of dopamine released per stimulus pulse at the beginning of a stimulation train, f is the short-term facilitation, d_1 is the short-term depression, and d_2 is the long-term depression. Each of these dynamic terms is multiplicative to give either an overall depression ($f * d_1 * d_2 < 1$) or an overall facilitation ($f * d_1 * d_2 > 1$) of release. Between stimulation events, each term decays exponentially with first order kinetics to its original value of 1, with a time constant τ_j^{-1}, with I_j representing any of the 3 variables in equation 1:

$$\frac{dI_j}{dt} = \tau_j^{-1}(1 - I_j) \quad (2)$$

This model was used to create a simulation program written in LabVIEW (National Instruments, Austin, TX). The program was then used to predict whether facilitation or depression would occur under specific stimulation conditions.

Chemicals

All chemicals and drugs were purchased from Sigma/Aldrich (St. Louis, MO) and used as received. Solutions were prepared using doubly distilled deionized water (Megapure system, Corning, NY). The TRIS buffer solution used for post-calibration was prepared using 12 mM TRIS, 140 mM NaCl, 3.2 mM KCl, 1.2 mM $CaCl_2$, 1.25mM

NaH_2PO_4, 1.2 mM $MgCl_2$, 2.0 mM Na_2SO_4 at pH 7.4. Drugs were dissolved in saline and injected intraperitoneally.

RESULTS

Paired-train paradigm

To examine how rapid changes in extracellular dopamine concentration could affect the dynamics of subsequent dopamine release in the caudate-putamen of anesthetized rats, we used the paired-train paradigm, where the maximal release evoked by one stimulus train is compared to the release evoked by a second stimulus train at some variable time in the future. This approach has been effective to study D2 inhibition of release in both brain slices, where local electrical stimulation has been used to evoke dopamine release (Kennedy et al. 1992; Phillips et al. 2002; Rice and Cragg 2004), as well as in vivo (Benoit-Marand et al. 2001). Trains with 12 pulses delivered at 50 Hz were used and the second train was initiated 0.5 to 25 s after the beginning of the first train (Fig. 2.1). When the second train was delivered 0.5 s after the first its amplitude was depressed (Fig. 2.1a). However, as the time between trains was increased, the depression diminished until at 8 s both trains produced similar magnitudes of dopamine release (Fig. 2.1c). Following a 0.5 mg/ kg i.p. injection of haloperidol, the amplitude of the first train doubled (n = 7 animals), clearly indicating that dopamine release is normally under D2 receptor control (Wiedemann et al. 1992). Consistent with prior experiments conducted in vivo and in brain slices, the relative amplitude of the second train was not attenuated as greatly at short intertrain intervals with the antagonist present. These experiments demonstrate that the D2 receptor can inhibit subsequent dopamine release on a time scale similar to the short-term depression factor captured by the model, 3.24 s (Montague et al. 2004).

Examination of facilitation and depression of dopamine release

To investigate the plasticity of dopamine release during stimulations, an extended series of trains (all 24 pulse, 50 Hz, 300 μA) separated by different times was

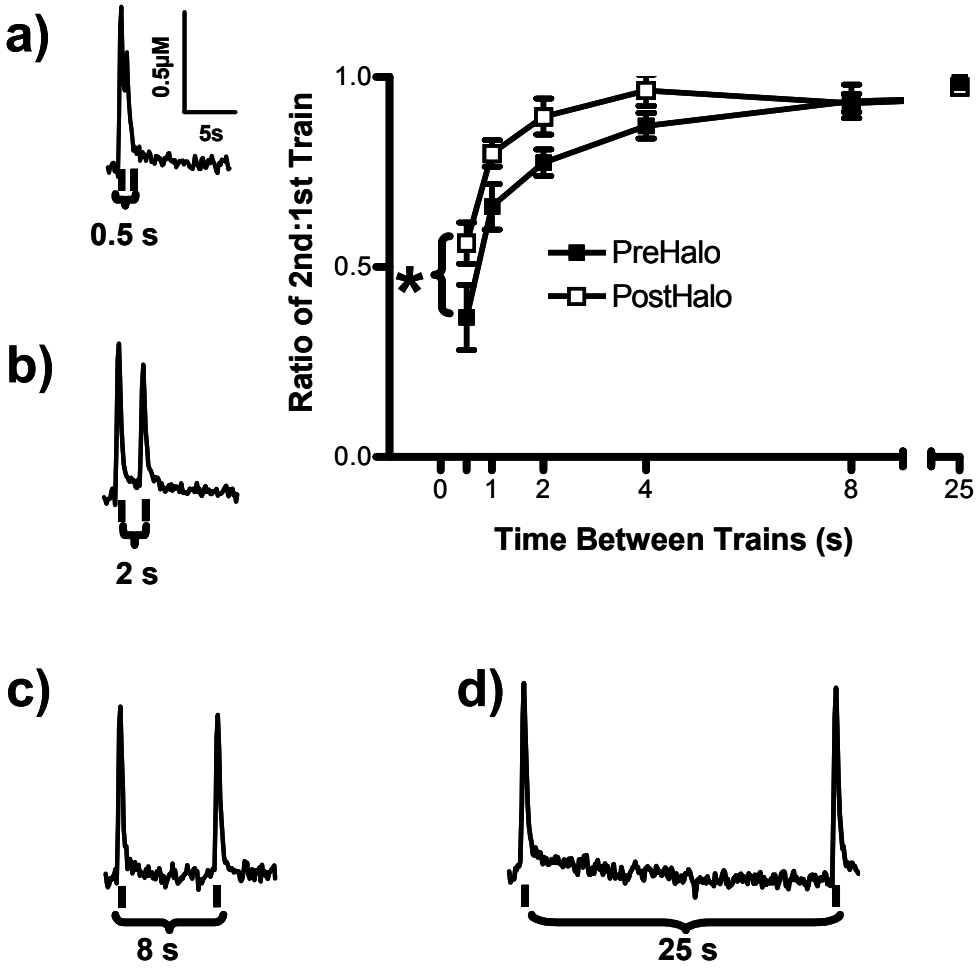

Figure 2.1. Effect of stimulation train spacing on autoreceptor function. Each panel shows the representative time course of dopamine evoked release in a single animal. Vertical bars indicate stimulus train (50Hz, 12p, 300µA) delivery. Time intervals between trains: **(a)** 0.5 s **(b)** 2 s **(c)** 8 s **(d)** 25 s. Inset: amplitude of the second peak normalized to the amplitude of the first peak in each train. This ratio was compared at different time intervals (n = 7), as well as before and after administration of a 0.5 mg/kg i.p. injection of haloperidol (n = 7). At spacing of 0.5 s, the pre and post drug values were significantly different ($F(1,91) = 9.202$, $p < 0.0031$, Bonferroni t-test). At time intervals larger than 8 s, both before and after haloperidol the normalized amplitudes were identical. Error bars represent SEM.

used (representative examples are shown in the A panels of Fig. 2.2 and 2.3). Prior to drug administration, stimulation sequences were repeated every five minutes until the release was stable between sequences. Within this stimulation pattern, the first five trains probed the short-term dynamics of dopamine release, while the later trains probed the dynamics of the longer-term component. There is some biological variability between animals in the pattern as demonstrated by the amplitude of dopamine release: some animals exhibit slight depression in the first 5 trains (Fig. 2.2a) while others exhibit slight facilitation (Fig. 2.3a). However facilitation occurs in later trains in both examples. For example, the responses to train 15 are approximately 25% larger than seen during train 11.

Effect of raclopride on dopamine release

The responses were compared before (Fig. 2.2a) and 20 min. after (Fig. 2.2b) a 1 mg/kg i.p. injection of the D2 antagonist raclopride. (Responses 20 min. after saline were virtually unchanged (vide infra)). Like haloperidol, raclopride caused approximately a two-fold increase in dopamine release on the first train of each pattern (Fig. 2.2b). However, the effect is less prominent during the next four trains as the amplitude of release diminishes. The within train facilitation observed between trains 11 and 15 is virtually abolished by raclopride administration (Fig. 2.2b).

The relative amplitude of the first five trains was pooled from several animals (Fig. 2.4, n = 6 for raclopride, n = 9 for saline). The maximum dopamine amplitude for each train was normalized by its pre-saline or pre-raclopride counterpart. For saline, the responses were essentially unity indicating no change in dopamine release in the 20 minute interval between train applications. In contrast, dopamine release in the first train was enhanced by a factor of 2.5 following raclopride (Fig. 2.4a). With each successive train, however, the enhancement of release diminished with the values decreasing

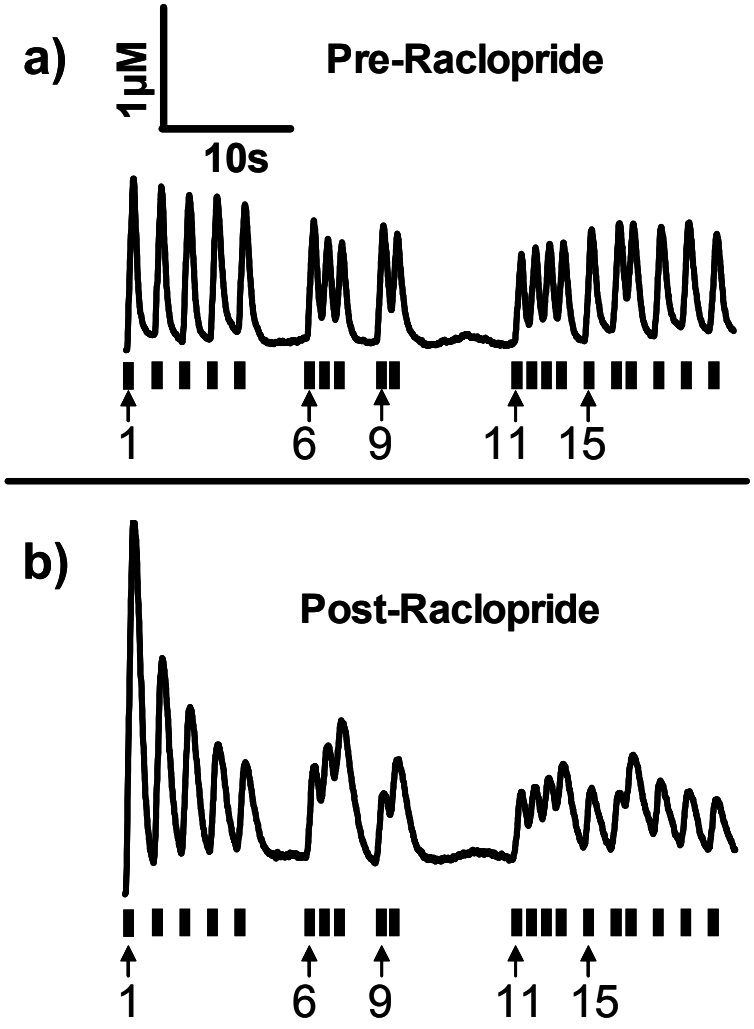

Figure 2.2. Effect of raclopride on stimulated dopamine release during a complex stimulation pattern. Each panel is a representative concentration versus time trace of dopamine release in a single animal. Vertical bars indicate stimulus train (50Hz, 24p, 300µA) delivery. Data were recorded every 20 minutes. **(a)** Trace of dopamine release before drug administration. **(b)** The effect of a 1 mg/kg i.p. injection of raclopride on stimulated dopamine release 20 minutes after administration.

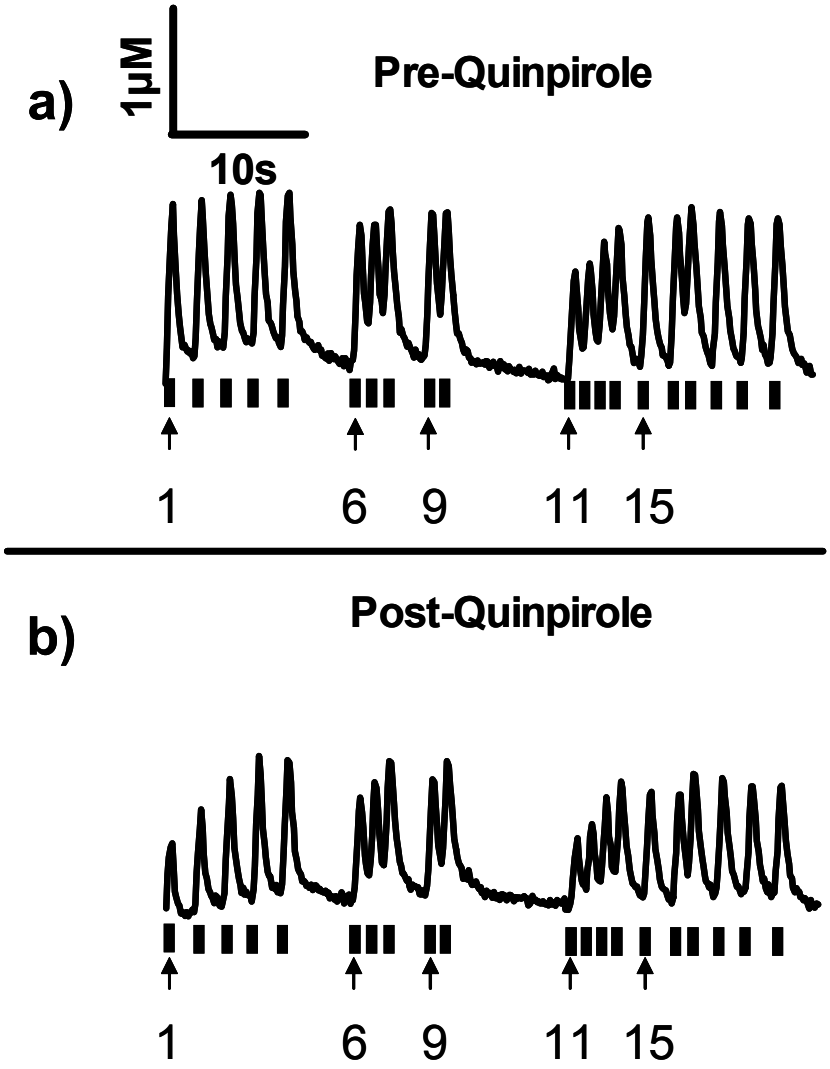

Figure 2.3. Effect of quinpirole on stimulated dopamine release during a complex stimulation pattern. Each panel is a representative concentration versus time trace of dopamine release in a single animal. Other conditions as in Fig. 2.2. **(a)** Trace of dopamine release before quinpirole administration. **(b)** The effect of a 1 mg/kg i.p. injection of quinpirole on stimulated dopamine release 20 minutes after administration.

toward unity ($F(1,65)=66.05$, $p<0.0001$, two-way ANOVA). Trains 1-4 exhibited significant difference from saline values ($p<0.001$ for trains 1, 2, and 3, $p<0.01$ for train 4, Bonferroni t-test). Train 5 was not significantly different from predrug values ($p>0.05$, Bonferroni t-test). Thus, administration of the D2 antagonist changes the release pattern to one of long-term depression.

We attempted to simulate these results with the Montague model (Fig. 2.4b). The predrug response, using kinetic values from Montague et al., (2004), predicts little change in maximal dopamine during the first 5 trains as is found in the experimental data (compare the left panel, Fig. 2.4b with the first five trains in Figs. 2.2a and 2.3a). Because D2 antagonists can enhance release (Fig. 2.1), we simulated the results after raclopride administration with an increased concentration of release (a_o) to account for this. Furthermore, we eliminated the short-term depression, d_1, as suggested by the data in Fig. 2.1. The simulation result (middle panel, Fig. 2.4b) predicts that dopamine release will be facilitated with each train, behavior unlike the experimental data. However, when both the short-term depression and facilitation, d_1 and f, were eliminated, stimulated release was predicted to decrease with each train as a consequence of the long-term depression, d_2. This trend closely resembles that obtained experimentally after raclopride (compare right panel, Fig. 2.4b, with Fig. 2.2b or the raclopride mean values Fig. 2.4a).

Effect of quinpirole on dopamine release

The effects of a 1 mg/kg i.p. dose of the D2 agonist quinpirole were examined. Release measurements were made twenty minutes after quinpirole was administered. The first release train was decreased by 50% consistent with previous reports (Joseph et al. 2002), but by the fourth train dopamine release had returned to its pre-drug value

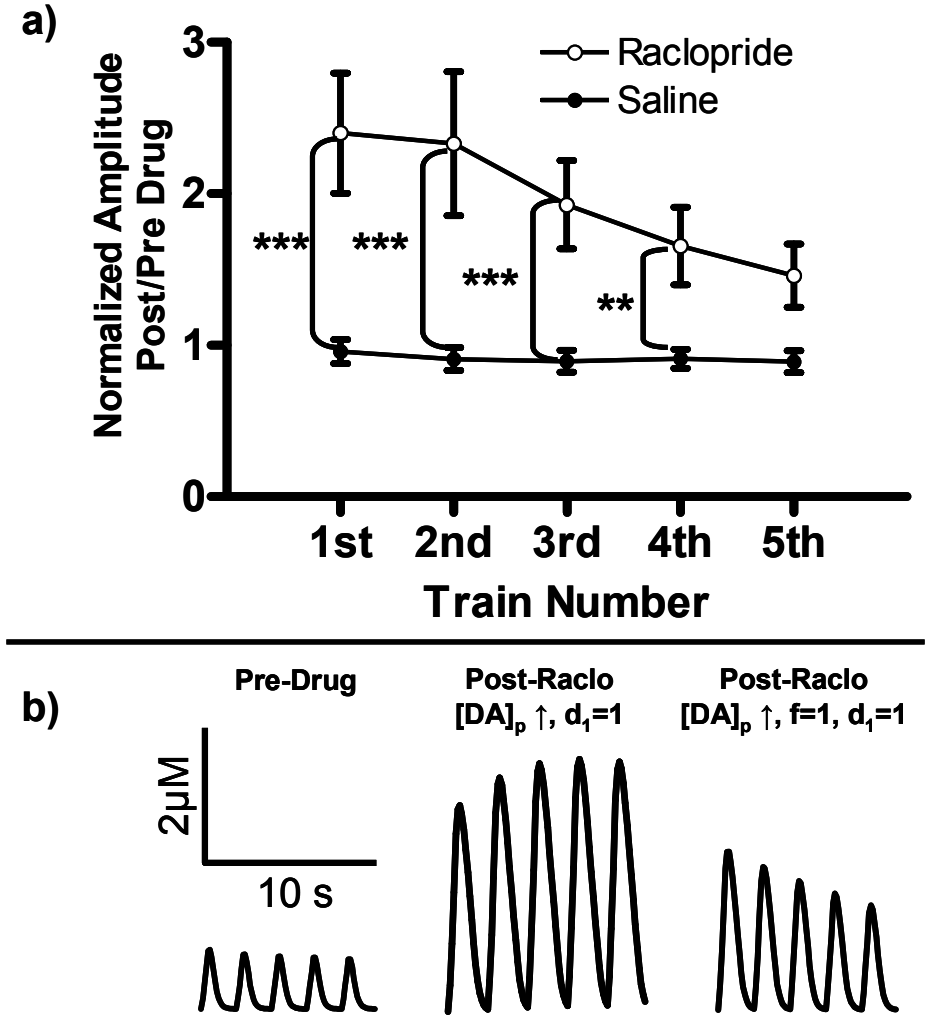

Figure 2.4. Effect of raclopride on dopamine release in consecutive trains. Release during 5 trains, 2 s apart, acquired as in Fig. 2.2. **(a)** Results following 1 mg/kg injection of raclopride (N=6) or saline (N=9) were normalized by the pre-injection maximal release amplitudes.was given i.p. Twenty minutes later, a second file was collected with the same stimulation parameters. There was significance between raclopride and saline in the first 4 trains ($p<0.001$, 0.001, 0.001, and 0.01 respectively, Bonferroni t-test). **(b)** Simulations of responses expected for the 5 stimulus trains. Left panel: Simulation of predrug response. Parameters used were A_o = 100 nM, uptake terms (K_m = 200 nM, V_{max} = 4 μM/s), kickback factors were: short-term facilitation = 1.01 with a time constant of 4.41 s, short-term depression = 0.989 with a time constant of 3.23 s, and long-term depression = 0.997 with a time constant of 840 s. Middle panel: simulation of post raclopride response with short-term depression removed. A_o was doubled, short-term kick back factor was set to one, and the other terms were left at their pre-drug value. Right panel: Identical to middle panel except short-term facilitation kick back factor was set to one. Error bars represent SEM.

(Fig. 2.3b). At the beginning of each subset of closely spaced stimulation trains (trains 1, 6, 9, and 11), release was inhibited but recovered by the end of the subset.

As with raclopride, maximal dopamine release from the first five trains from multiple animals (n = 7) following 1 mg/kg quinpirole were normalized to their corresponding predrug values and compared to release data collected in a similar way following saline (n = 9). The maximum dopamine concentration for each post-drug train was normalized to its corresponding response in the pre-drug train, with values less than 1 indicating decreased release relative to pre-drug values. Quinpirole caused dopamine release on the initial train to diminish by a factor of two (Fig. 2.5), consistent with previous experiments involving i.p. injection of quinpirole (Stamford et al. 1991). However, with each consecutive train, the amount of release incremented ($F(1,70)=5.331$, $p<0.0239$, two-way ANOVA). Other than for the 1st train, there was no significant difference between the values following saline and the quinpirole values ($p<0.01$ for train 1, $p>0.05$ for trains 2-5, Bonferroni t-test).

The results following quinpirole were also simulated with the Montague model (Fig. 2.5b). Because D2 agonists can enhance the short-term depression, we simulated the results after quinpirole administration with a decreased concentration of release, a_o, and with the short-term depression, d_1, enhanced. This simulation shows an overall decrease in the amount of dopamine release, while also increasing the amount of observed depression (middle panel, Fig. 2.5b), behavior unlike the experimental data. However, when both short-term depression and facilitation, d_1 and f, are enhanced, the observed trend closely resembles that obtained experimentally after quinpirole (compare right panel, Fig. 2.5b, with Fig. 2.3b or the quinpirole mean values Fig. 2.5a).

The effects of quinpirole on depression and facilitation of the later trains were also examined (Fig. 2.6). The inhibition is rapidly restored when there is a pause between stimulation trains. Between trains 5 and 6, there is approximately 5 s between

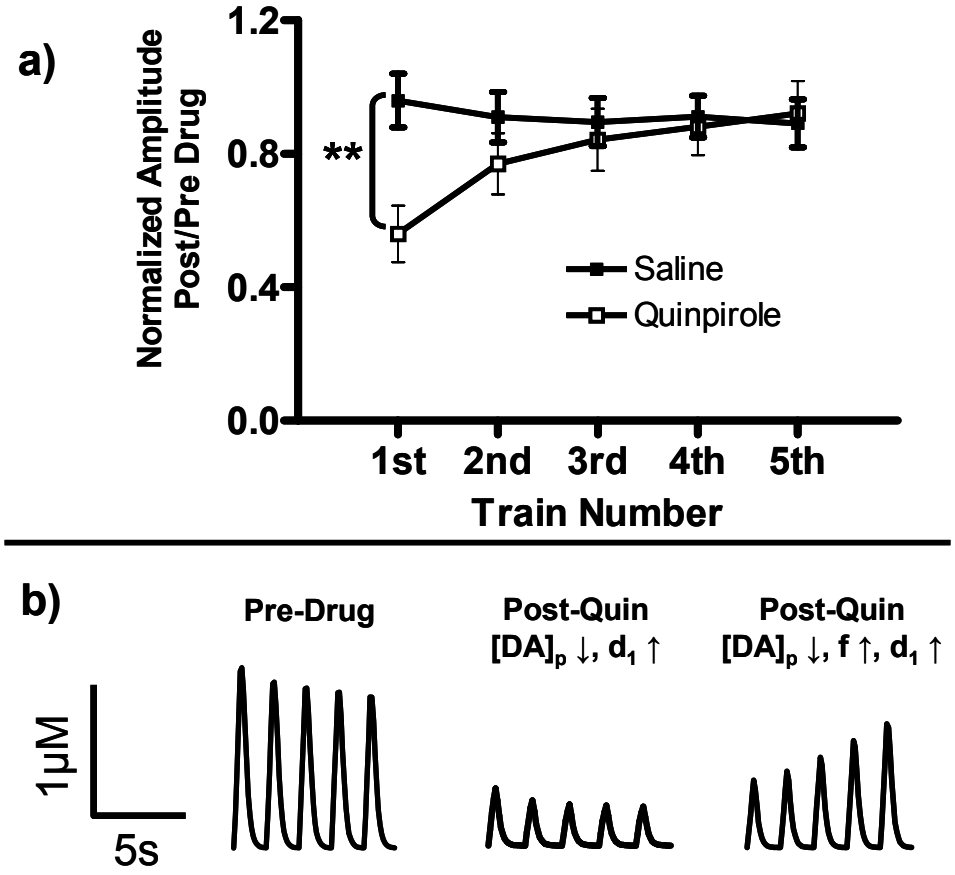

Figure 2.5. Effect of quinpirole on dopamine release in consecutive trains. Release during 5 trains, 2 s apart, acquired as in Fig. 2.2.3. **(a)** Results following a 1 mg/kg injection of quinpirole (N=7) or saline (N=9) were normalized by the pre-administration values. There was significance between quinpirole and saline in the first train ($p<0.01$, Bonferroni t-test). **(b)** Simulations of responses expected for the 5 stimulus trains. Left panel: Simulation of predrug response. Parameters used were A_o = 100 nM, uptake terms (K_m = 200 nM, V_{max} = 4 μM/s), kickback factors were: short-term facilitation = 1.01 with a time constant of 4.41 s, short-term depression = 0.989 with a time constant of 3.23 s, and long-term depression = 0.997 with a time constant of 840 s. Middle panel: Simulation of release following quinpirole with only the short-term depression increased. A_o was decreased in half to account for the reduced release and short-term depression was enhanced (kickback factor = 0.985). Right panel: same as middle panel except the short-term facilitation was also enhanced (kickback factor = 1.02). Error bars represent SEM.

stimulations, and, during this time, release reverts to a more inhibited state. During trains 6-8, the release increases, but during the pause between trains 8 and 9, there is again a reversion to more inhibited release. The time between trains 10 and 11 is relatively long (10 s), and dopamine release returns to an inhibited level similar to that caused by quinpirole on the first train. However, release facilitates quickly as is apparent in the trains immediately following trains 6, 9, and 11. Increasing the dose of quinpirole to 5 mg/kg caused increased inhibition on the first train, but the rate of facilitation is significantly lower (Fig. 2.6). The first train after each pause (trains 1, 6, 9, and 11) all have approximately the same value, but the rate of facilitation is slowed in the higher drug response files.

The D1 receptor was also investigated to ascertain its effect on facilitation and depression of release. A 1-mg/kg i.p. injection of the D1-antagonist SCH-23390 was given (data not shown). There was no significant difference between release following SCH-23390 and saline ($F(1,60)=1.931$, $p<0.168$, Bonferroni t-test) indicating that the D1 receptor is uninvolved.

Stimulation intensity

We wished to know how increased concentrations of the endogenous ligand, dopamine, could affect the dynamics of subsequent dopamine release. As above, the paired-train paradigm was used, where the effect of one stimulus train is compared to a second stimulus train at some time in the future. In this case, the number of stimulus pulses in the train was varied, which affects the amount of dopamine released (Wightman et al. 1988). 50 Hz trains spaced by 2 s containing at least 6 pulses were used to allow the effects of facilitation and depression to accumulate. At 6 pulses per train, the amplitude of the second train was smaller than that of the first train (Fig. 2.7a). Thus, as in Fig. 2.1, a small amount of depression of release occurs under these

conditions. At 60 pulses for each train, the results were dramatically different with the second train facilitated relative to the first train (Fig. 2.7a). Indeed, a trend of facilitation was seen with pulse numbers greater than 6 ($F(6,72)=4.302$, $p<0.0001$, two-way ANOVA). A 0.5 mg/kg i.p. dose of haloperidol blocked this apparent facilitation at 60 pulses (Fig. 2.7c).

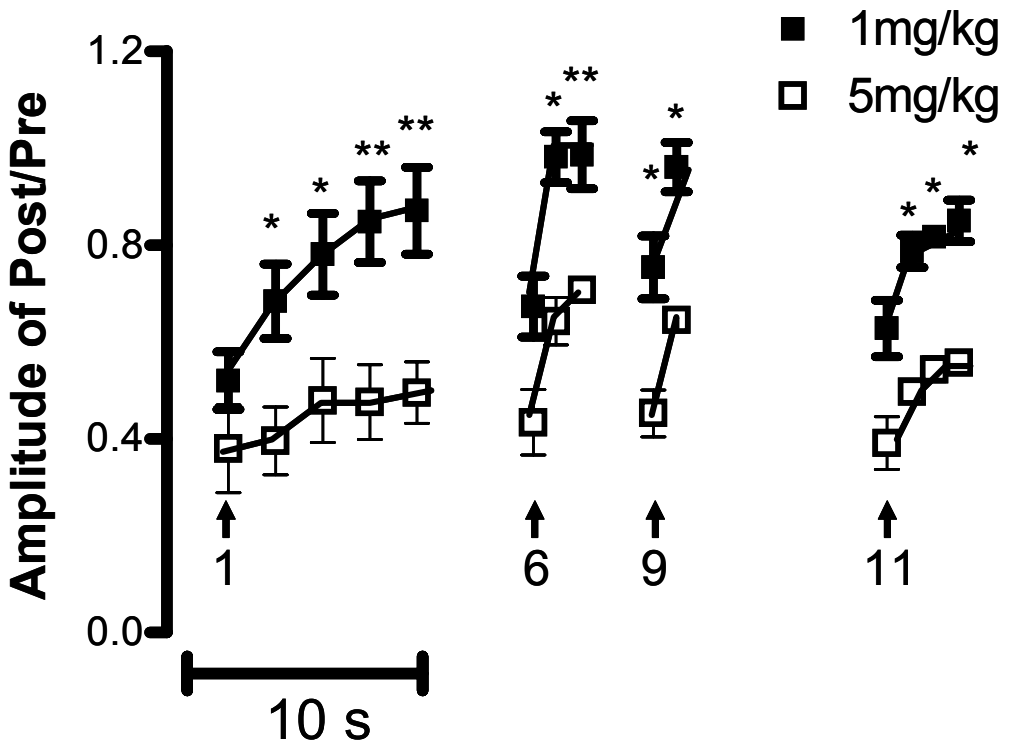

Figure 2.6. Effect of quinpirole concentration on stimulated dopamine release. Each data point is the maximal dopamine release induced by a 50Hz, 24p, 300 μA train normalized by release observed in the predrug train. Post-quinpirole files were collected 20 minutes after administration. Values <1 correspond to a depressed train, while values >1 correspond to a facilitated train. Two different doses of quinpirole were used, 1 mg/kg (N=6) and 5 mg/kg (N=5). Error bars represent SEM. There was significance in trains 2, 3, 4, 5, 7, 8, 9, 10, 12, 13, 14, 15 ($p < 0.05$ for all, except trains 4, 5, and 7 with $p < 0.01$).

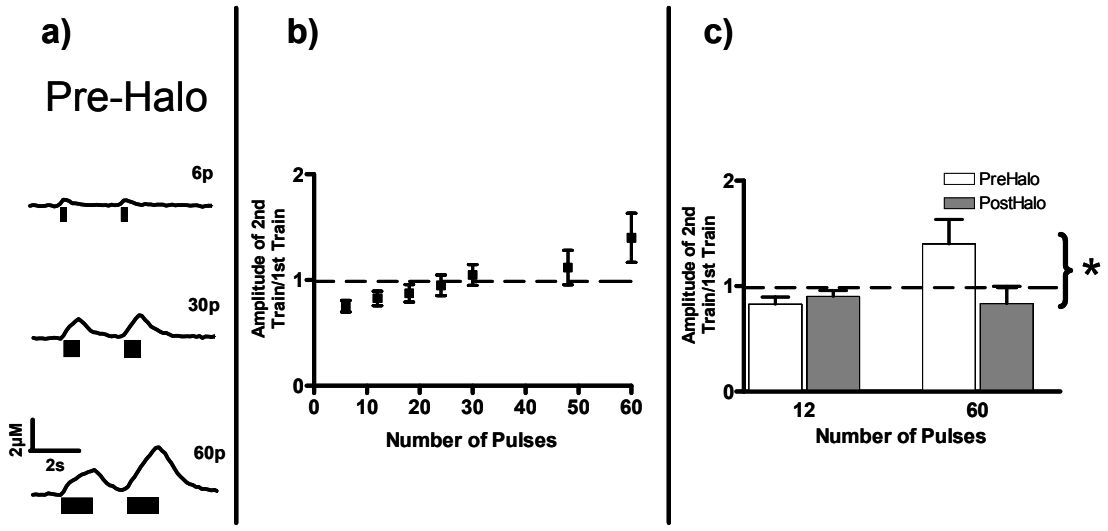

Figure 2.7. Effect of the number of stimulus pulses on dopamine release. Each train was at 50 Hz and 300 μA. **(a)** Representative traces of the paired train paradigm using 6p, 30p, and 60p before administration of haloperidol. **(b)** Panel showing the effect of 6p, 12p, 18p, 24p, 30p, 48p, and 60p on the paired-train paradigm. The amplitude of the second train was normalized to the amplitude of the first train. Depression occurred at low numbers of pulses, while facilitation occurred at higher numbers of pulses. This trend was continuous from 6p-60p ($F(6,72)=2.89$, $p<0.014$, two-way ANOVA). **(c)** Administration of haloperidol abolished facilitation at 60 pulses. Error bars represent SEM.

DISCUSSION

The experiments in this paper address mechanisms that govern dynamic fluctuations of dopamine release. They investigate whether the short-term depression identified by Montague et al. 2004 is in fact D2-mediated autoinhibition, while additionally revealing the paradoxical role of the D2 autoreceptor in facilitated dopamine release. Previous electrochemical measurements using the paired-pulse paradigm have shown that activation of D2 autoreceptors inhibits dopamine release on the second pulse (Limberger et al. 1991; Kennedy et al. 1992; Benoit-Marand et al. 2001; Phillips et al. 2002) and that this inhibition decays on a time scale of a few seconds. Our results with paired trains that directly evoke somatodendritic action potentials in dopamine neurons (Kuhr et al. 1987) produce the same results, and show that the time scale of the recovery during paired-trains (Fig. 2.1) is consistent with the short-term depression (τ = 3.2 s) described by Montague et al. (2004). We also demonstrate that release is depressed in the presence of a D2 agonist, quinpirole, for the first train. Repeated trains reveal more complex regulation. As previously shown (Yavich and MacDonald 2000), both facilitation and depression are apparent in the absence of drug (Fig. 2.2 and 2.3). Our work establishes that these processes are linked to the D2-receptor. First, an antagonist removes both short-term depression and facilitation of dopamine release (Fig. 2.4). Second, facilitation becomes more apparent with repeated trains in the presence of a D2 agonist, quinpirole (Fig. 2.5 and 2.6). Thus, the short-term dynamics of dopamine release, both facilitation and depression, are due to regulation by the D2-autoreceptor. As will be discussed below, the facilitation component may in fact be release from inhibition.

The D2-like population of dopamine receptors is comprised of the D_2-dopamine receptor that serves as the striatal dopamine autoreceptor (Benoit-Marand et al. 2001) and the D_3-dopamine receptor that plays only a minor role (Joseph et al. 2002).

Consistent with those prior findings, quinpirole, an agonist at both of these receptor types, inhibited maximal dopamine release evoked by the first train relative to its predrug value. Similarly, the increased dopamine release observed following raclopride or haloperidol, D2-receptor antagonists, is consistent with prior work (Gonon and Buda 1985; Stamford et al. 1988; Yavich 1996). D2 antagonists have also been shown to lower dopamine uptake rates (Wu et al. 2002), a factor clearly apparent in the prolonged responses of the dopamine signals after raclopride (Fig. 2.2, lower panel). The Montague model does not account for such changes in uptake. Therefore, we have not modeled the entire set of responses, but rather have used the predictions of the model to guide our experimental design and interpretation of the observed responses.

Although raclopride potentiated maximal dopamine release evoked by the first train, each subsequent train in a closely spaced series of stimulations exhibited less release (Fig. 2.4a), i.e., there was a predominant depression of release throughout the stimulation sequence. Similar results have been obtained in mouse striatum following repeated trains following haloperidol administration (Yavich 1996). This effect could be modeled by eliminating both the short-term depression (d_1) and facilitation (f) factors in the Montague model (Fig. 2.4b, right panel). Thus, the data are consistent with the concept that long-term depression of dopamine release is the sole adaptive factor when dopamine D2 receptors are blocked. This long-term depression is consistent with the slow time course of replenishing the readily releasable pool (Yavich 1996; Yavich and MacDonald 2000) from the recycling and reserve pools (Rizzoli and Betz 2005). With intense stimulations such as used here, sustained release requires mobilization of the reserve pool, which comprises the majority of vesicles (Richards et al. 2003). Alternatively, released dopamine may compete with raclopride at the D2 autoreceptor so that the dopamine released by each train may further reinstate a depression of release. While this could occur by simple binding competition (Ross 1989; Seeman et al. 1990), it

seems unlikely because the time scale of the depression responses are adequately described by the long-term depression described in the Montague model.

Although activation of the autoreceptor with quinpirole caused depression of the dopamine release evoked on the first train, dopamine release incremented for subsequent stimulations (Figs. 2.3 and 2.5). Similar behavior has also been observed for dopamine release under the control of nicotinic acetylcholine receptors. In that case, receptor activation leads initially to short-term depression, but the nicotinic receptor desensitizes resulting in an apparent facilitation (Rice and Cragg 2004). Similarly, in our case, the data following quinpirole could not be modeled by simply increasing the kick-back factor for short-term depression (d_1) but also required increasing it for the short-term facilitation (f) (Fig. 2.5b, right panel), suggesting a link between the two processes. Thus, while the data indicate that the short-term depression in the Montague model is mediated by the D2 autoreceptor, the short-term facilitation is consistent with desensitization of this pathway. When the full stimulation train was employed, it became apparent that at later trains (11-14), the likelihood of facilitation was much larger, presumably because of the prolonged activation and subsequent desensitization of the autoreceptor by dopamine (Figs. 2.2 and 2.3). The importance of the duration of activation of the autoreceptor was directly probed by increasing train duration; as the number of pulses in the paired-train paradigm was increased, the second train became increasingly larger than the first (Fig. 2.7a), again indicating desensitization via a dopamine dependent process. A major contributor to this effect was the depression of release on the first train. The greatest difference was found between the 6 pulse and 60 pulse trains: the maximal release was only 4.0 times greater with 60 pulses, far less than the 10 fold difference based upon the number of pulses. So, again, the apparent facilitation on the second train is actually due to depressed release on the first train. This facilitatory effect is D2-receptor mediated because it is abolished following

haloperidol (Fig. 2.7c). Careful inspection shows that all of the cases of apparent facilitation are actually a removal of depression (see, for example, Fig. 2.2a, trains 11-14, Fig. 2.3a and b, and Figs. 2.5-7).

Desensitization is a common feature of G-protein coupled receptors when they experience prolonged exposure to agonist (Leaney et al. 2004; Xu-Friedman and Regehr 2004). Our experiments provide twenty minutes between injection of the D2 agonist quinpirole and the measurements (Fig. 2.5). During this time, the D2 receptor could be primed for desensitization, for example by phosphorylation of the G-protein (Krasel et al. 2004). This prepares the protein for arrestin binding and subsequent desensitization upon agonist binding (Vilardaga et al. 2003; Sinclair et al. 2006), processes that occur on the 10-s time scale of our observations. An increased dose of quinpirole did not lead to a significantly greater inhibition on the first train. This ceiling effect is the asymptote of the intrinsic activity of quinpirole and has been demonstrated in brain slices where the maximum effect of quinpirole at D2 receptors is only a partial reduction of dopamine release (Joseph et al. 2002). At the same time, the apparent desensitization decreased (Fig. 2.6). The high dose of quinpirole may saturate the receptors, preventing subsequent release of dopamine from significantly affecting receptor dynamics. Indeed, throughout these studies, the competition between endogenous dopamine and exogenous drugs complicates quantitative interpretation of the data.

The presynaptic modulation of dopamine release, and its regulation by D2 receptors, will contribute to the complex modulation of the strength of cortico-striatal interactions. The plasticity in dopamine release seen here and in other in vivo work (Yavich and MacDonald 2000), as well as in brain slices (Cragg 2003; Rice and Cragg 2004), provides clear evidence that presynaptic plasticity does occur, a feature demonstrated in other preparations (Lu and Hawkins 2006). However, presynaptic

facilitation of neurotransmitter release is typically thought to involve intracellular calcium dynamics (Atluri and Regehr 1996; Zucker and Regehr 2002). Intracellular calcium influx after a conditioning stimulus does not immediately return to resting levels, and, upon subsequent stimulations, this "residual" calcium is summated with the subsequent influx to increase release probability. The D2 receptor can modulate intracellular calcium via its G-protein βγ subunits by activation of phospholipase C and by inhibition of calcium channels on the plasma membrane (Neve et al. 2004), providing another possible D2-controlled facilitation pathway.

Dopamine synapses are strategically located to modulate striatal neurons. Many are found on the neck of spines of medium spiny neurons, and the cortical inputs to these neurons, which use glutamate as their neurotransmitter, synapse on the head of the spines (Sesack et al. 1994). These cortico-striatal synapses can exhibit both LTD and LTP following tetanic stimulation (Charpier and Deniau 1997; Charpier et al. 1999; Nishioku et al. 1999). Furthermore, cortico-striatal LTP can be induced by bursts of dopamine release, either introduced by iontophoresis (Arbuthnott et al. 2000), pressure injection (Wickens et al. 1996) or released from endogenous stores using stimuli similar to those used in this work (Reynolds et al. 2001; Reynolds and Wickens 2002). Both D1 (Reynolds et al. 2001; Centonze et al. 2003) and D2 (Calabresi et al. 1997) receptors participate in the dopamine mediated synaptic plasticity. Our findings have direct pertinence to intracranial self-stimulation results, an experiment that evokes LTP (Reynolds et al. 2001), since our stimulation trains are the same as those used in intracranial self-stimulation experiments. The data demonstrate that D2 receptors provide a presynaptic component that not only can modulate autoinhibition, but also short-term facilitation of dopamine release, and therefore impacts both D1- and D2-mediated post-synaptic plasticity. Since phasic dopamine release occurs in response to cues predicting reward, the presynaptic plasticity observed here likely plays an important

role in the modulation of these types of responses as well (Schultz 1998; Carelli and Wightman 2004).

These findings have important implications for the downstream actions of D2-receptor ligands that are used clinically. For example, D2 receptor antagonists are used therapeutically for the management of schizophrenia (Seeman et al. 2006). These "typical" neuroleptics commonly have low affinity for dopamine D1-like receptors, and thus permit dopamine neurotransmission via this route. Our data predicts that this D1-mediated transmission will also be perturbed since there is gross loss of dynamic modulation, and therefore putative information content in the dopamine that is released to act upon these receptors. Thus, when reconciling the mechanisms involved in the unwanted side effects of neuroleptics, these important actions on presynaptic plasticity need to be considered.

REFERENCES

Arbuthnott G. W., Ingham C. A. and Wickens J. R. (2000) Dopamine and synaptic plasticity in the neostriatum. *J Anat* **196 (Pt 4),** 587-596.

Atluri P. P. and Regehr W. G. (1996) Determinants of the time course of facilitation at the granule cell to Purkinje cell synapse. *J Neurosci* **16,** 5661-5671.

Bath B. D., Michael B. J., Trafton B. J., Joseph J. D., Runnels P. L. and Wightman R. M. (2000) Subsecond adsorption and desorption of dopamine at carbon-fiber microelectrodes. *Anal Chem* **72,** 5994-6002.

Benoit-Marand M., Borrelli E. and Gonon F. (2001) Inhibition of dopamine release via presynaptic D2 receptors: time course and functional characteristics in vivo. *J Neurosci* **21,** 9134-9141.

Calabresi P., Saiardi A., Pisani A., Baik J. H., Centonze D., Mercuri N. B., Bernardi G. and Borrelli E. (1997) Abnormal synaptic plasticity in the striatum of mice lacking dopamine D2 receptors. *J Neurosci* **17,** 4536-4544.

Carelli R. M. and Wightman R. M. (2004) Functional microcircuitry in the accumbens underlying drug addiction: insights from real-time signaling during behavior. *Curr Opin Neurobiol* **14,** 763-768.

Centonze D., Grande C., Saulle E., Martin A. B., Gubellini P., Pavon N., Pisani A., Bernardi G., Moratalla R. and Calabresi P. (2003) Distinct roles of D1 and D5 dopamine receptors in motor activity and striatal synaptic plasticity. *J Neurosci* **23,** 8506-8512.

Charpier S. and Deniau J. M. (1997) In vivo activity-dependent plasticity at cortico-striatal connections: evidence for physiological long-term potentiation. *Proc Natl Acad Sci U S A* **94,** 7036-7040.

Charpier S., Mahon S. and Deniau J. M. (1999) In vivo induction of striatal long-term potentiation by low-frequency stimulation of the cerebral cortex. *Neuroscience* **91,** 1209-1222.

Chergui K., Suaud-Chagny M. F. and Gonon F. (1994) Nonlinear relationship between impulse flow, dopamine release and dopamine elimination in the rat brain *in vivo*. *Neuroscience* **62,** 641-645.

Cragg S. J. (2003) Variable dopamine release probability and short-term plasticity between functional domains of the primate striatum. *J Neurosci* **23,** 4378-4385.

Ewing A. G., Bigelow J. C. and Wightman R. M. (1983) Direct in vivo monitoring of dopamine released from two striatal compartments. *Science* **221,** 169-170.

Garris P. A., Kilpatrick M., Bunin M. A., Michael D., Walker Q. D. and Wightman R. M. (1999) Dissociation of dopamine release in the nucleus accumbens from intracranial self-stimulation. *Nature* **398,** 67-69.

Gonon F. G. and Buda M. J. (1985) Regulation of dopamine release by impulse flow and by autoreceptors as studied by in vivo voltammetry in the rat striatum. *Neurosci.* **14,** 765-774.

Joseph J. D., Wang Y. M., Miles P. R., Budygin E. A., Picetti R., Gainetdinov R. R., Caron M. G. and Wightman R. M. (2002) Dopamine autoreceptor regulation of release and uptake in mouse brain slices in the absence of D(3) receptors. *Neuroscience* **112,** 39-49.

Kennedy R. T., Jones S. R. and Wightman R. M. (1992) Dynamic observation of dopamine autoreceptor effects in rat striatal slices. *J Neurochem* **59,** 449-455.

Krasel C., Vilardaga J. P., Bunemann M. and Lohse M. J. (2004) Kinetics of G-protein-coupled receptor signalling and desensitization. *Biochem Soc Trans* **32,** 1029-1031.

Kuhr W. G., Wightman R. M. and Rebec G. V. (1987) Dopaminergic neurons: simultaneous measurements of dopamine release and single-unit activity during stimulation of the medial forebrain bundle. *Brain Res.* **419,** 122-128.

Leaney J. L., Benians A., Brown S., Nobles M., Kelly D. and Tinker A. (2004) Rapid desensitization of G protein-gated inwardly rectifying K(+) currents is determined by G protein cycle. *Am J Physiol Cell Physiol* **287,** C182-191.

Limberger N., Trout S. J., Kruk Z. L. and Starke K. (1991) "Real time" measurement of endogenous dopamine release during short trains of pulses in slices of rat neostriatum and nucleus accumbens: Role of autoinhibition. *Naunyn Schmiedebergs Arch.Pharmacol.* **344,** 623-629.

Lu F. M. and Hawkins R. D. (2006) Presynaptic and postsynaptic Ca(2+) and CamKII contribute to long-term potentiation at synapses between individual CA3 neurons. *Proc Natl Acad Sci U S A* **103,** 4264-4269.

Michael A. C., Ikeda M. and Justice J. B., Jr. (1987) Mechanisms contributing to the recovery of striatal releasable dopaine following MFB stimulation. *Brain Res.* **421,** 325-335.

Montague P. R., McClure S. M., Baldwin P. R., Phillips P. E., Budygin E. A., Stuber G. D., Kilpatrick M. R. and Wightman R. M. (2004) Dynamic gain control of dopamine delivery in freely moving animals. *J Neurosci* **24,** 1754-1759.

Neve K. A., Seamans J. K. and Trantham-Davidson H. (2004) Dopamine receptor signaling. *Journal of receptor and signal transduction research* **24,** 165-205.

Nishioku T., Shimazoe T., Yamamoto Y., Nakanishi H. and Watanabe S. (1999) Expression of long-term potentiation of the striatum in methamphetamine-sensitized rats. *Neurosci Lett* **268,** 81-84.

Pan W. X., Schmidt R., Wickens J. R. and Hyland B. I. (2005) Dopamine cells respond to predicted events during classical conditioning: evidence for eligibility traces in the reward-learning network. *J Neurosci* **25,** 6235-6242.

Phillips P. E., Hancock P. J. and Stamford J. A. (2002) Time window of autoreceptor-mediated inhibition of limbic and striatal dopamine release. *Synapse* **44,** 15-22.

Reynolds J. N. and Wickens J. R. (2002) Dopamine-dependent plasticity of corticostriatal synapses. *Neural Netw* **15,** 507-521.

Reynolds J. N., Hyland B. I. and Wickens J. R. (2001) A cellular mechanism of reward-related learning. *Nature* **413,** 67-70.

Rice M. E. and Cragg S. J. (2004) Nicotine amplifies reward-related dopamine signals in striatum. *Nat Neurosci* **7,** 583-584.

Richards D. A., Guatimosim C., Rizzoli S. O. and Betz W. J. (2003) Synaptic vesicle pools at the frog neuromuscular junction. *Neuron* **39,** 529-541.

Rizzoli S. O. and Betz W. J. (2005) Synaptic vesicle pools. *Nat Rev Neurosci* **6,** 57-69.

Ross S. B. J., David M. (1989) Kinetic properties of the accumulation of 3H-raclopride in the mouse brain in vivo. *Naunyn-Schmiedeberg's Archives of Pharmacology* **340,,** 6-12.

Schultz W. (1998) Predictive reward signal of dopamine neurons. *J Neurophysiol* **80,** 1-27.

Schultz W. and Dickinson A. (2000) Neuronal coding of prediction errors. *Annual review of neuroscience* **23,** 473-500.

Schultz W., Dayan P. and Montague P. R. (1997) A neural substrate of prediction and reward. *Science* **275,** 1593-1599.

Seeman P., Niznik H. B. and Guan H. C. (1990) Elevation of dopamine D2 receptors in schizophrenia is underestimated by radioactive raclopride. *Arch Gen Psychiatry* **47,** 1170-1172.

Seeman P., Schwarz J., Chen J. F., Szechtman H., Perreault M., McKnight G. S., Roder J. C., Quirion R., Boksa P., Srivastava L. K., Yanai K., Weinshenker D. and Sumiyoshi T. (2006) Psychosis pathways converge via D2high dopamine receptors. *Synapse* **60,** 319-346.

Sesack S. R., Aoki C. and Pickel V. M. (1994) Ultrastructural localization of D2 receptor-like immunoreactivity in midbrain dopamine neurons and their striatal targets. *J Neurosci* **14,** 88-106.

Sibley D. R. (1999) New insights into dopaminergic receptor function using antisense and genetically altered animals. *Annual review of pharmacology and toxicology* **39,** 313-341.

Sinclair J., Granfeldt D., Pihl J., Millingen M., Lincoln P., Farre C., Peterson L. and Orwar O. (2006) A biohybrid dynamic random access memory. *J Am Chem Soc* **128,** 5109-5113.

Stamford J. A., Kruk Z. L. and Millar J. (1988) Actions of dopamine antagonists on stimulated striatal and limbic dopamine release: an in vivo voltammetric study. *British Journal of Pharmacology* **94,** 924-932.

Stamford J. A., Kruk Z. L. and Millar J. (1991) Differential effects of dopamine agonists upon stimulated limbic and striatal dopamine release: in vivo voltammetric data. *British Journal of Pharmacology* **102,** 45-50.

Tobler P. N., Fiorillo C. D. and Schultz W. (2005) Adaptive coding of reward value by dopamine neurons. *Science* **307,** 1642-1645.

Venton B. J., Seipel A. T., Phillips P. E., Wetsel W. C., Gitler D., Greengard P., Augustine G. J. and Wightman R. M. (2006) Cocaine increases dopamine release by mobilization of a synapsin-dependent reserve pool. *J Neurosci* **26,** 3206-3209.

Vilardaga J. P., Bunemann M., Krasel C., Castro M. and Lohse M. J. (2003) Measurement of the millisecond activation switch of G protein-coupled receptors in living cells. *Nature biotechnology* **21,** 807-812.

Waelti P., Dickinson A. and Schultz W. (2001) Dopamine responses comply with basic assumptions of formal learning theory. *Nature* **412,** 43-48.

Wickens J. R., Begg A. J. and Arbuthnott G. W. (1996) Dopamine reverses the depression of rat corticostriatal synapses which normally follows high-frequency stimulation of cortex in vitro. *Neuroscience* **70,** 1-5.

Wiedemann D. J., Garris P. A., Near J. A. and Wightman R. M. (1992) Effect of Chronic Haloperidol Treatment on Stimulated Synaptic Overflow of Dopamine in the Rat Striatum. *Journal of Pharmacology and Experimental Therapeutics* **261,** 574-579.

Wightman R. M. and Robinson D. L. (2002) Transient changes in mesolimbic dopamine and their association with 'reward'. *Journal of Neurochemistry* **82,** 721-735.

Wightman R. M., Amatore C., Engstrom R. C., Hale P. D., Kristensen E. W., Kuhr W. G. and May L. J. (1988) Real-time characterization of dopamine overflow and uptake in the rat striatum. *Neuroscience* **25,** 513-523.

Wise R. A. (2004) Dopamine, learning and motivation. *Nat Rev Neurosci* **5,** 483-494.

Wu Q., Reith M. E. A., Walker Q. D., Kuhn C. M., Carroll F. I. and Garris P. A. (2002) Concurrent Autoreceptor-Mediated Control of Dopamine Release and Uptake during Neurotransmission: An In Vivo Voltammetric Study. *J. Neurosci.* **22,** 6272-6281.

Xu-Friedman M. A. and Regehr W. G. (2004) Structural contributions to short-term synaptic plasticity. *Physiological reviews* **84,** 69-85.

Yavich L. (1996) Two simultaneously working storage pools of dopamine in mouse caudate and nucleus accumbens. *Br.J.Pharmacol.* **119,** 869-876.

Yavich L. and MacDonald E. (2000) Dopamine release from pharmacologically distinct storage pools in rat striatum following stimulation at frequency of neuronal bursting. *Brain Research* **870,** 73-79.

Zucker R. S. and Regehr W. G. (2002) Short-term synaptic plasticity. *Annu Rev Physiol* **64,** 355-405.

CHAPTER 3 - Identification of an unknown signal using electrochemistry

INTRODUCTION

The mesolimbic pathway, which includes projections from the ventral tegmental area (VTA) to the nucleus accumbens (NAcc), has been implicated in reward circuitry (Pan et al. 2005) and many neurological disorders such as drug addiction (Di Chiara and Imperato 1988). This pathway uses dopamine as its primary neurotransmitter to communicate at neuronal terminals in the NAcc; however, recent research suggests that dopamine is also released at the dendrites of these same neurons (Beckstead et al. 2004; Beckstead et al. 2007). While neurons are chiefly designed to transmit action potentials from the cell bodies to the terminals, it has been demonstrated that midbrain dopaminergic neurons are also capable of backpropagating action potentials through the cell bodies (Gentet and Williams 2007). Measuring the release of dopamine at the cell bodies and dendrites is a difficult task as the dendrites are sparsely distributed and dopamine concentrations are significantly lower than that observed at the terminals. Thus measurement of evoked release requires a method that is both sensitive enough to record nanomolar concentrations and selective enough to effectively distinguish dopamine from other neurotransmitters such as norepinephrine and serotonin. The coupling of microelectrodes with fast-scan cyclic voltammetry (FSCV) provides sufficient resolution and sensitivity to allow measurement of these rapid fluctuations in concentration.

Though FSCV can initially provide excellent sensitivity and selectivity, it is often not sufficient to rely strictly on electrochemical measurements to identify neurochemical signals. Chemical identification of signals is a challenging process, and to aid in this process, a set of criteria was established several years ago to verify the identity of an unknown neurochemical signal (Wightman et al. 1987; Marsden et al. 1988; Phillips and Wightman 2003). First, and perhaps most important, is the verification of the signal using electrochemical measurements, as electrochemistry is the most direct form of

subsecond measurements. Comparison of an *in vivo* signal to an *in vitro* sample of known concentration provides a direct comparison between the unknown signal and a series of possible neurotransmitters. Additional verification of the signal using an independent chemical analysis can provide a secondary means of directly identifying the origin of an unknown signal; high performance liquid chromatography (HPLC) provides excellent selectivity, which can ultimately determine the presence and relative concentrations of potential neurotransmitters in the region of interest. Physiological characterization can be used to study the behavior of the signal in the presence of a changing physiological environment; this modulation can be performed via adjustment of the stimulation parameters to monitor the processes of release and uptake. The last criteria used for verification is pharmacological, as often the actual effects of the drugs cannot be fully understood until the signal has been appropriately characterized. Typical pharmacological manipulations include administration of an autoreceptor agonist or antagonist to either decrease or increase respectively the amplitude of measured signal (Benoit-Marand et al. 2001; Phillips et al. 2002). Additional drugs that are often used include uptake inhibitors, which can both increase the amplitude of release and delay the return to baseline.

Using *in vivo* FSCV coupled with microelectrodes, we measured an electrochemical signal in the VTA upon stimulation of the medial forebrain bundle (MFB). Verification that the evoked signal is due to dopamine release was performed using the above criteria (Wightman et al. 1987). Satisfaction of the electrochemical criterion was achieved via comparison of a cyclic voltammogram (CV) acquired from the VTA and CV's acquired both from the caudate-putamen (CP) and from *in vitro* flow cell calibrations. HPLC analyses were performed to certify the presence of dopamine in the VTA. The electrical stimulation parameters were varied to verify the vesicular nature of the released species. Pharmacological agents, including dopamine-specific

autoreceptor drugs, as well as selective uptake blockers for other neurotransmitters were administered to manipulate the evoked signal. The combined results from all four criteria conclusively prove that our signal is impulse-dependent somatodendritic dopamine release.

MATERIALS AND METHODS

Animals and surgery

Male Sprague-Dawley rats (225-350g; Charles River, Wilmington, MA) were anesthetized with urethane (1.5 g/kg, i.p.) and placed in a stereotaxic frame (Kopf, Tujunga, CA). A heating pad (Harvard Apparatus, Holliston, MA) maintained a constant body temperature of 37°C. Holes were drilled in the skull for the working, reference, and stimulation electrodes at coordinates selected from the atlas of Paxinos and Watson (Paxinos and Watson, 1986). The carbon-fiber microelectrode was placed in both the CP (AP +1.2, ML +2.0, and DV -4.5) as well as the VTA (AP -5.2, ML +1.0, and DV -8.0). The stimulating electrode was placed in the MFB (AP -1.8, ML +2.0, and DV -8.0). Both the carbon-fiber and stimulating electrodes were adjusted in the dorsal-ventral coordinate while stimulating to achieve maximal dopamine release. An Ag/AgCl reference was inserted in the contralateral region of the brain.

Electrical stimulation

An untwisted bipolar stimulating electrode (Plastics One, Roanoke, VA) was used to stimulate dopaminergic neurons. The stimulus was provided by an analog stimulus isolator (A-M Systems, Sequim, WA). The stimulation train consisted of biphasic pulses (± 300 μA, 2 ms/phase unless otherwise noted). The frequency and number of pulses per train were varied as noted in the text. The pulses were generated by a computer and applied between the cyclic voltammograms to avoid electrical interference.

Electrochemistry

Cylindrical carbon fiber microelectrodes were prepared using T650 carbon fibers (3 μm radius, Amoco) and encased in glass capillaries (A-M Systems, Sequim, WA) and pulled with a micropipette puller (Narashige, East Meadow, NY). The protruding fiber

was then cut to a length of 50-100 µm. On the day of use, the electrode was soaked for 10 minutes in isopropanol purified with activated carbon (Bath et al. 2000). To make contact with the carbon fiber, a backfill consisting of potassium acetate was injected into the glass capillary and a silver wire was inserted into the open end of the capillary and twisted to ensure solid contact with the carbon fiber. The reference electrode was chloridized by placing a silver wire in an HCl solution and applying 5V.

FSCV was used in all experiments (Bath et al. 2000). The instrumentation controlled the potential of the carbon-fiber electrode while the reference electrode was held at ground potential. The potential of the working electrode was held at -0.4 V vs Ag/AgCl between scans and was ramped to +1.3 V at 400 V/s and repeated at a frequency of 10 Hz. After the experiment the working electrode was calibrated *in vitro* using dopamine solutions of known concentration.

High performance liquid chromatography (HPLC)

Tissue samples were punched from brain slices (500 µm thickness) with a 2.5-mm diameter cork borer. The tissue was blotted dry with a Kimwipe, weighed dry, and homogenized with a sonic dismembrator (Fisher Sci., Model 60, Pittsburgh, PA, USA) in 200 µL of 0.1 N $HClO_4$ spiked with 1 µM hydroquinone (HQ). The homogenized tissue was centrifuged at 6000 rpm for 10 min, and the supernatant was removed and filtered using a 0.2-µm syringe microfilter (Millex-LG). Injections (10 µL) were made onto a reverse phase column (C-18, 5 µm, 4.8 x 250 mm, Waters symmetry 300). The mobile phase (prepared in HPLC grade water) contained 0.1 M citric acid, 1 mM hexyl sodium sulfate, 0.1 mm EDTA, and 10% methanol (pH 3.5) at a flow rate of 1 mL/min. Catecholamines were detected with a thin-layer radial electrochemical flowcell (BASi, West Lafayette, IN, USA) at a potential of 700 mV versus a Ag/AgCl reference electrode.

Catecholamine standards were prepared from 10 mM stock solutions in 0.1 N perchloric acid.

Data analysis

Data were analyzed in Graph Pad Prism (Graph Pad Software, San Diego, CA) and are expressed as mean ± SEM. Statistical significance was determined using a two-way ANOVA, and posthoc comparisons were performed using the method of least squares with a Bonferroni correction.

Chemicals and solutions

All chemicals and drugs were purchased from Sigma/Aldrich (St. Louis, MO) and used as received. Solutions were prepared using doubly distilled deionized water (Megapure system, Corning, NY). The TRIS buffer solution for flow cell analysis was prepared using 12 mM TRIS, 140 mM NaCl, 3.2 mM KCl, 1.2 mM $CaCl_2$, 1.25mM NaH_2PO_4, 1.2 mM $MgCl_2$, 2.0 mM Na_2SO_4 at pH 7.4. Drugs were dissolved in saline and injected intraperitoneally.

RESULTS

Electrochemical verification

As mentioned previously, verification of an unknown neurochemical signal requires satisfying a series of predetermined criteria. Figure 3.1 shows the electrochemical response of a carbon-fiber microelectrode upon exposure to a series of analytes collected *in vitro*. For each panel, 5 seconds of background current was collected before a 5 second bolus of electroactive species was injected. The resulting current was background-subtracted to give a cyclic voltammogram (CV) for each injected species. Each analyte had a signature CV; however, some of the CV's were remarkably similar; Fig. 3.1a-c possess visually identical CV's, while Fig. 3.1d-h all possess distinctive CV's. The molecule dopamine has a characteristic oxidation peak at approximately +600 mV and a reductive peak at approximately -200 mV; however, the molecules epinephrine and norepinephrine also have cathodic and anodic peaks at identical potentials.

The unknown *in vivo* neurochemical signal was obtained by placement of the stimulating electrode in the MFB, and by placement of the working electrode in the VTA. Electrical stimulation was administered to the MFB with a series of 60 biphasic, 300 μA electrical pulses delivered at 60 Hz. This electrical stimulation is designed to generate a series of action potentials that will lead to the vesicular release of neurotransmitter. Electrical stimulation of the MFB led to an increase in current, correlating to an increase in neurotransmitter concentration. The background-subtracted CV for the released substance has an oxidation potential at approximately +600 mV, and a reduction potential at approximately -200 mV (Fig. 3.2a). A background-subtracted CV for a 60 Hz, 40 pulse, 300 μA stimulation recorded in the dopamine-rich CP has an identical shape (Fig. 3.2b), suggesting the identity of the signal is either dopamine, epinephrine or norepinephrine.

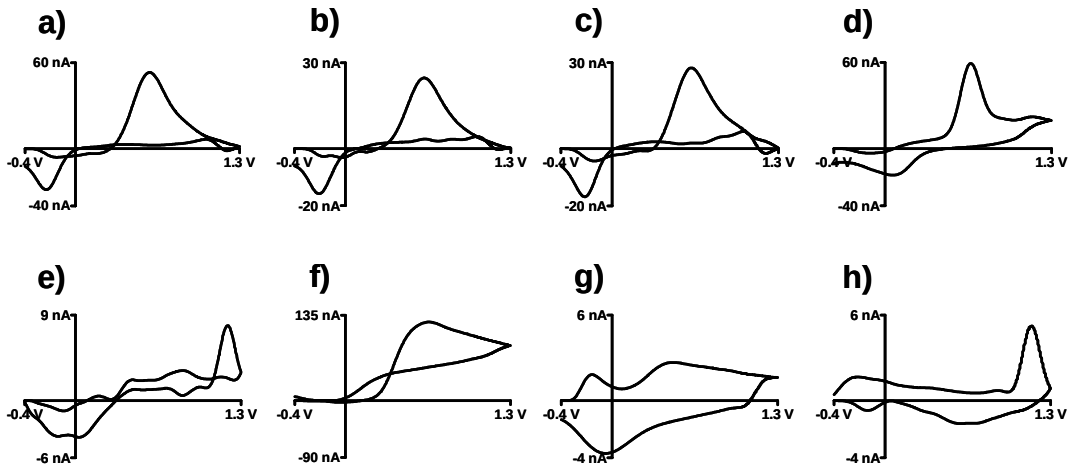

Figure 3.1. Background-subtracted CV's of electroactive neurochemicals. Voltammograms obtained for **(a)** 10 μM dopamine, **(b)** 10 μM norepinephrine, **(c)** 10 μM epinephrine, **(d)** 10 μM serotonin, **(e)** 10 μM histamine, **(f)** 100 μM ascorbate, **(g)** Δ pH +0.2, **(h)** Δ pH -0.2.

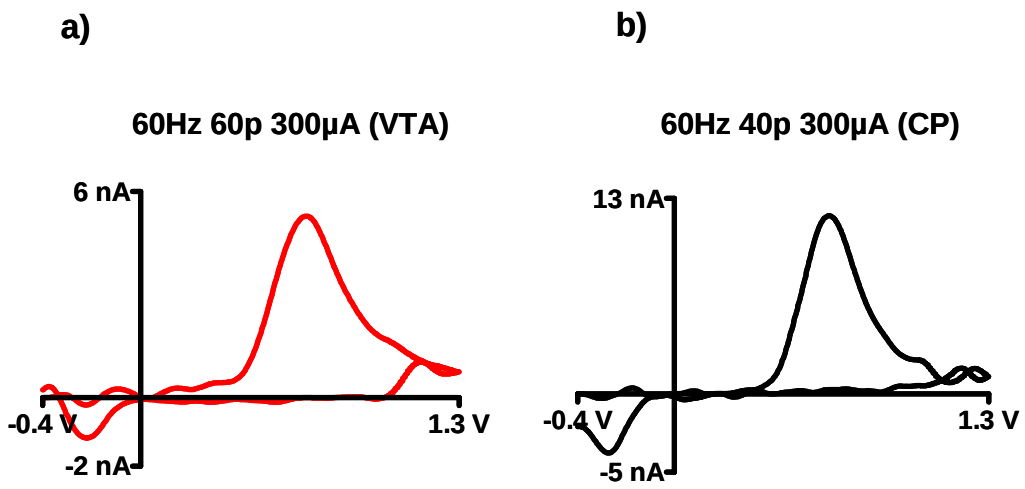

Figure 3.2. Comparison between CV's obtained in the VTA and CP. **(a)** Voltammogram obtained in the VTA upon electrical stimulation of the MFB (60 Hz, 60 p, 300 µA stimulation), **(b)** Voltammogram obtained in the CP upon electrical stimulation of the MFB (60 Hz, 40 p, 300 µA stimulation).

Physiological verification

To probe the physiology of our signal, the frequency of electrical stimulation was varied. Varying the frequency of electrical stimulation allows for a study of the release and uptake parameters of neurotransmitter release. The uptake of a released neurotransmitter that is transported into the neuron via an uptake transporter protein can be described by a modified form of the Michaelis-Menten equation (Wightman et al. 1988) (1):

$$\frac{d[NT]}{dt} = f \times [NT]_p - V_{max}(1 + K_m/[NT])^{-1} \qquad (1)$$

where the change in neurotransmitter concentration, [NT], as a function of time can be described by the release of neurotransmitter minus the amount cleared via uptake. F is the frequency of electrical stimulation, while $[NT]_p$ is the amount of neurotransmitter released per electrical pulse. V_{max} and K_m are the kinetic parameters associated with uptake, while [NT] is the absolute concentration of the neurotransmitter present at a given period in time. By increasing the frequency of electrical stimulation, the release of neurotransmitter overpowers the uptake component of transmission (Fig. 3.3). The concentration of dopamine released after a given stimulation was determined post-experiment using a calibration curve from data obtained in a flow cell, such that the dopamine concentration could be related to stimulation events. A plot of calculated dopamine concentration per stimulation frequency (Fig. 3.3) revealed a linear relationship between dopamine concentration and frequency of stimulation. The shape of release at 10 Hz (Fig. 3.3a) approaches a steady state where the release and uptake components are balanced. The release profile at 50 Hz is much sharper, demonstrating a much stronger component of release (Fig. 3.3c). These data are consistent with vesicular release seen at the terminal of dopaminergic neurons.

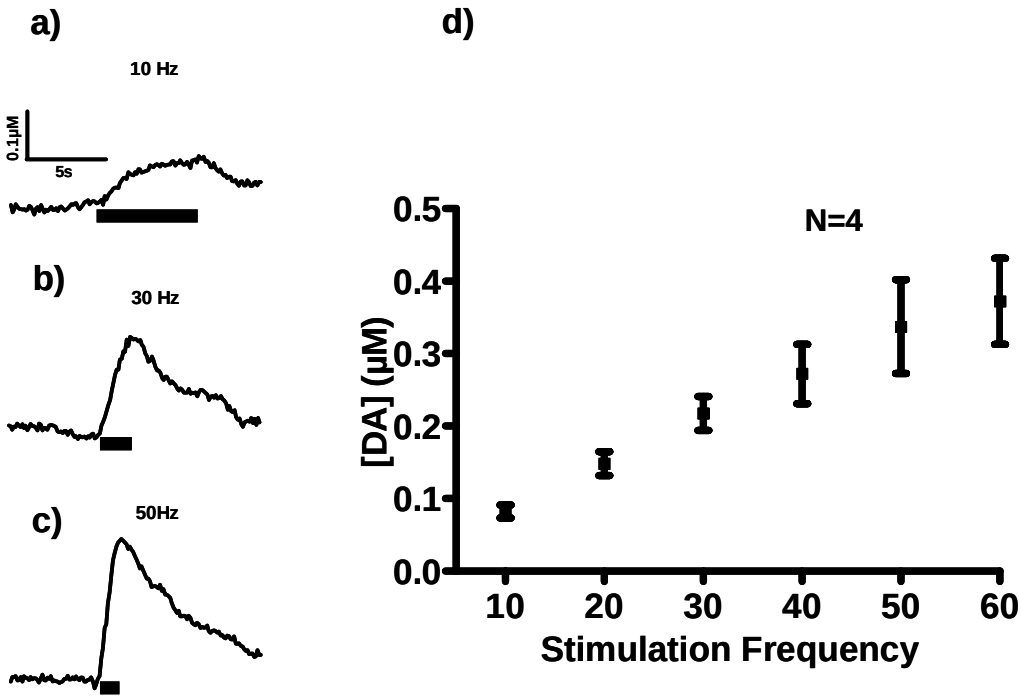

Figure 3.3. Effect of stimulation frequency on signal amplitude in the VTA. Representative traces obtained for a 60 p, 300 μA stimulation at **(a)** 10 Hz, **(b)** 30 Hz, **(c)** 50 Hz. **(d)** The effect of stimulation frequency can be seen with [DA] (μM) plotted as a function of the stimulation frequency (Hz). There is a linear increase as stimulation frequency increases.

To estimate the amount of release possible, an intense electrical stimulation was used to temporarily deplete the neurotransmitter stores. The MFB was electrically stimulated at 50 Hz for 50 s. The amplitude of release continued to rise until approximately 5 seconds after the stimulation begins. After this point the release slowly begins to return to baseline, demonstrating a depletion of the available neurotransmitter release (Fig. 3.4). A 60 Hz 60 pulse stimulation train immediately following the completion of the depletion stimulation led to a marked decrease in amplitude when compared to pre-depletion stimulation (data not shown).

Independent chemical analysis

Upon euthanization of the rat, the brain was removed and placed in PBS buffer. The brain was sectioned into 200μm slices using a vibratome, and the VTA was excised using a razor blade. The resulting VTA fragment was placed into perchloric acid and sonicated to degrade the tissue. The supernatant was then injected into an HPLC column to measure the resulting concentrations of neurotransmitters present. Under the conditions run, dopamine and serotonin were the primary neurotransmitters detected (Fig. 3.5). The HQ standard was used to quantify the amount of each neurotransmitter present. The dopamine peak eluted at 12.5 minutes, while the serotonin peak eluted at 18 minutes (Fig. 3.5). The concentration of dopamine in the VTA was 1.26 ± 0.08 μg/g, and the concentration of serotonin in the VTA was 0.86 ± 0.08 μg/g. Norepinephrine and epinephrine elute at 4.5 and 5.5 minutes respectively, and were not present in the trace.

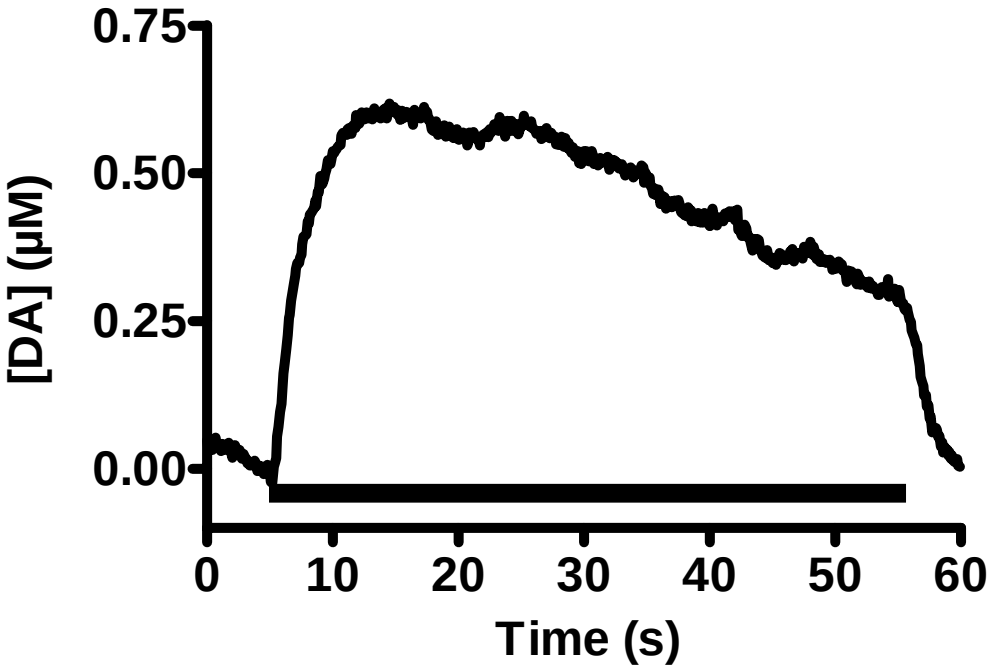

Figure 3.4. Effect of prolonged stimulation on electrically evoked dopamine release. Dopamine release was evoked by a 50 Hz, 500 p, 300 µA electrical stimulation. Dopamine release reached a steady state within 5 seconds and slowly returned to baseline over the course of 50 seconds.

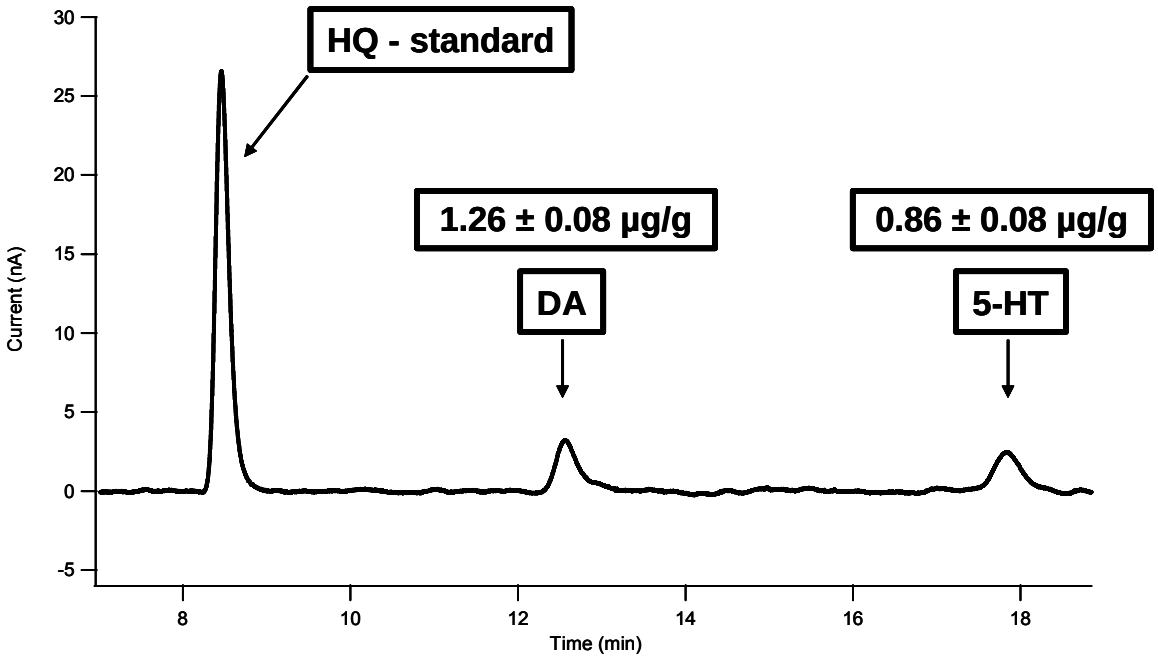

Figure 3.5. Neurotransmitter content obtained from the VTA. The content of both dopamine and serotonin was obtained by extracting brain tissue from the VTA and analyzing the resulting mixture using HPLC. The trace reveals 1.5 times more dopamine than serotonin. Concentrations were determined by comparing peak area to the HQ standard. The average concentration of dopamine measured in the VTA was 1.26 ± 0.08 µg/g, and the concentration of serotonin measured in the VTA was 0.86 ± 0.08µg/g. Norepinephrine and epinephrine, though not present in the VTA, would elute at 4.5 min and 5.5 min respectively.

Pharmacological verification

Further verification of the signal was provided via pharmacological manipulation of the measured signal. Concentrations of evoked dopamine release at the terminals in the CP can be modulated using dopamine specific drugs whose mechanism of action occurs at the autoreceptors. The D2 autoreceptor agonist, quinpirole, and the D2 autoreceptor antagonist, raclopride, should decrease and increase, respectively, the maximum amplitude of evoked dopamine in the CP via interactions with autoreceptors present on the dopamine terminals (Fig. 3.6). A 60 pulse, 60 Hz, 300 μA stimulation was applied every three minutes until the amplitude of release remained consistent for three consecutive files. Administration of a 1 mg/kg intraperitoneal injection of either the agonist, quinpirole, or the antagonist, raclopride, was given upon stabilization of the signal. The amplitude of release was then measured 20 minutes after administration of the drug. While there was a significant decrease of dopamine release ($N=6$, $p<0.01$) in the striatum upon administration of quinpirole (Fig. 3.6a, right panel), there was no significant decrease in signal in the VTA (Fig. 3.6a, left panel). Similarly, there was a significant increase in dopamine release ($N=6$, $p<0.001$) in the striatum upon administration of raclopride (Fig. 3.6b, right panel), while there was no significant decrease in signal in the VTA (Fig. 3.6b, left panel). These data suggest that the evoked neurotransmitter was not under autoregulation by the dopamine D2 autoreceptor.

Another method of modulating the concentration of evoked neurotransmitter is via administration of an uptake blocker. A non-selective uptake blocker, such as cocaine, prevents many neurons from uptaking the released neurotransmitter back to the cell, including dopamine, norepinephrine, epinephrine, and serotonin neurons (Iversen 2006). The result of this blockade would appear as a slower return to baseline after stimulation. Administration of 30 mg/kg cocaine (i.p. injection) significantly

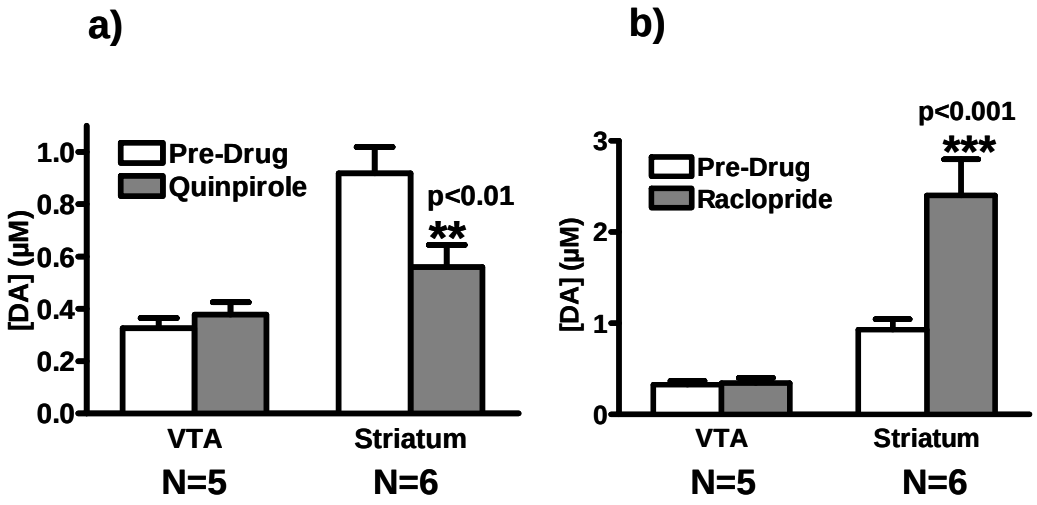

.

Figure 3.6. Effect of D2 autoreceptor drugs on release from the VTA and striatum. **(a)** Dopamine release was evoked using a 60 Hz, 60 p, 300 μA electrical stimulation both before and after administration of the D2 agonist quinpirole (1 mg/kg i.p. injection). There was no significant change in the VTA. There was a significant decrease in signal in the striatum ($p<0.01$). **(b)** Dopamine release was evoked using a 60 Hz, 60 p, 300 μA electrical stimulation both before and after administration of the D2 antagonist raclopride (1 mg/kg i.p. injection). There was no significant change in the VTA. There was a significant increase in signal in the striatum ($p<0.001$).

increased the amount of neurotransmitter evoked by a 60 p, 60 Hz, 300 μA stimulation, as well as inhibited the uptake of a representative trace (Fig. 3.9a). Twenty minutes after administration of cocaine, the maximal release was recorded and found to have increased significantly by a factor of approximately three (N=6, $p<0.007$) (Fig. 3.7b). The relative evoked concentration of neurotransmitter before administration of cocaine was 150 nM, which is significantly less than the 1 μM commonly seen in the CP.

A more selective uptake blocker, nomifensine (Lengyel et al. 2008), was used to bind selectively to the norepinephrine, epinephrine, and dopamine transporters, as well as any other tyrosine-derived neurotransmitters. Administration of a 20 mg/kg injection of nomifensine significantly increased the amount of neurotransmitter evoked by a 60 p 60 Hz 300 μA stimulation, as well as inhibited the uptake (Fig. 3.8a). Neurotransmitter release increased and was approximately 250% of saline controls (n=4, $p<0.0018$) (Fig. 3.8b). Files were collected every four minutes over the course of 2 hours to measure the duration of the increase in release caused by administration of nomifensine. The increase in release caused by nomifensine persisted at its maximal effect for approximately 40 minutes (Fig. 3.8a); the effects of the drug eventually wore off approximately 2 hours after administration (data not shown).

Now that it has been determined that the release of neurotransmitter is under transporter control, administration of selective uptake blockers should more directly determine the identity of the measured signal. Blockade of the serotonin transporter was performed using citalopram, a selective 5-HT transport inhibitor. A 20 mg/kg injection of citalopram did not significantly increase the concentration of evoked neurotransmitter (Fig. 3.9), while a 20 mg/kg injection of nomifensine 30 minutes later in the same animal was sufficient to increase release (Fig. 3.9). Additionally, a 20 mg/kg injection of desipramine, a selective norepinephrine transport inhibitor, produced no significant

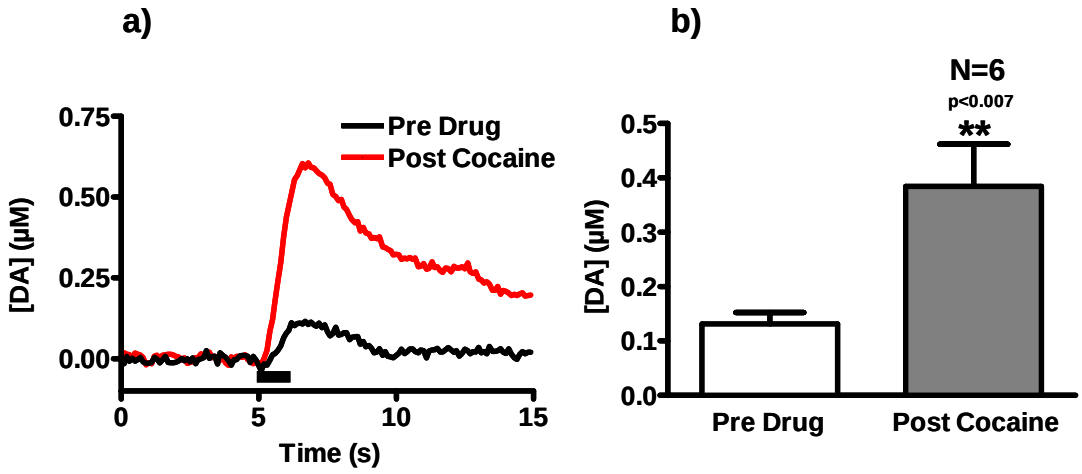

Figure 3.7. Effect of the non-selective monoamine uptake inhibitor cocaine. **(a)** Dopamine release was evoked by a 60 Hz, 60 p, 300 μA electrical stimulation (as noted by the black bar) in the MFB and recorded in the VTA. Representative traces are obtained both before and after administration of the non-selective monoamine uptake inhibitor cocaine (30 mg/kg i.p.). **(b)** An average of the effect of cocaine on amplitude of evoked release. Before cocaine administration, signal was approximately 150 nM (N=6). After cocaine administration, signal is significantly increased (N=6, $p<0.007$).

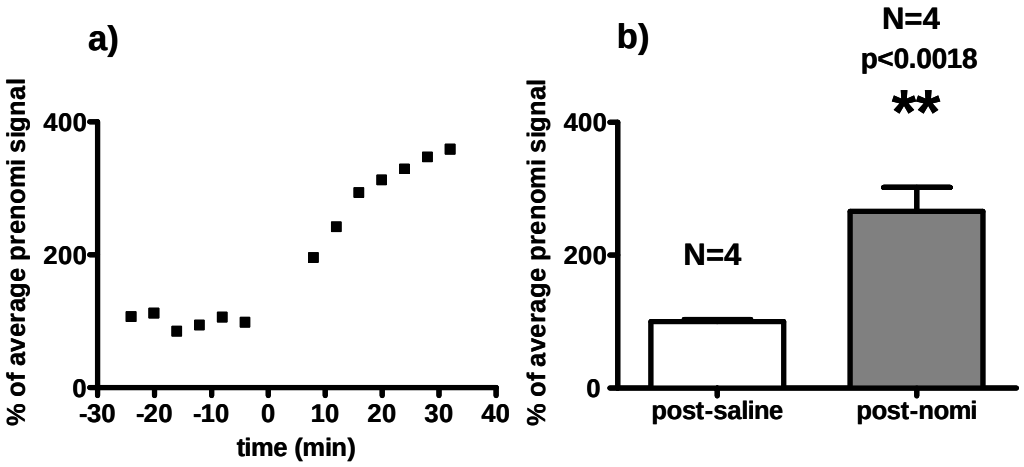

Figure 3.8. Effect of the catecholamine uptake inhibitor nomifensine. Dopamine release was evoked via a 60 Hz, 60 p, 300 μA electrical stimulation of the MFB. Signals were recorded in the VTA. **(a)** Representative trace of normalized dopamine signal. Data was collected for 30 minutes prior to nomifensine injection given at time 0 (20 mg/kg i.p.). Signals were normalized to pre-drug value and recorded every 4 minutes. Signal reached 400% of pre-drug values and persisted for one hour. **(b)** Average values for injections of saline and nomifensine. Saline injection had no effect. Nomifensine injection significantly increased signal (N=4, $p<0.0018$).

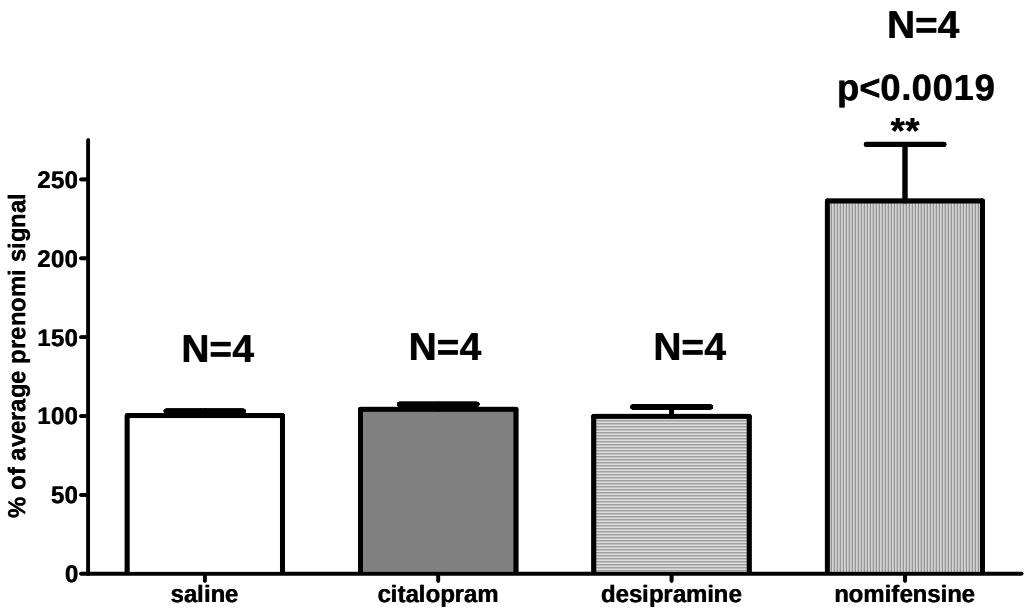

Figure 3.9. Effect of citalopram and desipramine on evoked signal. Release was evoked via a 60 Hz, 60 p, 300 μA electrical stimulation in MFB. Signals were recorded in the VTA before and after administration of saline, citalopram (20 mg/kg i.p.), desipramine (20 mg/kg i.p.) and nomifensine (20 mg/kg i.p.). Saline injection had no significant effect. The selective serotonin reuptake inhibitor had no significant effect. The selective norepinephrine reuptake inhibitor had no effect. Nomifensine administered 30 minutes after either citalopram or desipramine in the same rat significantly increased the signal (N=4, $p<0.0019$).

change (Fig. 3.9). Application of a 20 mg/kg injection of nomifensine 30 minutes after administration of desipramine in the same animal increased the maximal release by approximately 225% ($p<0.0019$). These secondary applications of nomifensine proved that the signals being recorded were responsive to uptake inhibition.

Summary

Summary of the results is noted in Table 1. For the electrochemical criterion, only dopamine, epinephrine, and norepinephrine possess the correct electrochemistry for the unknown signal. Serotonin has the appropriate oxidation potential; however, with the waveform used, the measured signal would be a non-physiological concentration. The physiological criterion proves that the signal mimics vesicular release at the terminals and has a finite pool of available molecules. This suggested that the signal was one of the neurotransmitters (Fig. 3.1a-e). The HPLC data confirmed the presence of both dopamine and serotonin in the VTA, and ruled out the possibility of norepinephrine and epinephrine. Data obtained upon pharmacological manipulation conclusively proved that the signal was not serotonin or norepinephrine, and the increase in release upon administration of nomifensine supported dopamine as the evoked signal.

	Electrochemical	Physiological	HPLC	Pharmacological
Dopamine	X	X	X	X
Serotonin		X	X	
Norepinephrine/ Epinephrine	X	X		
Histamine		X		
pH				

Table 3.1. Summary of experimental data. Of the four criteria used dopamine satisfied all 4. Serotonin, norepinephrine, and epinephrine each satisfied two criteria. Histamine satisfied one criterion, and changes in pH did not meet any of the criteria.

DISCUSSION

The experiments in this paper address the criteria needed to identify an unknown neurochemical signal. The unknown signal investigated was recorded in the VTA, and was evoked by electrical stimulation of the MFB. The hypothesis is that the unknown signal being measured is somatodendritic dopamine, which has not previously been measured on a subsecond time scale in an intact animal. Previous experiments have provided evidence for the existence of somatodendritic dopamine release (Rice et al. 1997; Hoffman and Gerhardt 1999; Falkenburger et al. 2001; Adell and Artigas 2004; Beckstead et al. 2007; John and Jones 2007); however, there remains some debate as to the manner in which dopamine is released and what function it might provide.

Before any insight can be offered into neurotransmitter function, it is imperative to ascertain the identity of the measured signal. Upon comparison of the *in vivo* signal (Fig. 3.2a) to the CV's obtained *in vitro* (Fig. 3.1), it became clear that the unknown signal most closely resembled dopamine, norepinephrine, epinephrine, or potentially serotonin. The pronounced peak at +600 mV unmistakably ruled out ascorbate, histamine, and pH as possible molecules being measured. Further comparison of the *in vivo* signal to the signal of dopamine obtained in the CP (Fig. 3.2b), suggests that the unknown signal was dopamine, norepinephrine, or epinephrine.

An independent chemical analysis using HPLC confirms the presence of both dopamine and serotonin in the VTA (Fig. 3.5). It is widely known that the VTA is heavily populated with dopaminergic cell bodies; additionally, serotonin receptors have been located in the VTA (Liu et al. 2006). Previous techniques such as microdialysis (Yan et al. 2005) and fluorescent histochemistry (Bjorklund and Lindvall 1975) have additionally confirmed the presence of releasable dopamine in the VTA.

The pharmacological studies performed provided information on the locations and function of various receptors and transport proteins in the VTA. A typical means of

modulating a known signal is to apply a selective drug designed to either increase or decrease its release. For the molecule dopamine, release can be modulated either by activation or blockade of the D2 autoreceptor. The D2 autoreceptor is responsible for autoregulating the release of the neurotransmitter for which it is selective. Administration of the D2 autoreceptor agonist, quinpirole, decreased release by approximately 50% in the CP (Fig. 3.6a), which is consistent with previous work (Benoit-Marand et al. 2001), while administration of the D2 autoreceptor antagonist, raclopride, effectively increased release by approximately 250% (Fig. 3.6b), consistent with previous work (Gonon and Buda 1985; Stamford et al. 1988; Yavich 1996). In the VTA, however, there appeared to be no significant effect on the amplitude of release upon administration of either quinpirole or raclopride (Fig. 3.6). Additionally, there was no secondary effect on uptake as a result of D2 autoreceptor drugs (Wu et al. 2002), further suggesting that there are no functional D2 autoreceptors present in the VTA. Other research groups have observed similar autoreceptor independence in the VTA, but substantial autoreceptor effects in the substantia nigra (Cragg and Greenfield 1997). While somatodendritic release of dopamine does not appear to self-regulate, one possible role for its release could be to regulate cell firing of the mesolimbic system; thus providing a secondary control of the concentration of evoked dopamine present in the NAcc. Typical regulation of dopamine concentration occurs at the terminals (Schmitz et al. 2003); however, somatodendritic dopamine release in the VTA has been shown to modulate the firing of the cell bodies under periods of intense stimulation, such as during burst firing (Kalivas 1993; Pucak and Grace 1994).

Other than selective autoreceptor drugs, a secondary means of modulating a neurochemical signal is via blockade of the specific transport molecule involved in uptake of the molecule into the neuron. Each neurotransmitter has its own selective transport system: dopamine = DAT (Kuhar et al. 1990), norepinephrine = NET (Kitayama

and Dohi 1996), and serotonin = SERT (Murphy and Lesch 2008). Initially, demonstration of an active uptake system was evaluated using the non-selective monoamine transport blocker cocaine (Fig. 3.7). The non-selective nature of cocaine ensures that many major neurotransmitter transporters will be inhibited upon cocaine binding. Administration of a 30 mg/kg intraperitoneal injection of cocaine was sufficient to elevate release as well as inhibit uptake of the unknown signal. Cocaine alone is not sufficient to discover the identity of the unknown signal. Further evaluation to determine the specific uptake transporter involved required using more selective transporter blockers. The catecholamine uptake inhibitor, nomifensine, also succeeded in increasing release and decreasing uptake (Fig. 3.8). More selective uptake inhibitors such as citalopram, a common selective serotonin reuptake inhibitor (SSRI), and desipramine, a selective norepinephrine reuptake inhibitor, had no effect on stimulated release (Fig. 3.9); however, reapplication of nomifensine was sufficient to elevate release in the same animal. By process of elimination, any signal that is elevated by both cocaine and nomifensine must be a catecholamine, and furthermore, as the selective uptake inhibitors citalopram and desipramine had no effect; the measured signal must be primarily dopamine.

Some controversy has arisen pertaining to the mechanism of somatodendritic release of dopamine. It was initially thought that the release of dopamine was through the reverse transport of dopamine through the dopamine transporter, which typically allows dopamine to re-enter the cell; however, recent research has demonstrated that the somatodendritic release of dopamine is dependent on Ca^{2+} concentration (Chen and Rice 2001), as well as tetrodotoxin (Santiago et al. 1992), a potent blocker of the Na^{+} channels necessary for the exocytotic, vesicular release of neurotransmitter. Our results clearly demonstrated that blockade of the uptake transporter, both through cocaine and nomifensine administration, facilitated release rather than preventing it (Fig. 3.7-9).

Blockade of the transporter would prevent the neuron from releasing neurotransmitter were it to be governed via a reverse transport mechanism. Additionally, change in response shape to varying frequencies of electrical stimulation suggests that the molecule being released is under conditions similar to what is experienced at the terminals of dopaminergic neurons, i.e. exocytotic release and uptake via the dopamine transporter.

As reported in Table 1, the only molecule which fully satisfied the criteria which were previously established (Wightman et al. 1987; Marsden et al. 1988; Phillips and Wightman 2003) is dopamine. Its electrochemical response is identical to that obtained in the CP, a dopamine-rich region, and an *in vitro* injection of 1 μM dopamine obtained in a flow cell. HPLC data (Fig. 3.5), as well as additional experiments performed in other labs (Bjorklund and Lindvall 1975; Yan et al. 2005) sufficiently supported the claim that dopamine is present in concentrations sufficient to be measured via FSCV. The pharmacology also supported the identity of dopamine; as selective uptake inhibitors citalopram and desipramine did not cause an increase in release, while an injection of nomifensine sufficiently increased the signal 2-fold. All of these criteria together combine to decisively identify the unknown electrochemical signal as dopamine.

REFERENCES

Adell A. and Artigas F. (2004) The somatodendritic release of dopamine in the ventral tegmental area and its regulation by afferent transmitter systems. *Neurosci Biobehav Rev* **28,** 415-431.

Bath B. D., Michael B. J., Trafton B. J., Joseph J. D., Runnels P. L. and Wightman R. M. (2000) Subsecond adsorption and desorption of dopamine at carbon-fiber microelectrodes. *Analytical chemistry* **72,** 5994-6002.

Beckstead M. J., Grandy D. K., Wickman K. and Williams J. T. (2004) Vesicular dopamine release elicits an inhibitory postsynaptic current in midbrain dopamine neurons. *Neuron* **42,** 939-946.

Beckstead M. J., Ford C. P., Phillips P. E. and Williams J. T. (2007) Presynaptic regulation of dendrodendritic dopamine transmission. *The European journal of neuroscience* **26,** 1479-1488.

Benoit-Marand M., Borrelli E. and Gonon F. (2001) Inhibition of Dopamine Release Via Presynaptic D2 Receptors: Time Course and Functional Characteristics In Vivo. *J. Neurosci.* **21,** 9134-9141.

Bjorklund A. and Lindvall O. (1975) Dopamine in dendrites of substantia nigra neurons: suggestions for a role in dendritic terminals. *Brain research* **83,** 531-537.

Chen B. T. and Rice M. E. (2001) Novel Ca2+ dependence and time course of somatodendritic dopamine release: substantia nigra versus striatum. *J Neurosci* **21,** 7841-7847.

Cragg S. J. and Greenfield S. A. (1997) Differential autoreceptor control of somatodendritic and axon terminal dopamine release in substantia nigra, ventral tegmental area, and striatum. *J Neurosci* **17,** 5738-5746.

Di Chiara G. and Imperato A. (1988) Drugs abused by humans preferentially increase synaptic dopamine concentrations in the mesolimbic system of freely moving rats. *Proc Natl Acad Sci U S A* **85,** 5274-5278.

Falkenburger B. H., Barstow K. L. and Mintz I. M. (2001) Dendrodendritic Inhibition Through Reversal of Dopamine Transport. *Science* **293,** 2465-2470.

Gentet L. J. and Williams S. R. (2007) Dopamine Gates Action Potential Backpropagation in Midbrain Dopaminergic Neurons, pp 1892-1901.

Gonon F. G. and Buda M. J. (1985) Regulation of dopamine release by impulse flow and by autoreceptors as studied by in vivo voltammetry in the rat striatum. *Neurosci.* **14,** 765-774.

Hoffman A. F. and Gerhardt G. A. (1999) Differences in pharmacological properties of dopamine release between the substantia nigra and striatum: an in vivo electrochemical study. *The Journal of pharmacology and experimental therapeutics* **289,** 455-463.

Iversen L. (2006) Neurotransmitter transporters and their impact on the development of psychopharmacology. *British journal of pharmacology* **147 Suppl 1,** S82-88.

John C. E. and Jones S. R. (2007) Voltammetric characterization of the effect of monoamine uptake inhibitors and releasers on dopamine and serotonin uptake in mouse caudate-putamen and substantia nigra slices. *Neuropharmacology* **52,** 1596-1605.

Kalivas P. W. (1993) Neurotransmitter regulation of dopamine neurons in the ventral tegmental area. *Brain Res Brain Res Rev* **18,** 75-113.

Kitayama S. and Dohi T. (1996) Cellular and molecular aspects of monoamine neurotransmitter transporters. *Japanese journal of pharmacology* **72,** 195-208.

Kuhar M. J., Sanchez-Roa P. M., Wong D. F., Dannals R. F., Grigoriadis D. E., Lew R. and Milberger M. (1990) Dopamine transporter: biochemistry, pharmacology and imaging. *European neurology* **30 Suppl 1,** 15-20.

Lengyel K., Pieschl R., Strong T., Molski T., Mattson G., Lodge N. J. and Li Y. W. (2008) Ex vivo assessment of binding site occupancy of monoamine reuptake inhibitors: Methodology and biological significance. *Neuropharmacology*.

Liu W., Thielen R. J., Rodd Z. A. and McBride W. J. (2006) Activation of serotonin-3 receptors increases dopamine release within the ventral tegmental area of Wistar and alcohol-preferring (P) rats. *Alcohol (Fayetteville, N.Y* **40,** 167-176.

Marsden C. A., Joseph M. H., Kruk Z. L., Maidment N. T., O'Neill R. D., Schenk J. O. and Stamford J. A. (1988) In vivo voltammetry--present electrodes and methods. *Neuroscience* **25,** 389-400.

Murphy D. L. and Lesch K. P. (2008) Targeting the murine serotonin transporter: insights into human neurobiology. *Nature reviews* **9,** 85-96.

Pan W. X., Schmidt R., Wickens J. R. and Hyland B. I. (2005) Dopamine cells respond to predicted events during classical conditioning: evidence for eligibility traces in the reward-learning network. *J Neurosci* **25,** 6235-6242.

Phillips P. E., Hancock P. J. and Stamford J. A. (2002) Time window of autoreceptor-mediated inhibition of limbic and striatal dopamine release. *Synapse* **44,** 15-22.

Phillips P. E. M. and Wightman R. M. (2003) Critical guidelines for validation of the selectivity of in-vivo chemical microsensors. *Trac-Trends in Analytical Chemistry* **22,** 509-514.

Pucak M. L. and Grace A. A. (1994) Regulation of substantia nigra dopamine neurons. *Critical reviews in neurobiology* **9,** 67-89.

Rice M. E., Cragg S. J. and Greenfield S. A. (1997) Characteristics of electrically evoked somatodendritic dopamine release in substantia nigra and ventral tegmental area in vitro. *Journal of neurophysiology* **77,** 853-862.

Santiago M., Machado A. and Cano J. (1992) Fast sodium channel dependency of the somatodendritic release of dopamine in the rat's brain. *Neuroscience letters* **148,** 145-147.

Schmitz Y., Benoit-Marand M., Gonon F. and Sulzer D. (2003) Presynaptic regulation of dopaminergic neurotransmission. *Journal of neurochemistry* **87,** 273-289.

Stamford J. A., Kruk Z. L. and Millar J. (1988) Actions of dopamine antagonists on stimulated striatal and limbic dopamine release: an in vivo voltammetric study. *British Journal of Pharmacology* **94,** 924-932.

Wightman R. M., Brown D. S., Kuhr W. G. and Wilson R. L. (1987) Molecular specificity of in vivo electrochemical measurements. *in Voltammetry in the Neurosciences***,** 103-138.

Wightman R. M., Amatore C., Engstrom R. C., Hale P. D., Kristensen E. W., Kuhr W. G. and May L. J. (1988) Real-time characterization of dopamine overflow and uptake in the rat striatum. *Neuroscience* **25,** 513-523.

Wu Q., Reith M. E. A., Walker Q. D., Kuhn C. M., Carroll F. I. and Garris P. A. (2002) Concurrent Autoreceptor-Mediated Control of Dopamine Release and Uptake during Neurotransmission: An In Vivo Voltammetric Study. *J. Neurosci.* **22,** 6272-6281.

Yan Q. S., Zheng S. Z., Feng M. J. and Yan S. E. (2005) Involvement of 5-HT1B receptors within the ventral tegmental area in ethanol-induced increases in mesolimbic dopaminergic transmission. *Brain research* **1060,** 126-137.

Yavich L. (1996) Two simultaneously working storage pools of dopamine in mouse caudate and nucleus accumbens. *Br.J.Pharmacol.* **119,** 869-876.

CHAPTER 4 - Neurobiological survey of the midbrain

INTRODUCTION

The mesolimbic dopaminergic pathway originates in the ventral tegmental area (VTA), a midbrain structure near the substantia nigra (SN). This is a major neuronal pathway stimulated during tasks such as intracranial self-stimulation (Olds and Milner 1954) and reward seeking behavior (Schultz 1998; Tobler et al. 2005). In addition, the midbrain contains many other structures including the SN. While investigating the SN and VTA in Chapter 3, it was discovered that other regions were capable of neurotransmitter release upon activation of the medial forebrain bundle (MFB) pathway. These included the intersitial medial longitudinal fasciculus (iMLF) and the red nucleus (RN). Fluorescent labeling of these regions using the rate limiting enzyme in dopamine synthesis, tyrosine hydroxylase (TH), demonstrated dopamine innervation in the iMLF, while fluorescent labeling of serotonin in these regions revealed serotonin innervation in the RN. Though the VTA has been shown to release dopamine (Bjorklund and Lindvall 1975; Cheramy et al. 1981; Falkenburger et al. 2001; Chen and Rice 2002; Adell and Artigas 2004), neither dopamine nor serotonin release has ever been measured in the iMLF or RN. To confirm the possibility of neurotransmitter release in these regions, it was necessary to record release using a subsecond electrochemical technique coupled with the criteria discussed in Chapter 3.

The three regions under investigation in this paper are the VTA, RN, and iMLF. The VTA is widely studied for its role in initiating the mesolimbic dopaminergic reward pathway. Its projections extend through the MFB and terminate in the nucleus accumbens (NAcc). Activation of the MFB has been shown to evoke release of dopamine in both the NAcc (Phillips et al. 2003) and dendritic projections of the VTA (Zhang et al. 1994) in rats. Another region of the midbrain connected to the MFB is the RN (Breese 1975), situated anterior to the VTA. The RN has been mostly studied with respect to its role in the circadian cycle (Licata et al. 2001), with its primary regulating

neurotransmitter being serotonin (Palkovits et al. 1974; Bosler et al. 1983). The other region in the midbrain which expressed significant TH labeling is the iMLF, situated in the thalamus, which has been shown to regulate oculomotor movements (Daroff 1987; Yan et al. 2001) and to deteriorate in Parkinson's disease (Racette et al. 2004) where dopamine has been implicated (Coulter et al. 1996; Toonen et al. 1998).

While neurotransmitter release has been measured in the midbrain, specifically the VTA, using microdialysis (Yan et al. 2005) and in-vitro fast-scan cyclic voltammetry (Cragg and Greenfield 1997), subsecond measurements of neurotransmitter release in the midbrain upon electrical stimulation of the MFB have not been observed in the intact animal. To determine the relative distributions of each neurotransmitter throughout the three target regions of the midbrain, we used a combination of immunohistochemical and electrochemical techniques. Cyclic voltammetric experiments performed in the rat brain confirmed the presence of evoked neurotransmitter in all three regions upon MFB stimulation, which was further supported using local stimulations in a murine brain slice. Immunohistochemical data were obtained to determine the relative distribution of dopaminergic structures in each region. The VTA had the highest dopamine intensity, followed by the iMLF, and lastly the RN possessed faint fluorescence. Results from the murine brain slice experiments indicated the presence of releasable pools of both neurotransmitters in all three regions, with serotonin being present in higher concentration in both the iMLF and the RN, and dopamine being present in higher concentration in the VTA. While local stimulations do not directly address which neurotransmitters are released upon MFB activation, they do confirm the presence of releasable dopamine and serotonin in all three regions.

MATERIALS AND METHODS

Anesthetized rat preparations

Animals and surgery

Male Sprague-Dawley rats (225-350g; Charles River, Wilmington, MA) were anesthetized with urethane (1.5 g/kg, i.p.) and placed in a stereotaxic frame (Kopf, Tujunga, CA). A heating pad (Harvard Apparatus, Holliston, MA) maintained a constant body temperature of 37°C. Holes were drilled in the skull for the working, reference, and stimulation electrodes at coordinates selected from the atlas of Paxinos and Watson (Paxinos and Watson, 1986). The carbon-fiber microelectrode was placed in both the caudate-putamen (CP, AP +1.2, ML +2.0, and DV -4.5) as well as the VTA (AP -5.2, ML +1.0, and DV -8.0). The stimulating electrode was placed in the MFB (AP -1.8, ML +2.0, and DV -8.0). Both the carbon-fiber and stimulating electrodes were moved in the dorsal-ventral direction while stimulating to find sites of maximal dopamine release. An Ag/AgCl reference was inserted in the contralateral side.

Electrical Stimulation

An untwisted bipolar stimulating electrode (Plastics One, Roanoke, VA) was used to stimulate dopaminergic neurons. The stimulus was provided by an analog stimulus isolator (A-M Systems, Sequim, WA). The stimulation train consisted of biphasic pulses (± 300 µA, 2 ms/phase unless otherwise noted). The frequency and number of pulses per train were varied as noted in the text. The pulses were generated by a computer and applied between the cyclic voltammograms to avoid electrical interference.

Electrochemistry

Cylindrical carbon fiber microelectrodes were prepared using T650 carbon fibers (3 µm radius, Amoco) and encased in glass capillaries (A-M Systems, Sequim, WA) and

pulled with a micropipette puller (Narashige, East Meadow, NY). The protruding fiber was then cut to a length of 50-100 µm. On the day of use, the electrode was soaked for 10 minutes in isopropanol purified with activated carbon (Bath et al. 2000). To make contact with the carbon fiber, a wire coated with silver paint was inserted into the open end of the capillary and twisted to ensure solid contact with the fiber. The wire was then secured using epoxy. The reference electrode was chloridized by placing a silver wire in an HCl solution and applying 5V.

Fast-scan cyclic voltammetry was used (Bath et al. 2000). The instrumentation controlled the potential of the carbon-fiber electrode while the reference electrode was held at ground potential. The potential of the working electrode was held at -0.4 V vs Ag/AgCl between scans and was ramped to +1.3 V at 400 V/s and repeated at a frequency of 10 Hz. After the experiment the working electrode was calibrated *in vitro* using dopamine solutions of known concentration. For serotonin measurements, the potential of the working electrode was held at +0.1 V vs Ag/AgCl between scans and was ramped to +1.0 V at 1000 V/s and subsequently ramped to -0.2 V before returning to the holding potential of +0.1 V and repeated at a frequency of 10 Hz.

Immunohistochemistry

For confocal microscopy experiments six rats were anesthesized with urethane (1.5 g/kg, i.p.) and perfused transcardially with 80 ml of 0.9% saline, followed by 80 ml of 4% paraformaldehyde. The brains were removed immediately after fixation and post-fixed for one hour in 4% paraformaldehyde. After one hour, the brains were transferred to phosphate buffered saline at a pH of 7.4 and kept in the refrigerator overnight. The brains were then cut on a microtome into 200 µm slices and collected in artificial cerebral sprinal fluid. The resulting slices were transferred to a pre-blocking solution containing 10 mL of PBS at pH 7.4, 0.1 g of bovine serum albumin (BSA), 1.0 mL of normal goat

serum, and 30 µL of Triton-X 100 and allowed to incubate for 2 hours. The slices were then incubated in a solution of primary anitbody (rabbit anti-TH polyclonal, Chemicon cat# AB 152) or (rabbit anti-serotonin polyclonal, Invitrogen, Carlsbad, CA) at a concentration of 1:200. The slices were then kept on a shaker plate overnight at 4^{o}C. The primary antibody was rinsed off with six aliquots of PBS at pH 7.4 for one hour. The slices were then incubated in a solution of secondary antibody (Invitrogen Alexa Fluor(R) 555 goat/anti-rabbit) at a concentration of 1:200 for 24 hours on a shaker plate at 4^{o}C. The secondary antibody was rinsed off with six aliquots of PBS at pH 7.4 for one hour. The slides were mounted on glass slides using BioRad Fluoroguard Antifade Reagent mounting media and analyzed on a Leica SP2 Laser Scanning Confocal Microscope (Leica Microsystems Inc., Bannockburn, IL).

Murine brain slices

Slice preparation

Mice were deeply anesthetized by ether inhalation and decapitated. The brain was immediately removed and placed in ice-cold aCSF. The aCSF solution consisted of (in mM): NaCl 126, KCl 2.5, NaH_2PO_4 1.2, $CaCl_2$ 2.4, $MgCl_2$ 1.2, $NaHCO_3$ 25, HEPES 20, D-glucose 11. The pH was adjusted to 7.4 with 5 M NaOH and the buffer was continuously saturated with 95% O_2/5% CO_2. The cerebellum was sliced off with a razor blade and the brain was mounted on a Teflon block using Krazy Glue ®. Brain slices were made using an NVSL vibratome (World Precision Instruments, Sarasota, FL, USA). Coronal slices containing the SN and VTA were obtained at -2.8 to -3.3 mm from bregma. Brain slices were stored in ice-cold aCSF. A single slice was submerged under aCSF maintained at 34°C and continuously flowing (2 mL/min) through a superfusion chamber (Warner Instruments, Hamden, CT, USA). Each brain slice was equilibrated for 30 min prior to obtaining measurements.

Electrochemistry

Carbon-fiber cylinder microelectrodes were made as previously described (Kawagoe et al. 1993) using T650 carbon fibers (Amoco, Greenville, SC, USA) cut to a length of 25 µm. Electrodes were epoxied (Miller-Stevenson, Danbury, CT, USA) to ensure a good seal, and dipped immediately in acetone for a few seconds to remove residual epoxy from the carbon fiber. A triangular waveform, starting at -0.4 V, increasing to 1.0 V, and scanning back to -0.4 V, was applied to the carbon-fiber working electrode, versus a Ag/AgCl reference electrode, at a scan rate of 600 V/s. For serotonin detection, the triangular waveform begins at 0.2 V, ramps to 1.0 V, ramps down to -0.1 V and returns to the resting potential of 0.2 V at a scan rate of 1000 V/s. An update rate of 10 Hz was used for all experiments.

The carbon fiber was inserted until the tip was 60-70 µm below the surface of the brain slice in the dorsolateral caudate region of the striatum between the prongs of a bipolar stimulating electrode (FHC, Bowdoinham, ME, USA), situated 200 µm apart. To evoke dopamine release, 20 pulses at 60 Hz (2 ms each phase, 350 µA in amplitude) were applied to the stimulating electrode. The current arising from dopamine oxidation (at about 0.6 V) in successive voltammograms was measured and plotted versus time. Electrodes were calibrated against dopamine standards of known concentrations in a flow cell after each brain slice experiment.

Data analysis

Data were analyzed in Graph Pad Prism (Graph Pad Software, San Diego, CA) and are expressed as mean ± SEM. Statistical significance was determined using a two-way ANOVA, and posthoc comparisons were performed using the method of least squares with a Bonferroni correction.

Chemicals and solutions

All chemicals and drugs were purchased from Sigma/Aldrich (St. Louis, MO) and used as received. Solutions were prepared using doubly distilled deionized water (Megapure system, Corning, NY). The TRIS buffer solution for flow cell analysis was prepared using 12 mM TRIS, 140 mM NaCl, 3.2 mM KCl, 1.2 mM $CaCl_2$, 1.25mM NaH_2PO_4, 1.2 mM $MgCl_2$, 2.0 mM Na_2SO_4 at pH 7.4. Drugs were dissolved in saline and injected intraperitoneally.

RESULTS

Dopamine localization in the midbrain via immunohistochemistry

Evaluation of dopamine localization was performed using immunohistochemistry, using specific antibodies labeled with fluorescent markers to examine each region of the midbrain. To locate dopamine innervation in the midbrain, tyrosine hydroxylase (TH), an enzyme critical to dopamine synthesis, was labeled with a primary antibody (rabbit/anti-TH). A secondary antibody, Alexa-555/anti-rabbit, was used to provide visual evidence of TH. A coronal view of the slice under investigation demonstrates the three regions of interest. The VTA is located in the ventral portion of the slice, spanning the midline (Fig. 4.1). The RN is situated dorsal to the VTA (Fig. 4.2), and the iMLF, labeled iMLF, is positioned dorsal to the RN (Fig. 4.3).

Verification of the specificity of the antibody was performed by first investigating the cell bodies of the VTA, which is the area responsible for the synthesis of dopamine in the mesolimbic dopaminergic pathway. An image of the transmitted light can be used to orient the slice. The midline of the brain runs directly from top to bottom of the image (Fig. 4.1a). The Alexa-555 antibody clearly demonstrates the specific binding of the protein based on the bright circular shapes, corresponding to dopaminergic cell bodies, surrounded by wispy projections, corresponding to dendrites (Fig. 4.1b-c). The antibody labels symmetrically on both sides, and at the midline, the bright labeling continues upward toward the top of the image. Further magnification of the image yields a clearer picture of the structure of dopaminergic neurons. The cell bodies can be more easily observed (Fig. 4.1c, white arrows), and the structure of the dendrites is more defined.

Reorienting the image to include only one hemisphere allows the observation of more structure in the slice. The transmitted light image indicated that the midline is located at the left edge, and showed the presence of the VTA, SN, and the RN (Fig. 4.2a). Fluorescent labeling again demonstrated intense labeling of the cell bodies and

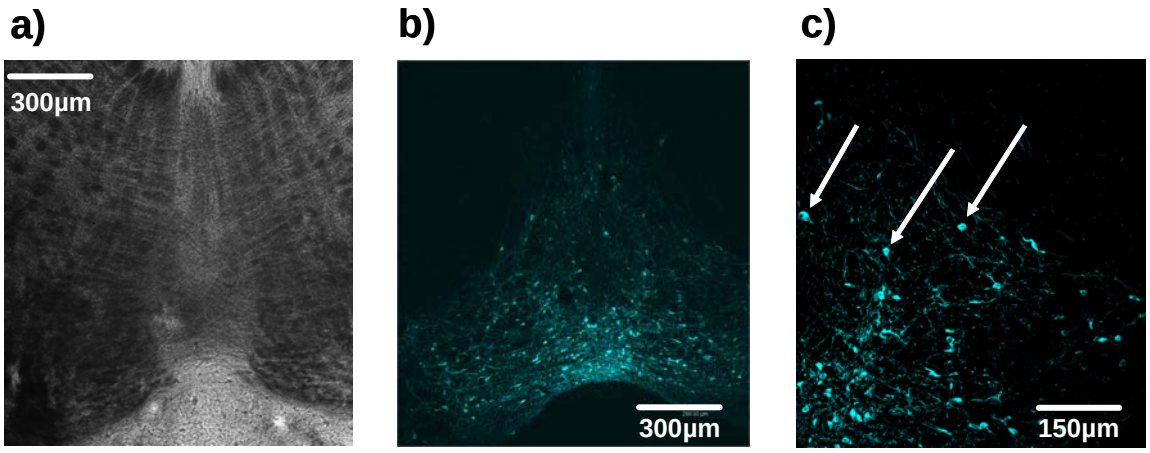

Figure 4.1. Dopaminergic structures in the ventral tegmental area (VTA). To locate dopamine innervation in the midbrain, TH was labeled with a primary antibody (rabbit/anti-TH). A fluorescent secondary antibody, Alexa-555/anti-rabbit, was used to provide a marker for TH. **(a)** This panel is a 10X transmitted light image showing the midline structure in the center of the image, and the VTA symmetrically placed about the midline. **(b)** A 10X fluorescent image showing the cyan-colored fluorescent labeling of TH in both hemispheres of the VTA. The bright dots indicate cell bodies. The line structures correspond to dendrites. **(c)** A 20X fluorescent image of the right hemisphere of the VTA. The cell bodies can be more clearly distinguished at this magnification. They appear as bright circular structures (white arrows), while the dendrites appear as wispy structures.

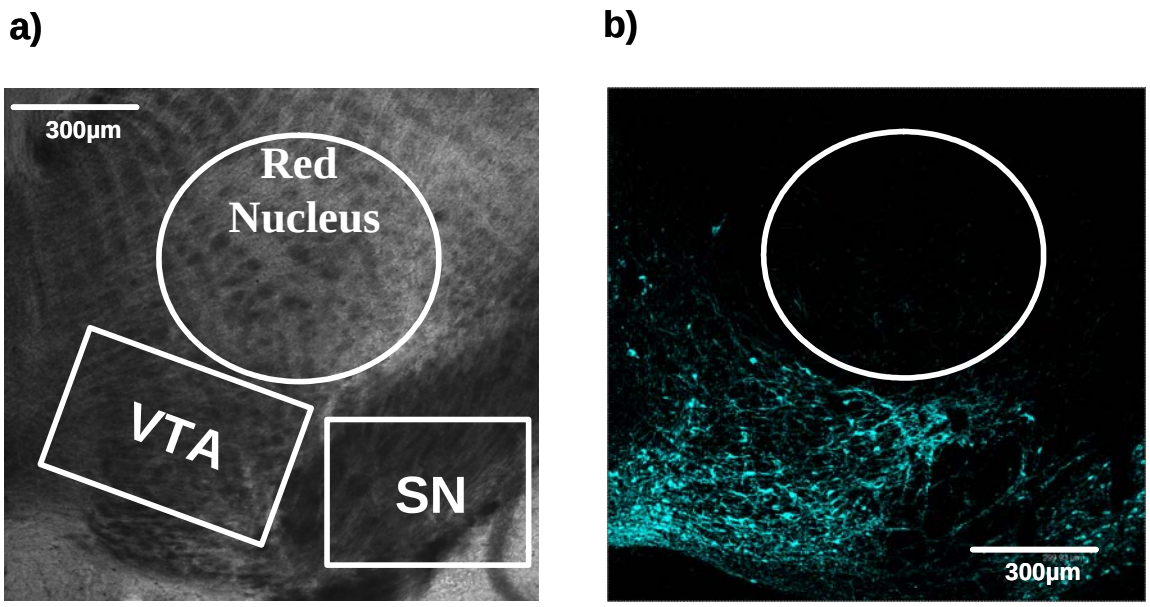

Figure 4.2. Dopaminergic structures along the ventral midline. To locate dopamine innervation in the midbrain, TH labeling was done as in Figure 4.1. Each panel represents the right hemisphere containing the VTA, red nucleus, and the substantia nigra (SN). The image has the midline located on the left edge. **(a)** This panel is a 10X transmitted light image of the right hemisphere of the ventral midbrain. The lower portion of the image is separated into the VTA (on left) and the substantia nigra (on the right). The circular structure located above the VTA is the red nucleus. **(b)** The cyan regions indicate the presence of fluorescently labeled TH neurons in the VTA and substantia nigra. The bright circular structures represent cell bodies and the wispy structures represent dendrites. The area directly above the VTA, the red nucleus displays only modest staining, suggesting only minor TH presence.

dendrites in the VTA (Fig. 4.2b). At the right side of the image, the VTA terminated and formed a junction with the SN, another dopamine rich region of the midbrain. The white circle indicates the location of the RN (Fig. 4.2b). Though there appear to be a few illuminated areas within the RN, the labeling is significantly less in this region, which indicates to a decreased dopaminergic innervation.

The iMLF is approximately 1.5 mm more dorsal from the image containing the RN and VTA. The transmitted light image verified the position of the midline on the left edge of the image (Fig. 4.3a). The iMLF is shown as a circular region in the transmitted light image (Fig 4.3a). Note the presence of a small portion of the RN located in the lower portion of the image. Examination of the fluorescent image verifies the presence of dopaminergic innervation in the iMLF (Fig. 4.3b). The only other labeling present in the area is located along the midline which suggests fairly specific binding. The confocal microscope was also used to produce layered images which can be summated to provide an image indicating the maximum fluorescent intensity for each pixel. Increasing the magnification by a factor of four (40X magnification) gives more detail of the iMLF region (Fig. 4.3c). The image represents 30 layers of approximately 10 nm each, corresponding to an overall thickness of 300 nm. The max projection image indicates that the labeled structures are more terminal-like, as there are no brightly labeled cell bodies present in the image (Fig. 4.3c).

Serotonin localization in the midbrain via immunohistochemistry

Regions containing significant concentrations of serotonin were identified using serotonin specific antibodies. Locating serotonin was performed using a rabbit/anti serotonin primary antibody. A secondary antibody was then used to visualize the bound serotonin. Once again, the Alexa-555 conjugated goat/anti-rabbit secondary antibody was selected to detect the serotonin fluorescently.

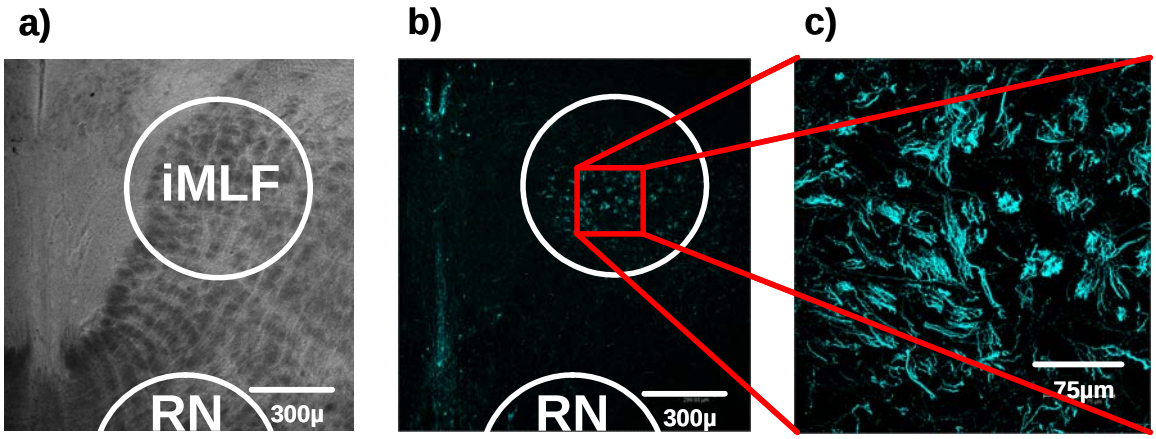

Figure 4.3. Dopaminergic structures in the ventral tegmental area (VTA). To locate dopamine innervation in the midbrain, TH labeling was done as in Figure 4.1. Each panel represents the area in the right hemisphere 5-7 mm ventral from the top of the brain. The circular region represents the interstitial medial longitudinal fasciculus (iMLF), with a small portion of the red nucleus (RN) still visible in the ventral portion of the image. **(a)** This panel represents a 10X transmitted light image of the right hemisphere lateral to the third ventricle. The midline is on the left edge and the iMLF is located in the center of the image. **(b)** A 10X fluorescent image of the iMLF. The cyan-colored regions indicate the presence of TH-positive neurons. The iMLF demonstrates a circular staining which is consistent with the structure observed in the atlas (Paxinos and Watson). The contrast and brightness of the image have been enhanced to observe the staining in the iMLF. The relative brightness is significantly lower than the fluorescent signals obtained in the VTA. **(c)** 40X image of the iMLF centered about the red square from panel **(b)**. The image is displayed as the summation of a series of 30 layers, each of 10 nm thickness. The brightest pixel from each layer is displayed in the final image to give a 3D appearance. The summated image demonstrates linear structures that are more commonly observed at the terminals.

The specificity of the antibody was evaluated via labeling of regions rich in serotonin. The dorsal raphe nucleus was selected as one of the serotonergic regions, due to the high concentration of serotonin present and its role in depression (Michelsen et al. 2007). Fluorescent labeling of the region demonstrated regionally specific labeling of the serotonin cell bodies (Fig. 4.4a). Fluorescence for the serotonin antibody is shown in magenta. The cell bodies of the dorsal raphe are indicated by the white arrows, and they appear as bright circular shapes. The image is displayed at a magnification of 20X to visualize each cell body more clearly.

Once the specificity of the antibody had been determined, the midbrain was investigated to determine serotonin content. The SN labeled strongly for serotonin (Fig. 4.4b), consistent with previous findings in the region (John and Jones 2007). Surprisingly, intense serotonin labeling was also present in the VTA (Fig. 4.4c); however, the presence of serotonin does not definitively mean that serotonin is released upon MFB stimulation, which was proven in Chapter 3.

The RN also displayed strong serotonin labeling. The midline is located at the left edge of the image, and the VTA and SN are located along the lower edge of the image. Both the VTA and SN contain serotonin as shown previously (Fig. 4.4b-c), and the intensity of serotonin labeling in the RN is roughly equivalent to the intensity obtained in the SN (Fig. 4.4d). The shape of the serotonin labeling roughly corresponds to the circular structure of the RN, further verifying the presence of releasable serotonin in the RN. Fluorescent labeling in the iMLF is non-existent (Fig. 4.4e). The midline and ventricle are located on the left edge of the image, and possess only faint labeling; however, the region containing the iMLF is almost black, which suggests minimal serotonin involvement in the iMLF.

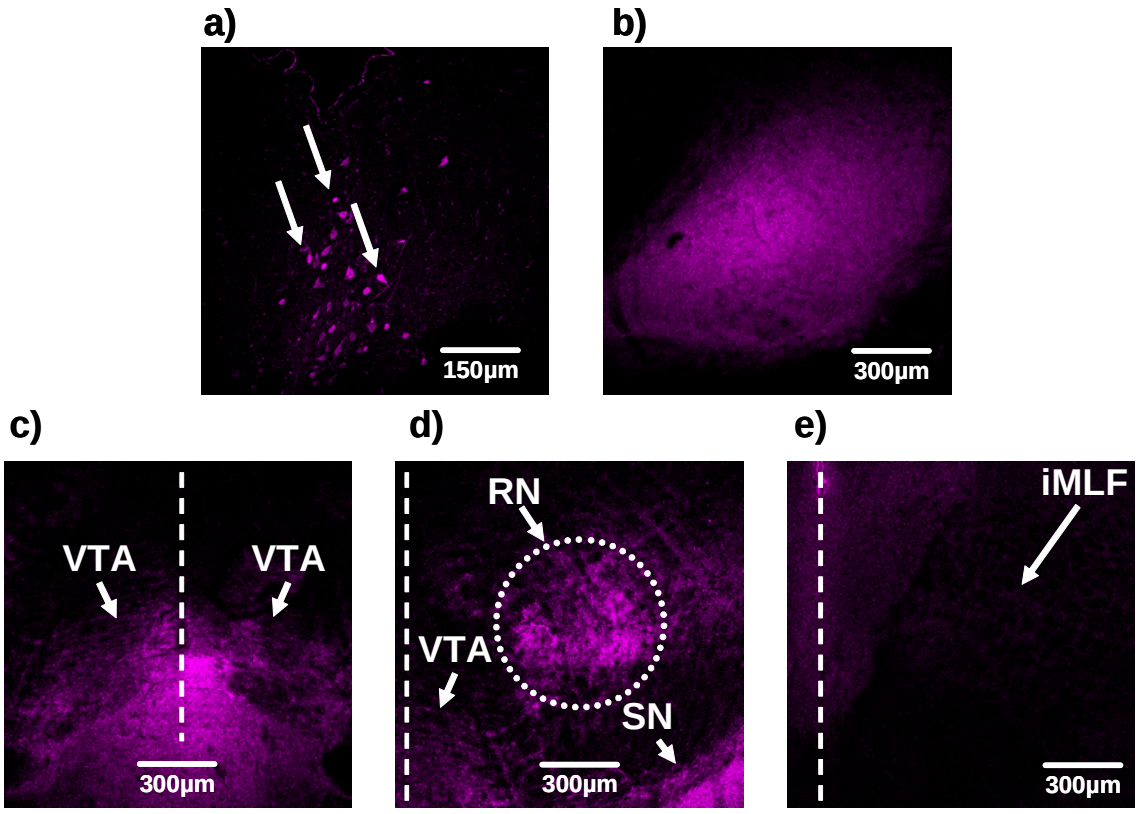

Figure 4.4. Serotonin labeling in the midbrain. Coronal brain slices were labeled with a rabbit/anti-serotonin primary antibody. A fluorescent secondary antibody, Alexa-555/anti-rabbit, was used to provide a marker for serotonin. The dashed line represents the midline. **(a)** Slice obtained -7.0 mm from bregma containing the dorsal raphe nucleus. Image magnified using 20X objective. Bright circular shapes indicate the presence of serotonergic cell bodies (white arrows). **(b)** Coronal slice obtained -5.2 mm from bregma containing the SN. Image magnified using 10X objective. **(c)** Slice obtained -5.2 mm from bregma containing both hemispheres of the VTA. Image magnified using 10X objective. **(d)** Slice obtained -5.2 mm from bregma containing the RN, VTA, and SN. Image magnified using 10X objective. The RN is shown as a dotted circle. The intensity of the labeling is roughly equivalent to the intensity obtained in the neighboring VTA and SN. **(e)** Slice obtained -5.2 mm from bregma containing the iMLF. Image magnified using 10X objective.

Anatomical verification

To measured subsecond release in the midbrain, it is first important to confirm placement of the working and stimulating electrodes. Anatomical specificity of the electrochemical signal was provided via maneuvering both electrodes. Placement of the stimulating electrode was confirmed via placement of the working electrode into the densely dopaminergic caudate-putamen (CP) region (AP +1.2, ML +2.0, DV -4.5). The stimulating electrode was placed at (AP -1.8, ML +2.0) and lowered in 200 µm increments. The location was chosen based on the midpoint directly between the terminals and cell bodies of dopaminergic cells projecting from the VTA toward the NAcc (Fig. 4.5a). At each position of the stimulating electrode, an electrical stimulation was applied (40 p, 60 Hz, 300 µA). The voltammetric current was measured and the maximum amplitude of the release profile was recorded (Fig. 4.5b). For each experiment, the amplitude at each location was normalized to the location which yielded the highest response. In this way each brain could be appropriately compared. The normalized dopamine response was graphed on the x-axis, with depth from the top of the brain (in mm) plotted on the y-axis (Fig. 4.5b). The cyclic voltammogram obtained throughout the MFB possessed the characteristic dopamine oxidation peak at +0.6 V and reduction peak at -0.2 V (Fig. 4.5b, inset). Dopamine release was not apparent until the stimulating electrode had reached a depth of approximately 7.5 mm, which correlates roughly with the location of the MFB (Fig. 4.5b). Upon completion of the experiment, the animal was anesthetized, and the brain removed to determine the final location of the stimulating electrode. The final location of the stimulating electrode can be seen as a small black square (n=4, Fig. 4.5a).

Once the optimal stimulating electrode position had been determined, the working electrode was lowered through the CP and into the NAcc (AP +1.2, ML +2.0) (Fig. 4.6a). As the MFB is known to project to both the CP and the NAcc, it was

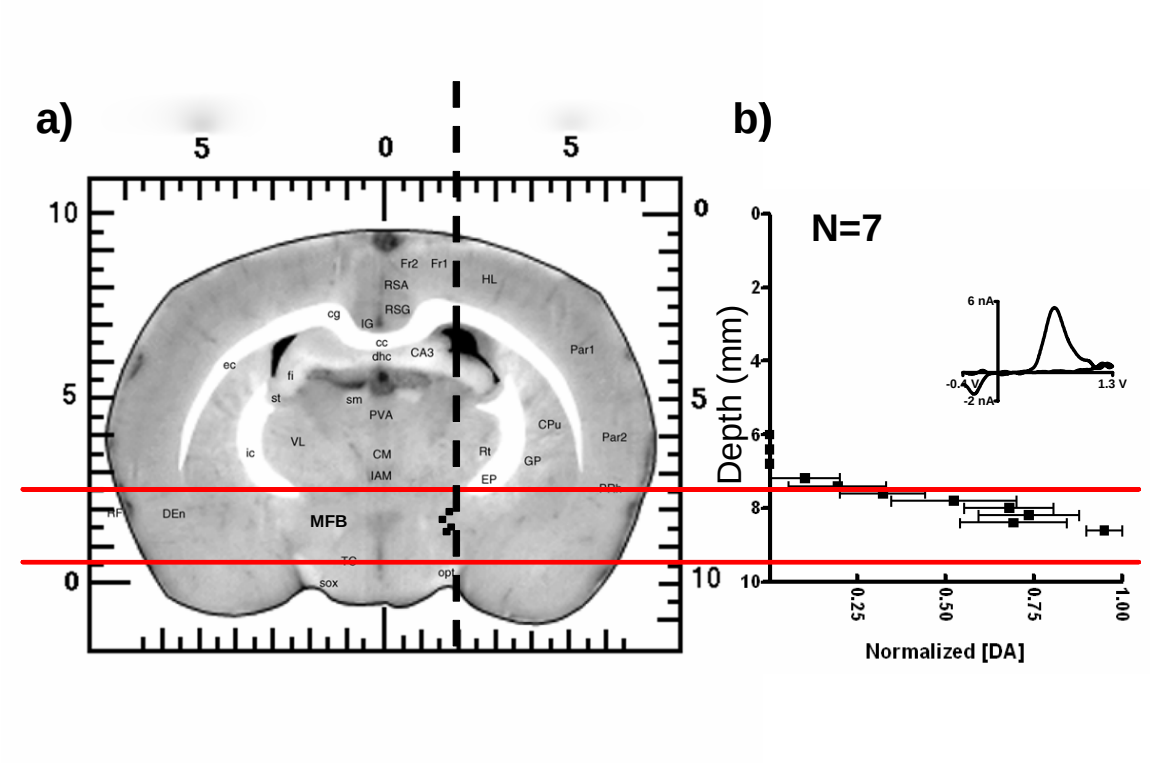

Figure 4.5. Anatomical verification of stimulating electrode placement. The placement of the stimulating electrode was determined by manually lowering the stimulating electrode through the brain. Signals were recorded in the CP during a 60 Hz, 40 p, 300 µA electrical stimulation. **(a)** Brain slice atlas image obtained -2.04 mm posterior from bregma. The brain structures at 2.04 and 2.00 mm posterior from bregma are virtually identical and can be used as a comparison for the placement of the stimulating electrode. Black squares indicate final position of the electrode determined via imaging upon euthanization of the animal. The target region for the stimulating electrode placement is the medial forebrain bundle (MFB). The dashed line represents the track of the stimulating electrode. **(b)** The normalized concentration of evoked dopamine was measured in 200 µm increments as the stimulating electrode was lowered. In each animal, the signal at each data point was normalized to the maximum amplitude of release obtained from the animal. The red lines indicate the estimated height of the MFB in the rat brain atlas image. The measured signals are roughly encompassed by the red lines. (inset) CV obtained *in vivo* in the CP upon electrical stimulation of the MFB.

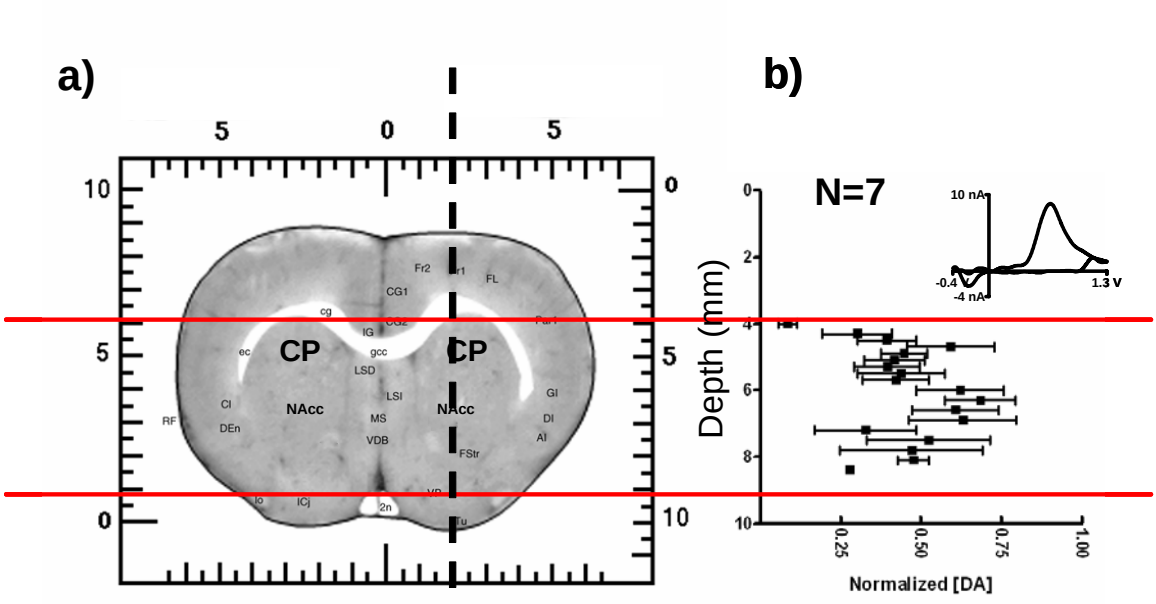

Figure 4.6. Anatomical verification of working electrode placement in the forebrain. The placement of the working electrode was determined by manually lowering the electrode through the forebrain while holding the stimulating electrode fixed in the MFB. Signals were recorded in the CP and NAcc upon a 60 Hz, 40 p, 300 µA electrical stimulation of the MFB. **(a)** Brain slice obtained +0.96 mm anterior from bregma. The brain structures at 0.96 and 1.00 mm anterior from bregma are virtually identical and can be used as a comparison for the placement of the working electrode. The target areas in the forebrain are CP and the NAcc. The dashed line represents the track of the working electrode. **(b)** The normalized concentration of evoked dopamine was measured in 200 µm increments as the working electrode was lowered. Data normalized as in Figure 4.5. The red lines indicate the estimated height of the two forebrain structures in the rat brain and encompass the bimodal measured signal. (Inset) Cyclic voltammogram (CV) obtained *in vivo* in the CP upon electrical stimulation of the MFB.

important to measure release in both regions to confirm that the stimulating electrode was activating the entire MFB. Stimulation and recording parameters are the same as with the stimulating electrode placement. At each 200 µm increment of the carbon fiber, the maximal release was recorded, normalized and plotted as a function of electrode depth (Fig. 4.6b). Release can be described in a bimodal distribution correlating to the CP and NAcc (Fig. 4.6b). Evoked release from both the CP and the NAcc indicate that fibers originating from both the VTA and the SN were stimulated. The cyclic voltammograms obtained throughout the CP and NAcc possessed the characteristic dopamine oxidation peak at +0.6 V and reduction peak at -0.2 V (Fig. 4.6b, inset).

The working electrode was then moved to the midbrain region to record from the iMLF (AP -5.2, ML +1.0, DV -6.5), the RN (AP -5.2, ML +1.0, DV -7.5), and the VTA (AP -5.2, ML +1.0, DV -8.5) (Fig. 4.7a). The carbon fiber electrode was lowered in a series of 200 µm increments and the maximal release was recorded in response to an electrical stimulation (60 p at 60 Hz, 300 µA each phase). The higher number of pulses was necessary due to decreased amplitude of release throughout the midbrain. Measured signals were not confined to the VTA, but were also present in the iMLF, and the RN (Fig. 4.7b). The cyclic voltammograms obtained throughout the midbrain are not conclusively dopaminergic (Fig. 4.7b, inset). The characteristic +0.6 V oxidation peak is present; however, due to the lower concentration measured in these regions, the reduction peak is not clearly defined. An unclearly defined reduction peak may suggest the presence of both dopamine and serotonin. The final position of the working electrode in the VTA was determined via electrical lesioning of the carbon fiber working electrode. A small current was applied between the reference and working electrodes to create a lesion which was visually detected upon euthanization of the rat. Each location can be seen as a small black square (n=4, Fig. 4.7a).

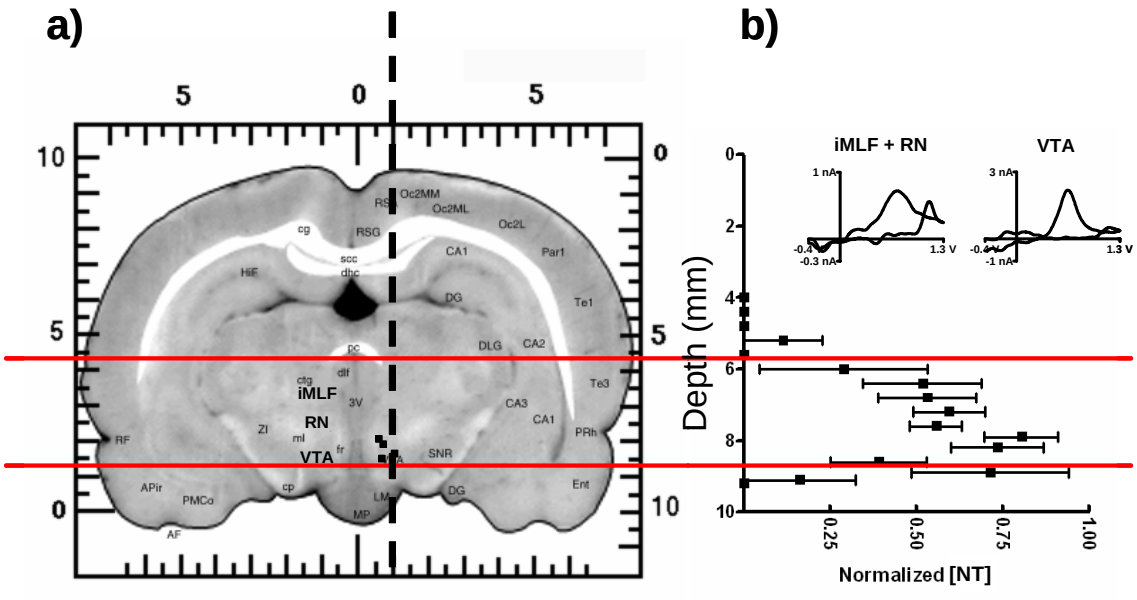

Figure 4.7. Anatomical verification of working electrode placement in the midbrain. The placement of the working electrode was determined via manually lowering the working electrode through the midbrain, while holding the stimulating electrode fixed in the MFB. Signals were recorded in the midbrain upon a 60 Hz, 60 p, 300 µA electrical stimulation of the MFB. **(a)** Brain slice obtained -5.20 mm posterior from bregma. Black squares indicate final position of the electrode determined via imaging upon euthanization of the animal. The areas under investigation include the iMLF, RN and the VTA. Regions labeled in the left hemisphere are structurally identical to the regions in the right hemisphere. The dashed line represents the track of the working electrode. **(b)** The normalized concentration of evoked neurotransmitter (NT) was measured in 200 µm increments as the working electrode was lowered. Data normalized as in Figure 4.5. The red lines indicate the estimated height of the three midbrain stuctures and encompass the measured signal. (inset) Representative cyclic voltammograms obtained from both the iMLF and RN (left panel) and the VTA (right panel).

Selective detection of serotonin in these three regions was performed by modifying the applied waveform. Rather than use the traditional -400 mV → +1300 mV, the modified serotonin waveform was used (See Methods). The same procedure was performed as previously (Fig. 4.7). Measurements were taken every 200 µm. As the working electrode was lowered through the brain, no signal was recorded during the first 6.0 mm. Serotonin was detected in both the RN and the iMLF (Fig. 4.8), with the maximum signal obtained in the RN (Fig. 4.8b). These results are consistent with the imaging data which demonstrated the highest serotonin fluorescent intensity in the RN. A representative CV is shown (Fig. 4.8b, inset). Though the *in vivo* CV does not directly match the CV obtained in a flow cell, an *in vivo* microinjection of serotonin into the brain adjacent to the working electrode results in a CV identical to that obtained during the experiment (data not shown).

Differential distribution of dopaminergic and serotonergic neurons

As electrochemical differentiation proved unfeasible in both the iMLF and RN, of the anesthetized rat, experiments were performed in murine brain slices to investigate releasable pools of neurotransmitter in the midbrain. A transgenic mouse line in which catecholamine containing cells express the gene for the enhanced green fluorescent protein (Kessler et al. 2003) was used to allow visualization of dopaminergic regions. To determine the relative concentrations of dopamine and serotonin in the three regions of interest, the working electrode was placed directly into each region using a confocal microscope to visualize the GFP fluorescently-labeled regions. Neurotransmitter release was evoked via local electrical stimulation using a bipolar stimulating electrode. To measure both serotonin and dopamine in the same region of the brain, the waveform was alternated between the traditional dopamine waveform and the modified waveform for serotonin (See Methods). As the dopamine waveform detects both serotonin and

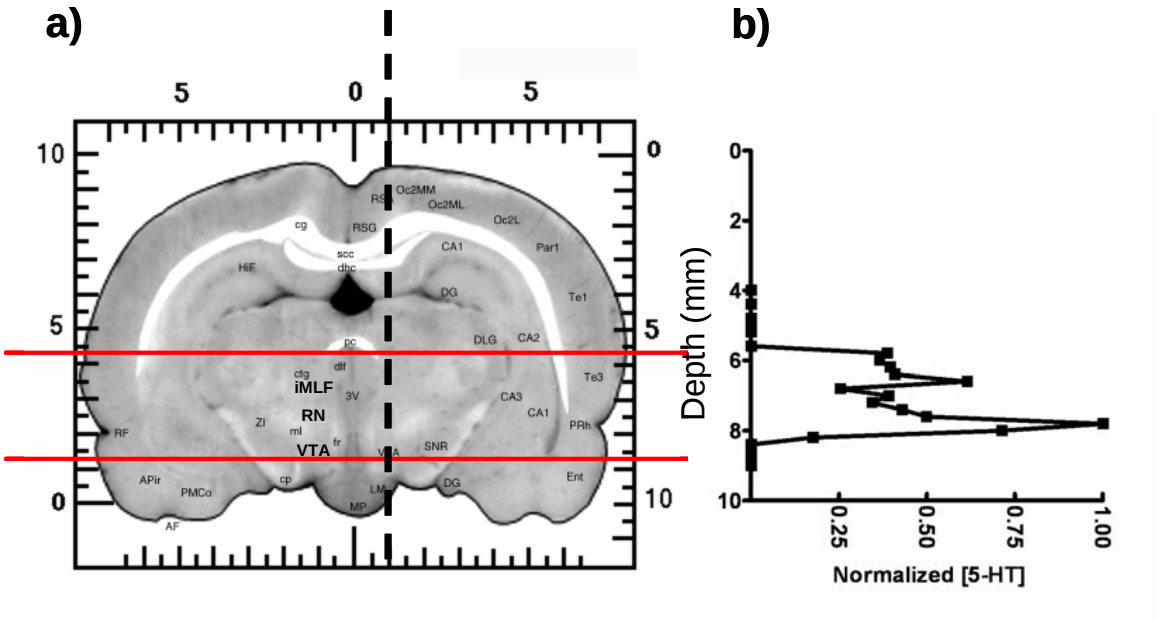

Figure 4.8. Anatomical verification using serotonin specific waveform. The placement of the working electrode was determined via manually lowering the working electrode through the midbrain, while holding the stimulating electrode fixed in the MFB. Signals were recorded in the midbrain upon a 60 Hz, 60 p, 300 µA electrical stimulation of the MFB. The serotonin waveform was applied to the carbon fiber as described in Methods. **(a)** Brain slice obtained -5.20 mm posterior from bregma. The areas under investigation include iMLF, RN and the VTA. Regions labeled in the left hemisphere are structurally identical to the regions in the right hemisphere. The dashed line represents the track of the working electrode. **(b)** The normalized concentration of evoked serotonin (5-HT) was measured in 200 µm increments as the working electrode was lowered. Data normalized as in Figure 4.5. The red lines indicate the estimated height of the three midbrain structures and encompass the measured signal, with the maximum signal occurring in the RN. (inset) Representative cyclic voltammogram obtained from the RN. The obtained cyclic voltammogram is consistent with CV's obtained upon *in vivo* microinjections of serotonin.

dopamine, it was used to calculate the combined contribution of both neurotransmitters in all three regions (Fig. 4.9b, DA panel). The serotonin waveform was then used to measure the serotonin signal alone (Fig. 4.9b, 5-HT panel). The two signals could then be subtracted from each other to yield the concentration of each neurotransmitter individually (Fig. 4.9a). *In vitro* flow cell experiments confirmed the viability of this method.

Each region had one predominant neurotransmitter. In the VTA, there was an approximately two-fold higher concentration of dopamine as compared to serotonin (Fig. 4.9a). There was an average release of 192 ± 95 nM for dopamine and 96 ± 32nM for serotonin. The values were not significantly different, but there was a distinct trend. The RN which was expected to contain more serotonin (Palkovits et al. 1974; Bosler et al. 1983) had approximately three times more serotonin than dopamine (Fig. 4.9a). The amount of neurotransmitter released in the RN was significantly less than that observed in the VTA; however, there was approximately 54 ± 10 nM of serotonin released, and approximately 16±4 nM of dopamine released (Fig. 4.9a). The iMLF possessed a mixed signal of both dopamine and serotonin. Serotonin release was 164 ± 87 nM, and dopamine release was 83 ± 30 nM (Fig. 4.9a). While these results are from mice, not anesthetized rats, they do indicate that there is a distribution of releasable serotonin and dopamine in all three regions.

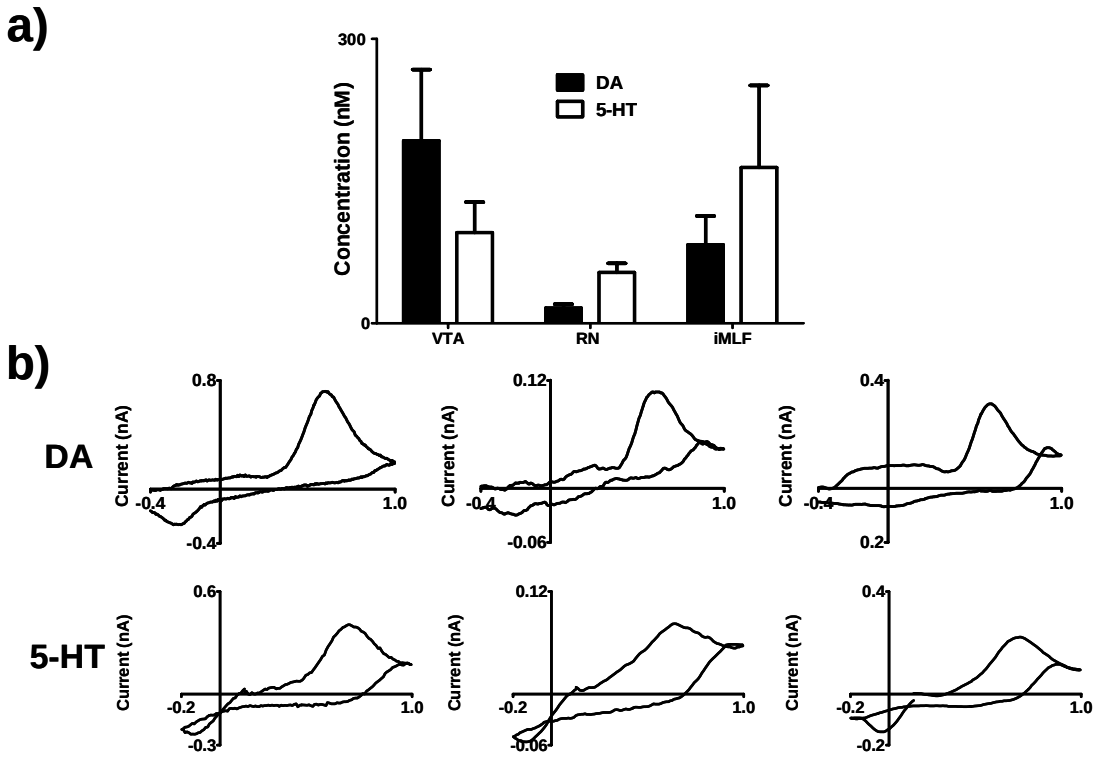

Figure 4.9. Concentrations of DA and 5-HT obtained in the midbrain. The concentrations of both dopamine and serotonin were obtained in murine brain slice preparations. Mixed solutions of the two chemicals were analyzed to calibrate the electrodes. **(a)** The VTA contained approximately two times more dopamine than serotonin. The red nucleus (RN) contained approximately three times more 5-HT than dopamine, and the iMLF contained approximately two times more 5-HT than dopamine (N=5). **(b)** Representative cyclic voltammograms obtained from all 3 brain regions. For each brain region, both the dopamine waveform (labeled DA) and the serotonin waveform (labeled 5-HT) were used.

DISCUSSION

From the results obtained it is clear that in addition to projections from the MFB toward the CP and NAcc, projections also exist which communicate with both the RN and iMLF. This realization suggests that each time the mesolimbic dopamine pathway is activated, it is also activating these secondary areas which are involved in the circadian cycle (Izac and Eeg 2006) and oculomotor movements (Yan et al. 2001). Further investigation into these midbrain structures is necessary to fully understand the role played by dopamine and serotonin in midbrain structures other than the VTA and SN.

An excellent complement to electrochemical experiments in the brain is the use of a secondary technique that can indicate the presence of specific neuromolecules. Here, TH was targeted with antibodies to pinpoint areas containing dopaminergic structures. The fluorescent staining correlated well with the electrochemical data (Fig. 4.1-6). The RN possessed only faint TH staining, suggesting significantly less dopamine release than other regions such as the VTA or iMLF (Fig. 4.2b), while the VTA exhibited intense TH staining. The iMLF possessed faint but regionally distinctive features (Fig. 4.3c). Closer examination of these features in the iMLF suggested that the observed structures were terminals (Fig. 4.3c), which strengthens the case for terminal release of dopamine in this region.

Using a primary antibody selective to serotonin, several structures rich in serotonin were identified. The dorsal raphe nucleus, a region known to be high in serotonin concentration, possessed strong serotonin labeling (Fig. 4.4a). The SN and VTA also possessed significant serotonin labeling. The two regions of interest, the iMLF and RN, labeled contrarily to the results obtained with TH labeling. While the iMLF had significant TH labeling (Fig. 4.3c), serotonin labeling was not present (Fig. 4.4e). The RN was void of TH labeling (Fig. 4.2b); however, serotonin labeling revealed a structurally specific arrangement of serotonergic cells in the RN. These

immunohistochemical experiments are useful for verifying locations of specific neurotransmitters throughout the brain; in this case, it proved the presence of serotoninergic innervation in the RN and dopaminergic innervation in the iMLF.

Verifying the placement of the electrodes is crucial to any statements regarding the location of neurotransmitter release. Placing the working electrode into a 2 mm by 2 mm area, rich in dopamine release, ensures that at least one electrode is properly situated initially (Fig. 4.5a). Slowly lowering the stimulating electrode ventrally through the brain while holding the working electrode fixed allows placement of the stimulating electrode along the relatively confined MFB (Fig. 4.5b). Measurement of dopamine in the CP under these conditions ensures that the electrical stimulation is activating at least a portion of the MFB. By subsequently lowering the working electrode through both the CP and the NAcc, we can ensure that the entire MFB is receiving the electrical stimulation (Fig. 4.6b). Dopamine release in both the CP and NAcc indicates that projections from both the VTA and SN are being activated.

In the anesthetized rat, it is typically not feasible to switch back and forth between waveforms as the carbon fiber surface rapidly fouls in the presence of both serotonin and dopamine. For this reason, the waveform used to measure release in the three midbrain regions was the traditional dopamine waveform. The waveform has a higher sensitivity to dopamine; however, the signal is confounded in the presence of substantial quantities of serotonin release. The dopamine waveform measured signals above baseline beginning at 6 mm ventral from the top of the brain (Fig. 4.3b). This correlates with the beginning of the iMLF (Fig. 4.3a). The signal continued at varying amplitudes throughout the remainder of the midbrain until the terminal region of the brain was reached (Fig. 4.3b). Experiments were also performed using the serotonin waveform to get an idea of the amount of serotonin release upon MFB stimulation. The overall shape of the depth profile for the serotonin waveform (Fig. 4.8b) was similar to

that obtained with the dopamine waveform (Fig. 4.7b); however, there was no serotonin measured in the VTA. Additionally, there was a greater concentration of serotonin measured in the RN as opposed to the iMLF. The depth profile obtained with each waveform provides useful information as to the relative concentrations of neurotransmitter present in each region; however, because serotonin rapidly fouls the electrode during measurement, it makes it challenging to accurately evaluate the concentration of each neurotransmitter.

Further experiments to obtain the relative concentrations of both serotonin and dopamine were performed in murine brain slices. The mouse model was selected because mice expressing GFP on catecholaminergic cells were developed which can aid in the placement of the working electrode into each brain region. Without GFP fluorescence, placement of the working electrode in brain slices is quite difficult. Though the preparation is not in a rat, it can still provide evidence regarding the neurotransmitter content in these three regions. A coronal section was taken containing all three brain regions. By alternating between the serotonin and dopamine waveforms, the relative concentration of each neurotransmitter was determined upon local stimulation. Somewhat surprisingly, each region contained both neurotransmitters at detectable concentrations. The VTA which was expected to contain releasable dopamine (John and Jones 2006), released twice as much dopamine as serotonin (Fig. 4.9a); however the presence of a serotonin signal measured in the VTA is contrary to current literature which has proven that the only releasable neurotransmitter in the area is dopamine (Rice et al. 1997; John et al. 2006; John and Jones 2007). Additionally, data presented in Chapter 3 also demonstrated that the neurotransmitter released under our conditions was dopamine. The measurement of serotonin in this region further accentuates the difference between these two preparations, as local stimulation does not directly mimic a propagating action potential.

It is important to note the distinction between the two preparations used to measure the concentration of neurotransmitter release. In the anesthetized rat, the electrical stimulation is occurring 3 mm away from the site of the working electrode. This ensures that the evoked release is due to the propagation of an action potential, rather than the direct opening of the ion channels needed to initiate release. The drawback to anesthetized experiments is the inability to visualize the placement of the electrodes as well as the inability to utilize two alternating waveforms. By using GFP-positive mice, visualization of each region can be achieved, allowing for more accurate placement of the working and stimulating electrodes. The other advantage to using murine brain slices is that as a result of the buffer constantly flowing over the brain slice, electrode-fouling serotonin metabolites can be washed away before the electrode becomes fouled. The combination of the two preparations can be used to provide a much more complete picture than can be obtained in one preparation alone.

The RN and iMLF also exhibited a combination of both serotonin and dopamine signals (Fig. 4.9a and Fig. 4.7b, inset). The RN possessed three times more releasable serotonin, and the iMLF possessed 2 times more releasable dopamine (Fig. 4.9a). Neither region is very well understood due to the prior lack of a technique capable of selectively measuring neurotransmitter release on the subsecond time scale. The presence of dopamine transporter has been previously measured in the iMLF (Coulter et al. 1996) suggesting a potential role for dopamine release. The presence of dopamine in the iMLF is consistent with the function of the region, as the iMLF has been implicated in Parkinsonian behavior (Racette et al. 2004), which is the degeneration of nigrostriatal dopaminergic neurons. The identification of both dopamine and serotonin in these midbrain regions will also provide useful information for further investigation into the major serotonin pathways studied with regards to the circadian cycle.

These experiments open up the possibility of recording serotonin and dopamine in the midbrain under conditions of reward, addiction, or motor movements. Current investigation of reward, addiction, and motor movements typically involves measurements in the CP and NAcc; however, the knowledge of these additional projections will serve to enhance our understanding of the factors which are involved in the regulation of the mesolimbic pathway. Further studies need to be performed to fully grasp the regulatory role that each region is playing in the overall mesolimbic system.

REFERENCES

Adell A. and Artigas F. (2004) The somatodendritic release of dopamine in the ventral tegmental area and its regulation by afferent transmitter systems. *Neurosci Biobehav Rev* **28,** 415-431.

Bath B. D., Michael B. J., Trafton B. J., Joseph J. D., Runnels P. L. and Wightman R. M. (2000) Subsecond adsorption and desorption of dopamine at carbon-fiber microelectrodes. *Analytical chemistry* **72,** 5994-6002.

Bjorklund A. and Lindvall O. (1975) Dopamine in dendrites of substantia nigra neurons: suggestions for a role in dendritic terminals. *Brain research* **83,** 531-537.

Bosler O., Nieoullon A., Onteniente B. and Dusticier N. (1983) In vitro radioautographic study of the monoaminergic innervation of cat red nucleus. Identification of serotoninergic terminals. *Brain research* **259,** 288-292.

Breese G. (1975) Chemical and immunochemical lesions by specific neurotoxic substances and antisera. *In: Iversen LL, Iversen SD, Snyder SH (eds) Handbook of Psychopharmacology* **Vol I.,** New York, Plenum, pp 137-174.

Chen B. T. and Rice M. E. (2002) Synaptic regulation of somatodendritic dopamine release by glutamate and GABA differs between substantia nigra and ventral tegmental area. *Journal of neurochemistry* **81,** 158-169.

Cheramy A., Leviel V. and Glowinski J. (1981) Dendritic release of dopamine in the substantia nigra. *Nature* **289,** 537-542.

Coulter C. L., Happe H. K. and Murrin L. C. (1996) Postnatal development of the dopamine transporter: a quantitative autoradiographic study. *Brain Res Dev Brain Res* **92,** 172-181.

Cragg S. J. and Greenfield S. A. (1997) Differential autoreceptor control of somatodendritic and axon terminal dopamine release in substantia nigra, ventral tegmental area, and striatum. *J Neurosci* **17,** 5738-5746.

Daroff R. B. (1987) Progressive supranuclear palsy: a brief personalized history. *The Yale journal of biology and medicine* **60,** 119-122.

Falkenburger B. H., Barstow K. L. and Mintz I. M. (2001) Dendrodendritic Inhibition Through Reversal of Dopamine Transport. *Science* **293,** 2465-2470.

Izac S. M. and Eeg T. R. (2006) Basic anatomy and physiology of sleep. *American journal of electroneurodiagnostic technology* **46,** 18-38.

John C. E. and Jones S. R. (2006) Exocytotic release of dopamine in ventral tegmental area slices from C57BL/6 and dopamine transporter knockout mice. *Neurochemistry international* **49,** 737-745.

John C. E. and Jones S. R. (2007) Voltammetric characterization of the effect of monoamine uptake inhibitors and releasers on dopamine and serotonin uptake in mouse caudate-putamen and substantia nigra slices. *Neuropharmacology* **52,** 1596-1605.

John C. E., Budygin E. A., Mateo Y. and Jones S. R. (2006) Neurochemical characterization of the release and uptake of dopamine in ventral tegmental area and serotonin in substantia nigra of the mouse. *Journal of neurochemistry* **96,** 267-282.

Kawagoe K. T., Zimmerman J. B. and Wightman R. M. (1993) Principles of Voltammetry and Microelectrode Surface-States. *Journal of neuroscience methods* **48,** 225-240.

Kessler M. A., Yang M., Gollomp K. L., Jin H. and Iacovitti L. (2003) The human tyrosine hydroxylase gene promoter. *Brain Res Mol Brain Res* **112,** 8-23.

Licata F., Li Volsi G., Di Mauro M., Fretto G., Ciranna L. and Santangelo F. (2001) Serotonin modifies the neuronal inhibitory responses to gamma-aminobutyric acid in the red nucleus: a microiontophoretic study in the rat. *Experimental neurology* **167,** 95-107.

Michelsen K. A., Schmitz C. and Steinbusch H. W. (2007) The dorsal raphe nucleus--from silver stainings to a role in depression. *Brain research reviews* **55,** 329-342.

Olds J. and Milner P. (1954) Positive reinforcement produced by electrical stimulation of septal area and other regions of rat brain. *Journal of comparative and physiological psychology* **47,** 419-427.

Palkovits M., Brownstein M. and Saavedra J. M. (1974) Serotonin content of the brain stem nuclei in the rat. *Brain research* **80,** 237-249.

Phillips P. E. M., Stuber G. D., Heien M. L. A. V., Wightman R. M. and Carelli R. M. (2003) Subsecond dopamine release promotes cocaine seeking. *Nature* **422,** 614-618.

Racette B. A., Esper G. J., Antenor J., Black K. J., Burkey A., Moerlein S. M., Videen T. O., Kotagal V., Ojemann J. G. and Perlmutter J. S. (2004) Pathophysiology of parkinsonism due to hydrocephalus. *Journal of neurology, neurosurgery, and psychiatry* **75,** 1617-1619.

Rice M. E., Cragg S. J. and Greenfield S. A. (1997) Characteristics of electrically evoked somatodendritic dopamine release in substantia nigra and ventral tegmental area in vitro. *Journal of neurophysiology* **77,** 853-862.

Schultz W. (1998) Predictive reward signal of dopamine neurons. *Journal of neurophysiology* **80,** 1-27.

Tobler P. N., Fiorillo C. D. and Schultz W. (2005) Adaptive coding of reward value by dopamine neurons. *Science* **307,** 1642-1645.

Toonen M., van Dijken H., Holstege J. C., Ruigrok T. J., Koekkoek S. K., Hawkins R. K., Teune T. M., vd Burg J. and De Zeeuw C. I. (1998) Light microscopic and ultrastructural investigation of the dopaminergic innervation of the ventrolateral outgrowth of the rat inferior olive. *Brain research* **802,** 267-273.

Yan Q. S., Zheng S. Z., Feng M. J. and Yan S. E. (2005) Involvement of 5-HT1B receptors within the ventral tegmental area in ethanol-induced increases in mesolimbic dopaminergic transmission. *Brain Research* **1060,** 126-137.

Yan Y. J., Cui D. M. and Lynch J. C. (2001) Overlap of saccadic and pursuit eye movement systems in the brain stem reticular formation. *Journal of neurophysiology* **86,** 3056-3060.

Zhang H., Kiyatkin E. A. and Stein E. A. (1994) Behavioral and pharmacological modulation of ventral tegmental dendritic dopamine release. *Brain research* **656,** 59-70.

CHAPTER 5 - Fabrication and characterization of a nitric oxide sensor

INTRODUCTION

The molecule nitric oxide has proven to be an important regulatory agent throughout the body, in particular in its role as a vasodilator (Miki et al. 1977; Ignarro et al. 1987; Moncada et al. 1991; Moncada and Higgs 1993). More recently, however, nitric oxide has been discovered to play a role in neurotransmission as a glutamate stimulated, retrograde messenger (Garthwaite et al. 1988; Gally et al. 1990; Montague et al. 1991; Garthwaite and Boulton 1995; Venton et al. 2003). The current hypothesis of nitric oxide release is that evoked glutamate release activates proteins that subsequently activate nitric oxide synthases, potentially implicating nitric oxide in learning and memory (Piedrafita et al. 2007). However, much about the molecule still remains unanswered due to the lack of a sensor capable of measuring nM concentration of nitric oxide on a time scale consistent with many transient biological processes. A microsensor with the capabilities just described would be a significant addition to the field of nitric oxide study.

As a reactive, gaseous molecule, nitric oxide presents some interesting analytical challenges as it pertains to *in vivo* measurements. Throughout the years, many methods have been developed to measure changes in nitric oxide both directly and indirectly (Archer 1993; Bryan and Grisham 2007). The original method, or the Griess reaction (Griess 1879), measures the concentrations of both nitrite and nitrate, the degradation products of nitric oxide (Tsikas 2007). Citrulline, the molecule concurrently formed upon nitric oxide synthesis, is also measured as an indirect correlation of nitric oxide concentration using HPLC (Guthohrlein and Knappe 1968). Other methods for measuring nitric oxide include chemiluminescence (Robinson et al. 1999), fluorescence (Gomes et al. 2006; Lim and Lippard 2007), and gas chromatography (Helmke and Duncan 2007); however, these methods lack the temporal resolution afforded by electrochemistry (Bedioui and Villeneuve 2003; de Vooys et al. 2004; Zhang 2004). Detection of nitric oxide via electrochemistry is typically performed using an electrode

modified with an electrocatalyst to facilitate measurements (Shibuki 1990; Malinski and Taha 1992; Diab et al. 2005; Pereira-Rodrigues et al. 2005). More recent designs include amperometric sensors with organically modified membranes to enhance selectivity (Friedemann et al. 1996; Lee et al. 2004; Shin et al. 2005). These designs still lack the spatial resolution necessary to record subsecond changes in small brain microenvironments.

The first step toward understanding changes in nitric oxide concentration in the brain is to develop a miniaturized sensor with subsecond temporal resolution without sacrificing nitric oxide specificity. Toward this end, a xerogel-modified platinized microelectrode was designed capable of measuring nitric oxide on a subsecond time scale. The multilayered electrode design consists of a tungsten conical microelectrode, plated with both platinum and platinum black, and covered with a permselective fluorinated xerogel. At each step of the fabrication process, the electrode was characterized both optically and electrochemically to probe the surface characteristics. Additionally, the sensitivity and selectivity of each layer was measured to determine the optimal sensor design. The sensitivity was found to increase with each layer of platinum deposit, and the selectivity was found to increase upon coverage by the xerogel. The electrode was exposed to a variety of interferents known to participate in neuronal signaling, including dopamine, oxygen and pH. The rise time of the electrode upon exposure to an *in vitro* bolus of nitric oxide was approximately 800 ms; thus making *in vivo* measurements of nitric oxide a possibility. Using *in vivo* microinjections, the diffusion of nitric oxide was measured and calculated demonstrating the presence of a significant clearance of nitric oxide in the brain.

MATERIALS AND METHODS

Reagents

Hydrofluoric acid (48 wt % in water) was purchased from Aldrich (Milwaukee, WI). (Heptadecafluoro-1,1,2,2-tetrahydrodecyl)trimethoxysilane (17FTMS) was purchased from Gelest (Tullytown, PA). Methyltrimethoxysilane (MTMOS) was purchased from Fluka (Buchs, Switzerland). Sodium nitrite and dopamine hydrochloride were purchased from Sigma (St. Louis, MO). An electrocleaning solution, 32.6g/L (Electrocleaner) was purchased from Shor International (Mt. Vernon, NY). Platinum TP solution (acidic plating solution) was purchased from Technic, Inc. (Cranston, RI). A platinizing solution (3% chloroplatinic acid in water) was purchased from LabChem (Pittsburgh, PA). Nitric oxide (NO; 99.5% and 24.1 ppm, balance nitrogen), argon (Ar), and nitrogen (N_2) gases were obtained from Linde Gas (Morrisville, NC) and National Welders Supply (Raleigh, NC). Other solvents and chemicals were analytical-reagent grade and used as received. A Millipore Milli-Q UV Gradient A10 System (Bedford, MA) was used to purify distilled water to a final resistivity of 18.2 MΩ·cm and a total organic content of ≤6 ppb.

Preparation of NO ultramicroelectrodes

For the preparation of platinum ultramicroelectrodes, a tungsten substrate with a diameter of 125 μm and AC resistance of 0.5 MΩ and insulated with parylene-C via a vacuum deposition was used (A-M Systems; Sequim, WA). The exposed tips (typically 50 – 60 μm length) were cleaned for 10 s in hydrofluoric acid (48 wt % in water), electrolyzed for 30 s at 50 ^{o}C in an electrocleaning solution at an applied potential of -5 V (vs a platinum electrode), and rinsed with water (Hermans and Wightman 2006). The conical electrode was then transferred into an acidic platinum electroplating solution, plated for 5 s at 50 ^{o}C at an applied potential of -0.5 V (vs a platinum electrode), and

rinsed with water and ethanol (Hermans and Wightman 2006). The ensuing platinum-deposited working electrode was platinized in 3% chloroplatinic acid (v/v in water) by cycling the potential from +0.6 to –0.35 V (vs Ag/AgCl) at a scan rate of 20 mV/sec using a CH Instruments 730B bipotentiostat (Lee et al. 2004; Shin et al. 2005). Finally, the multilayered ultramicroelectrode (i.e., platinum black/platinum/tungsten, Pt-B/Pt/W) was modified with the optimized fluorinated xerogel-derived permselective membrane by dip-coating the sensor tip into a sol solution. The sol solution was prepared by combining, in order, 300 μL of ethanol, 60 μL of MTMOS, 15 μL of 17FTMS, 80 μL of water, and 5 μL of 0.5 M HCl. The HCl was added immediately after the addition of water to facilitate hydrolysis. The solution was incubated on the Vortex for 1 hour; after which the Pt-B/Pt/W electrodes were dipped three times. After allowing the xerogel "film" to cure for 10 min, the process was repeated two additional times. The xerogel-modified electrode was then allowed to dry for 24 h under ambient conditions.

Surface characterization

Scanning electron microscope (SEM) images of the platinized ultramicroelectrode were collected on a Hitachi S4700 field-emission SEM (Tokyo, Japan) using an accelerating voltage of 15 keV (source working distance of 13.5 mm). To obtain high-quality images, samples were coated with a thin layer of gold (ca. 5 nm thickness) using a Cressington 108auto sputter-coater (Watford, England).

Voltammetric characterization

Cyclic voltammograms were acquired with the EI-400 potentiostat (Ensman Instrumentation, Bloomington, IN), locally constructed hardware, and software written in LabVIEW (National Instruments, Austin, TX) that has been described previously (Michael et al. 1999). The electrochemical cell was placed inside a grounded Faraday cage to

minimize electrical noise. For background-subtracted cyclic voltammograms the electrode was positioned at the outlet of a 6-port rotary valve. The loop injector was mounted on an actuator (Rheodyne model 5041 valve and 5701 actuator) that was controlled by a 12-V DC solenoid valve kit (Rheodyne, Rohnert Park, CA). This introduced the analyte to the electrode surface. Solution was driven with a syringe infusion pump (2 mL/min, Harvard Apparatus Model 940, Holliston, MA) through the valve and the electrochemical cell. For all experiments a Ag-AgCl reference electrode (Bioanalytical Systems, West Lafayette, IN) was used.

To evaluate the analytical performance of the NO sensors, cyclic voltammetric and amperometric measurements were performed using a CH Instruments 730B bipotentiostat (Austin, TX). The electrode assembly (3-electrode configuration) consisted of a xerogel-modified Pt working electrode (2-mm diameter), a Pt-coiled counter electrode (0.6-mm diameter), and a Ag/AgCl reference electrode (Bioanalytical Systems, West Lafayette, IN).

Two standard NO solutions (1.9 mM and 41 nM) were prepared by purging TRIS buffer solution (15 mM TRIS, 140 mM NaCl, 3.25 mM KCl, 1.2 $CaCl_2$, 1.25 mM NaH_2PO_4, 1.2 mM $MgCl_2$ and 2.0 mM Na_2SO_4, was adjusted to pH 7.4) with Ar for 30 min to remove oxygen, then NO (99.5% and 24.1 ppm) for 30 min. The NO gas was purified before use by passing it through a column packed with KOH pellets to remove trace NO degradation products. Solutions of NO and interfering species (pH and dopamine) were prepared freshly every day and stored at 4 ºC. All sensors were pre-polarized for at least 10 minutes and tested in deoxygenated TRIS (prepared by purging with N_2) at room temperature with constant stirring. Electrooxidation currents of NO and interfering species were recorded at an applied potential of +0.8 V (vs Ag/AgCl). Sensors were stored in TRIS at room temperature between measurements.

Animals and surgery

Male Sprague-Dawley rats (225-350g; Charles River, Wilmington, MA) were anesthetized with urethane (1.5 g/kg, i.p.) and placed in a stereotaxic frame (Kopf, Tujunga, CA). A heating pad (Harvard Apparatus, Holliston, MA) maintained a constant body temperature of 37°C. Holes were drilled in the skull for the working, and reference electrodes and at coordinates selected from the atlas of Paxinos and Watson (Paxinos and Watson, 1986). The fluorinated xerogel microsensor was placed in the caudate-putamen (CP) (AP +1.2, ML +2.0, and DV -4.5). An Ag/AgCl reference was inserted in the contralateral region of the brain.

Microinjections

The microinjection configuration involved affixing the NO microsensor to a 2.5 µL syringe (Hamilton Company, Reno, NV). To test the electrodes, a 100 nL, 300 µm radius droplet of 1.9 mM nitric oxide was injected approximately 500 µm from the microsensor. The size of the droplet and distance between the syringe and microsensor were measured under the microscope. The electrochemical response upon microinjection was measured in 0.6% w/v agarose gel and in the caudate-putamen of the rat brain.

RESULTS AND DISCUSSION

Evaluation of electrode surface

Critical to the construction of the microsensor is an understanding of the electrode surface. At each step in the electrode fabrication process, the surface structure was analyzed. As described in the Materials and Methods section, a tungsten conical microelectrode is the substrate for the microsensor. There are two important steps to the fabrication of a functional microelectrode. The first issue is minimizing the resistance between the substrate and the metal being used for the electrochemistry, and the second critical step is ensuring that the deposited metal have a smooth and durable coat (Hermans and Wightman 2006). The first step in the electrode fabrication process is electroplating a smooth platinum layer via constant potential electroplating, and the second step is the electrodeposition of platinum black to enhance sensitivity. The electrochemistry at tungsten is significantly different than electrochemistry at platinum (Hermans and Wightman 2006); thus cyclic voltammetry is a suitable means of evaluating each of the platinum layers on the electrode. Sulfuric acid can be used to distinguish tungsten from platinum by its cyclic voltammogram (Fig. 5.1). A tungsten electrode cyclic voltammogram obtained in a 0.5 M solution of sulfuric acid demonstrated no distinctive background peaks (Fig. 5.1a); whereas the electroplated platinum electrode demonstrated two reversible hydrogen adsorption peaks and one quasi-reversible oxygen peak (Fig. 5.1b). Additionally the amplitude of the background has increased, suggesting an increase in electroactive surface area (Fig. 5.1a-b). Upon deposition of the platinum black, the overall amplitude of the background increased an order of magnitude (Fig. 5.1c), indicating a further increase in the electroactive area. A glass encased, platinum disk electrode gives an identical cyclic voltammogram (Fig. 5.1d), which is consistent with reported literature (Bard and Faulkner 2001). Cyclic voltammetry in sulfuric acid is an excellent means of evaluating the quality of the

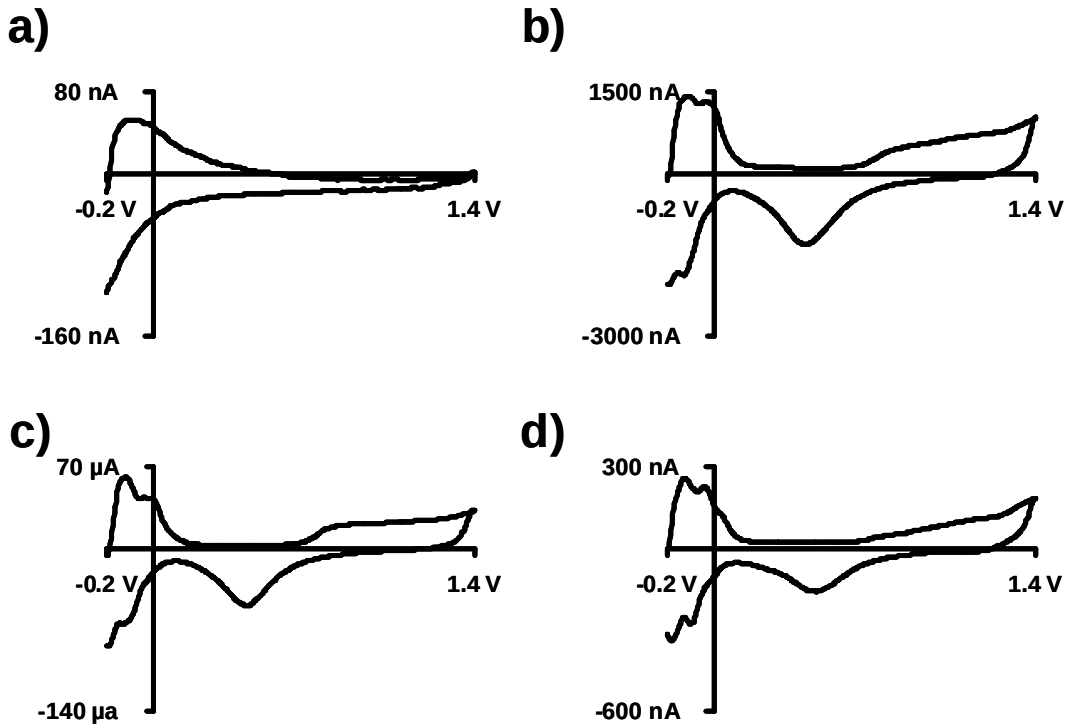

Figure 5.1. Characterization of the electrode surface using cyclic voltammetry. Each electrode is analyzed using cyclic voltammetry at 10 V/s in 0.5 M sulfuric acid. **(a)** Tungsten conical microelectrode showing no characteristic platinum peaks in sulfuric acid. **(b)** Platinum-plated tungsten microelectrode showing two distinctive Pt-H adsorption peaks. **(c)** Platinum black tungsten microelectrode showing increased background current as a result of increased surface area. **(d)** Glass-encased platinum disk electrode.

platinum deposits; a severe ramping current at higher potentials demonstrates incomplete coverage of the tungsten substrate.

Impedance measurements were also used to characterize the relative electroactive surface areas. By applying a 1000 Hz, 20 mV_{p-p}, sine wave and recording the resulting current, the impedance of the electrode was measured (Fig. 5.2a). The dotted line represents the sinusoidal waveform applied to a platinum plated electrode, and the solid line represents the resulting current. The resulting current is not symmetrical about the x-axis until the third cycle of the sine wave; thus the impedance is derived from the fourth cycle. Another method of displaying the data is by plotting the current versus the applied potential, known as a Lissajous figure (Fig. 5.2b). This is useful for measuring the phase difference between the current and voltage. The impedance for each electrode can be determined using equation 1:

$$\mathbf{V} = \mathbf{I} \times \mathbf{Z} \qquad (1)$$

where V is the applied voltage, I is the measured current, and Z is the unknown impedance of the electrode. Dividing the applied voltage by the measured current yields the impedance. The average impedance of a hydrofluoric acid cleaned, bare tungsten microelectrode is 368±37 kΩ (Fig. 5.2c). The electroplated platinum (first layer) had an average impedance of 66±9 kΩ, which is a decrease in the impedance by a factor of 5, indicating an increase in electroactive surface area. Exposed tungsten typically has a highly resistive surface oxide layer, preventing the occurrence of electrochemical process; the deposition of platinum blocks the oxide layer and allows for the charging of the double layer. The second layer of platinum further decreased the impedance by an order of magnitude to 4.70±0.25 kΩ (Fig. 5.2c). This is consistent with the goal of the platinum black to increase the sensitivity of the electrode by increasing the surface area; thus, a decrease in impedance correlates to an increase in surface area. The addition of the hydrophobic fluorinated xerogel membrane increased the impedance by a factor of

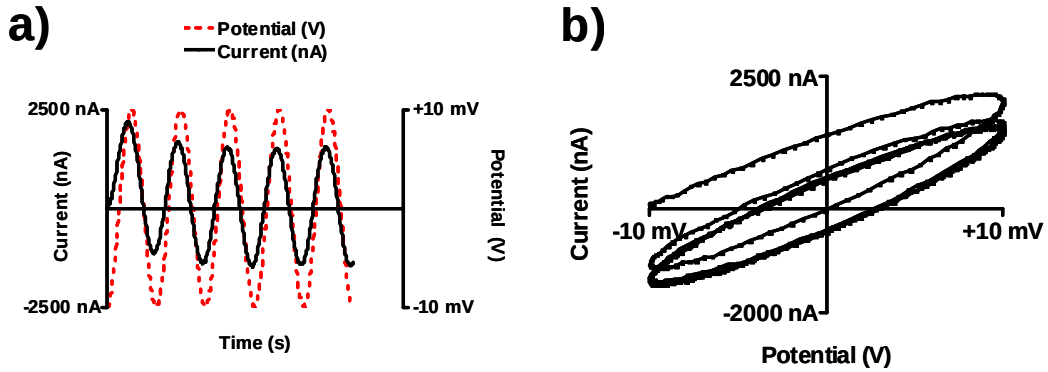

c)

	Electrode	Tungsten	Pt-plated	Pt-platinized	Membrane
Impedance (kΩ)	#1	295.81	47.27	4.38	6.39
	#2	421.24	64.68	5.44	7.16
	#3	443.07	91.62	4.45	10.24
	#4	311.72	61.92	4.53	6.01
	Average	367.96	66.37	4.70	7.45
	SEM	37.47	9.24	0.25	0.96

Figure 5.2. Analysis of microelectrode impedance. To determine impedance of each electrode, a sinusoidal wave was applied from -10 to +10 mV at 1000 Hz. **(a)** The dotted red line indicates the applied potential plotted on the right y-axis. The black solid line represents the resulting current at a representative platinized electrode. The current used for impedance calculation was obtained by measuring the peak amplitude of the fourth wave. **(b)** The Lissajous figure showing the current to voltage relationship for a representative platinized electrode. The phase can be determined by measuring the slope of the ovular structure. **(c)** Graph demonstrating the impedance for a set of 4 electrodes. Each column indicates the step in the fabrication process. The average impedance and SEM for each step are displayed at the bottom of each column.

two, which is to be expected with the addition of a hydrophobic layer to the electrode surface. This small impedance change suggests that the membrane should not significantly affect electrochemistry at the surface as the ohmic drop is not significant.

SEM images of the electrode surface confirm the presence of each layer of the platinum process (Fig. 5.3a-c). The tungsten microelectrode possesses a smooth featureless surface with an approximately one micron thick insulation of parylene-c (Fig. 5.3a). The electroplated platinum surface demonstrates a slightly rougher surface but at the one micron scale, is still relatively smooth (Fig. 5.3b). Addition of the platinum black layer significantly increases the size and surface area of the electrode (Fig. 5.3c). Each cluster of platinum atoms is designed to catalytically increase the oxidation of nitric oxide at the surface. Due to the roughened amorphous surface, addition of the approximately one micron thick membrane coating is not apparent (Fig. 5.3d). The apparent lack of visible membrane is likely due to differences in cluster formations between the two electrodes (Fig. 5.3c-d).

Electrode performance

In addition to pure platinum surface coverage, durability and reproducibility are also crucial to the electrode performance. An important characteristic of an *in vivo* sensor is that the sensor maintains its sensitivity over the course of an experiment. To evaluate the reproducibility of the electrode, the membrane covered electrode was exposed to a series of injections separated by three minutes. Each bolus of 37 nM nitric oxide produced roughly the same current response over the course of 30 minutes, approximately 400 pA (Fig. 5.4a). An additional injection given 1.5 hours after the last injection elicited the same response suggesting the response to identical exposures was consistent over the course of a two hour period (data not shown). A typical recording

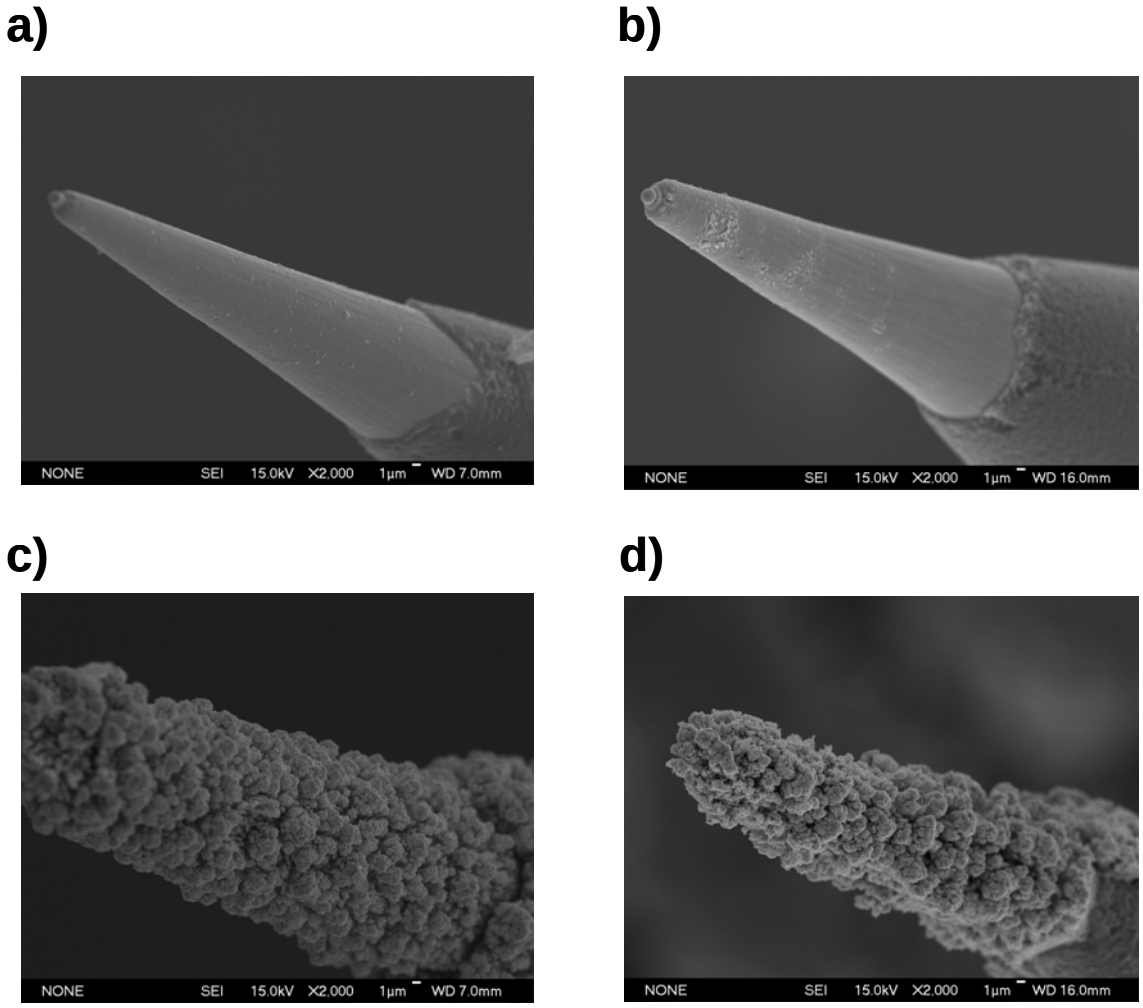

Figure 5.3. SEM imaging of the microelectrodes. Each panel represents a 2000X magnified SEM image. **(a)** Bare tungsten microelectrode, **(b)** platinum-plated microelectrode, **(c)** platinum black microelectrode, and **(d)** membrane coated microelectrode.

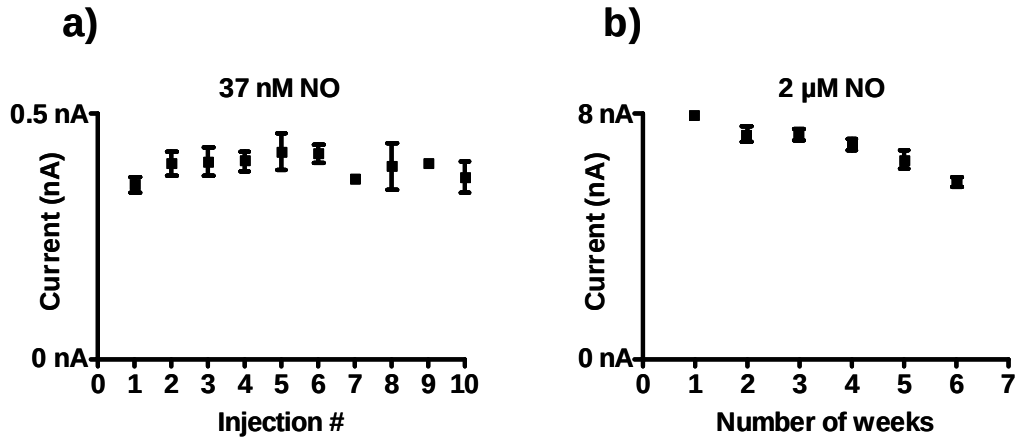

Figure 5.4. Evaluation of sensor reproducibility. The sensor was held at +0.8 V vs a Ag/AgCl electrode. **(a)** To evaluate sensor reproducibility over the course of an experiment, a bolus of 37 nM nitric oxide (NO) was passed through a flow cell and repeated every 3 minutes for thirty minutes. There was no significant change in NO sensitivity over the course of the experiment (n=5). **(b)** To evaluate sensor reproducibility over several weeks, a bolus of 2 µM nitric oxide was passed through a flow cell and repeated once a week for 6 weeks. Sensitivity did not significantly change during the first 4 weeks; however, sensitivity reached 75% after 6 weeks.

session for recording in a single brain region is approximately 3 hours, so the performance of the electrode with its current design should be satisfactory.

Another important requirement of an in vivo sensor is that the sensitivity remains constant over extended periods of time upon completion of the fabrication process. A long period of viability simplifies the fabrication process and allows for mass production, rather than constant daily construction. Similar to the previous experiment, the membrane covered electrode was exposed to a series of 2 μM nitric oxide boluses over the course of several weeks. One data point is plotted from each week demonstrating that the electrode is slowly losing sensitivity; however the electrode maintains 90% of its signal even one month after the first file is collected (Fig. 5.4b), and only after 2 months does the electrode approach 75% of its initial sensitivity.

Nitric oxide is a molecule that has a short half-time; thus, it is imperative that the electrode be able to measure rapid changes in nitric oxide concentration. The temporal resolution of the membrane covered electrode was measured by injecting various concentrations of nitric oxide to the electrode and measuring the subsequent rise time of the electrode in response to each injection. For each of the concentrations investigated, 400 nM, 1 μM, and 4 μM, the rise time of the signal was approximately identical (Fig. 5.5a). A closer inspection into the rise time reveals that the rise time for each injection was approximately 300 ms (Fig. 5.5b), which is approximately the same temporal resolution achieved by a carbon fiber microelectrode used to measure dopamine with background subtracted cyclic voltammetry (Bath et al. 2000).

Selectivity and sensitivity

Interferents commonly encountered in dopamine rich regions of the brain include pH changes, oxygen changes, and dopamine fluctuations (Venton et al. 2003). To determine the selectivity of the electrode to each of these species, the electrode, in

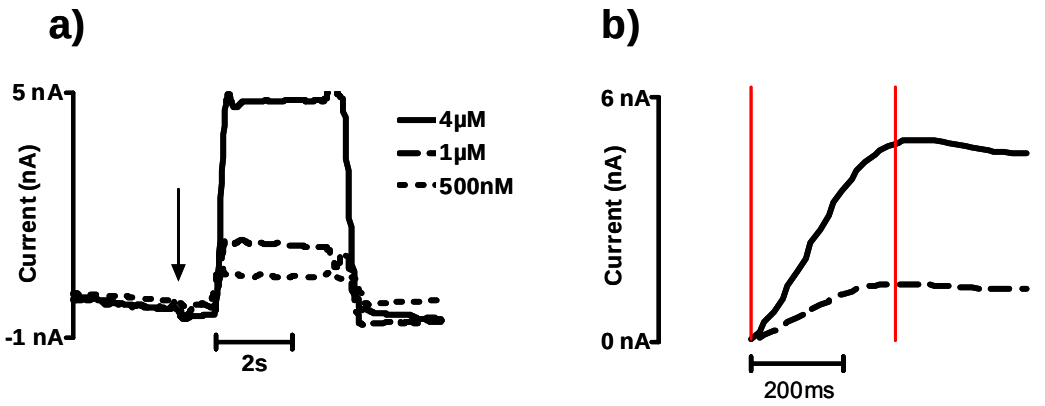

Figure 5.5. Evaluation of the time response of the electrode. The sensor was held at +0.8 V vs a Ag/AgCl electrode. **(a)** To determine the temporal response of the electrode, the electrode was exposed to three different concentration of nitric oxide: 500 nM, 1 μM and 4 μM. The injection of the solution occurred at the black arrow. There was one second of dead time for the injection to reach the electrode. The upward slope for each concentration was identical. **(b)** Representative trace of an electrode being exposed to a 4 μM solution of nitric oxide. Zooming in by a factor of 10 reveals the actual time response of the electrode. Once the electrode begins to sense the nitric oxide, it takes approximately 300 ms to reach the maximum amplitude before reaching a plateau.

various stages of fabrication, was exposed to a series of *in vitro* injections. When recording in the dopamine rich caudate-putamen using cyclic voltammetry, changes in pH are commonly encountered (Venton et al. 2003). By using constant potential amperometry coupled with a fluorinated xerogel membrane, we hoped to eliminate the pH interference normally present. Injections of buffer at various pH were presented to the electrode to determine the sensitivity of the electrode to changes in pH. Typical pH changes observed *in vivo* range from ±0.2 pH units. In our *in vitro* experiments, there was no significant increase in signal in response to injections ranging from pH 7.2 – 7.6 (Fig. 5.6). Additionally, Injection of the mobile phase with room temperature oxygen saturation also produced no significant electrochemical response (Fig. 5.6).

The major interferent encountered in the caudate of the rat brain is dopamine. To test for the interference caused by dopamine exposure, the electrode was evaluated during each phase of the fabrication process. For each platinum layer, the electrode was exposed to 0.5, 1, 5, and 10 μM dopamine injections (Fig. 5.7). For the electroplated platinum, the sensitivity to dopamine was 0.054 nA/μM (Fig. 5.7a), which is only slightly less than the amperometric response at a carbon fiber (unpublished observation). The addition of a second layer of platinum through the deposition of platinum black increased the sensitivity to dopamine by a factor of five, 0.244 nA/μM.

Ideally the sensitivity to nitric oxide would be greater than dopamine at a platinum electrode. At the first electroplated platinum layer, the sensitivity to nitric oxide was 0.319 nA/μM which is significantly greater than the sensitivity to dopamine at the same surface ($p<0.0015$). Further platinization through deposition of platinum black increased the sensitivity to nitric oxide to 22.19 nA/μM (Fig. 5.8b), which is also significantly greater than the sensitivity to dopamine observed at the platinum black surface ($p<0.0001$). Even without a membrane, the selectivity for nitric oxide as compared to dopamine is a factor of nearly 100.

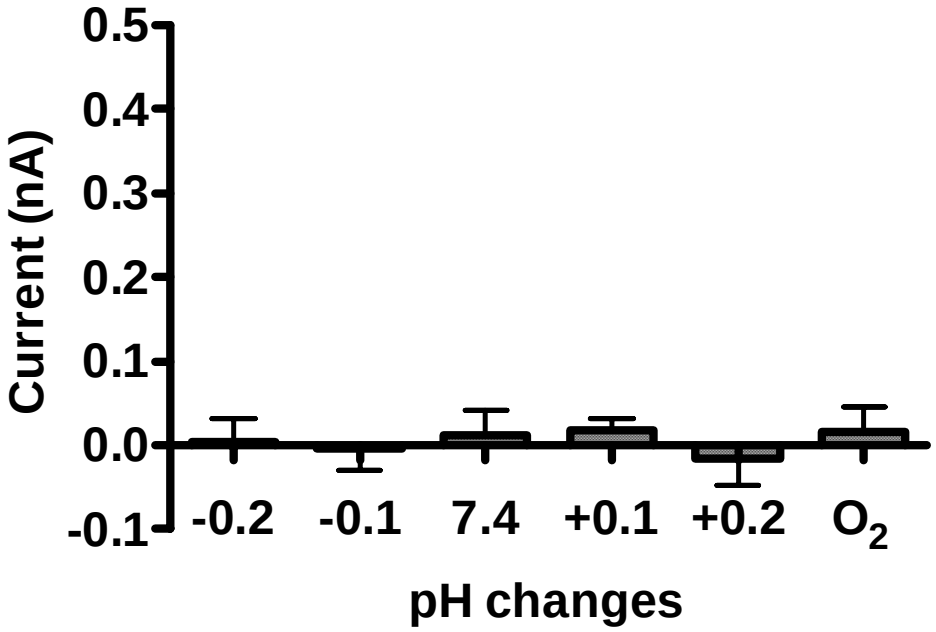

Figure 5.6. Sensitivity of the sensor to changes in pH and oxygen concentration. The sensor was held at +0.8 V vs a Ag/AgCl electrode. To establish a baseline, the sensor was placed in a TRIS buffer of pH 7.4 in a flow cell. Injections of TRIS buffered solutions at different pH's were analyzed. There was no significant change in signal in response to injections of pH 7.2, 7.3, 7.4, 7.5, or 7.6 (n=5). These pH's correspond to pH changes of -0.2, -0.1, 0, +0.1, and +0.2 respectively. Additionally, to measure the interference of oxygen, the sensor was placed in the flow cell with deoxygenated TRIS buffer. To measure oxygen, a room temperature oxygen saturated solution of TRIS buffer was injected. There was no significant change (n=5).

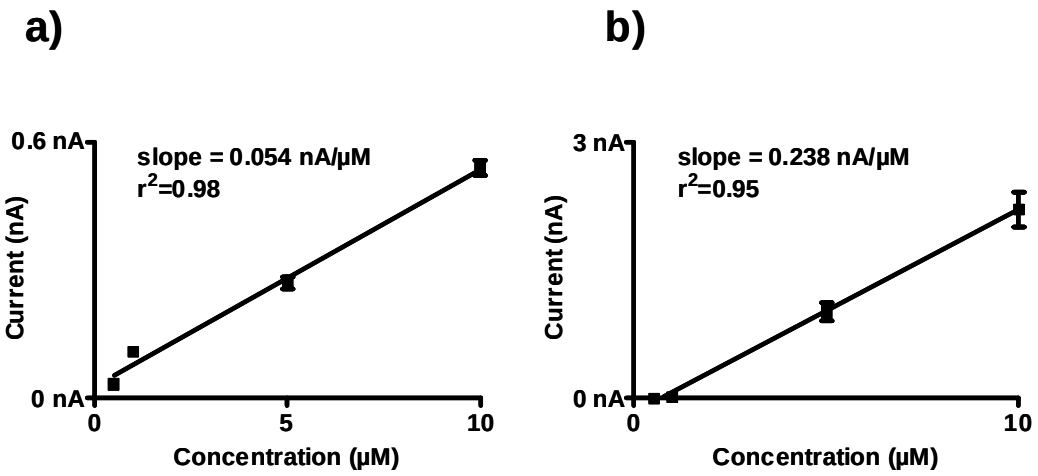

Figure 5.7. Sensitivity of the platinum electrode to dopamine. The sensor was held at +0.8 V vs a Ag/AgCl electrode. **(a)** A platinum-plated tungsten microelectrode was placed in a flow cell and exposed to various concentrations of dopamine, including 0.5, 1, 5, and 10 µM dopamine. The sensitivity of the platinum-plated electrode to dopamine was 0.054 nA/µM (r^2=0.98). **(b)** A platinum black tungsten microelectrode was placed in a flow cell and exposed to various concentrations of dopamine, including 0.5, 1, 5, and 10 µM dopamine. The sensitivity of the platinum black electrode to dopamine was 0.238 nA/µM (r^2=0.95).

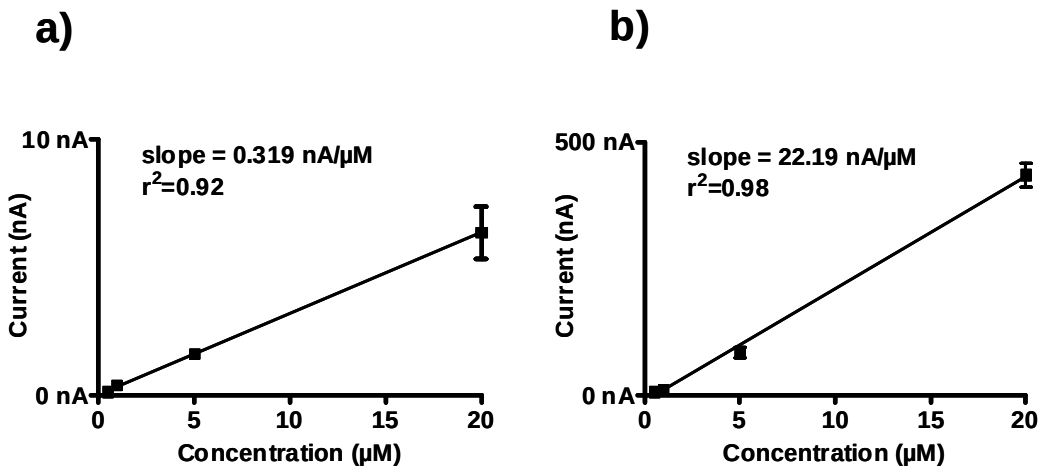

Figure 5.8. Sensitivity of the platinum electrode to nitric oxide. The sensor was held at +0.8 V vs a Ag/AgCl electrode. **(a)** A platinum-plated tungsten microelectrode was placed in a flow cell and exposed to various concentrations of nitric oxide, including 0.5, 1, 5, and 20 µM nitric oxide. The sensitivity of the platinum-plated electrode to nitric oxide was 0.319 nA/µM (r^2=0.92). **(b)** A platinum black tungsten microelectrode was placed in a flow cell and exposed to various concentrations of nitric oxide, including 0.5, 1, 5, and 20 µM nitric oxide. The sensitivity of the platinum black electrode to nitric oxide was 22.19 nA/µM (r^2=0.98).

The addition of the fluorinated xerogel membrane, which as a hydrophobic membrane should prevent the entry of all polar species, including dopamine, produced mixed results. The sensitivity to dopamine decreased from its previous value of 0.244 nA/μM to 0.062 nA/μM, which is a reduction of a factor of 4 (Fig. 5.9a). However, the sensitivity to nitric oxide decreased from its previous value of 22.19 nA/μM to 1.45 nA/μM (Fig. 5.9b). The decrease in sensitivity to nitric oxide appeared to be as a result of fouling of the electrode in response to higher concentrations of nitric oxide. To confirm this hypothesis, Injections of 20 μM nitric oxide were given every 3 minutes, which led to an initial current amplitude of 70 nA and a slow decay to approximately 20 nA (data not shown). The mixed results demonstrate the effectiveness of the membrane to prevent the entry of molecules previously accessible to the platinum surface; however, it also suggests that the electrochemical products of nitric oxide oxidation, nitrite and nitrate, are unable to escape the membrane and are effectively fouling the surface.

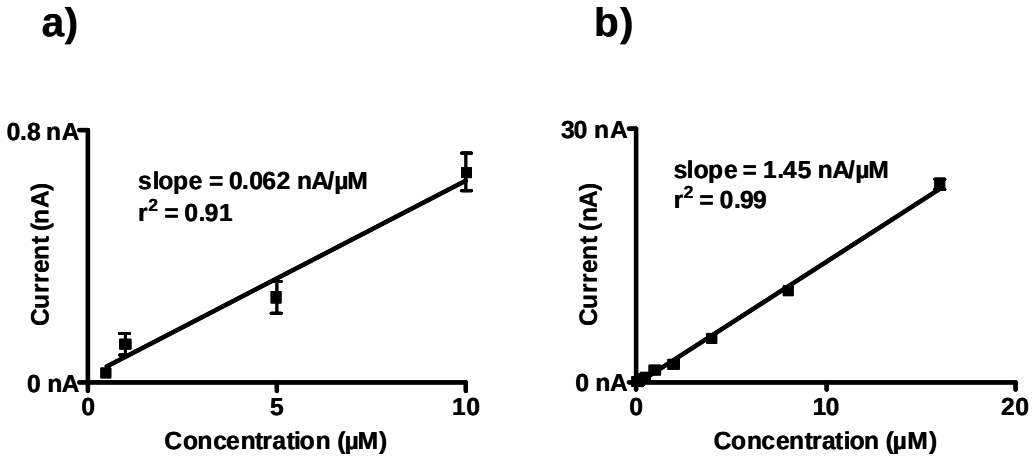

Figure 5.9. Selectivity of the fluorinated sensor to both dopamine and nitric oxide. The sensor was held at +0.8 V vs a Ag/AgCl electrode. **(a)** A membrane-coated sensor was placed in a flow cell and exposed to various concentrations of dopamine, including 0.5, 1, 5, and 10 µM dopamine. The sensitivity of the membrane-coated sensor to dopamine was 0.062 nA/µM (r^2=0.91). **(b)** A membrane-coated sensor was placed in a flow cell and exposed to various concentrations of nitric oxide, including 100 nM, 200 nM, 400 nM, 1 µM, 2 µM, 4 µM, 8 µM, 16 µM, and 32 µM. The sensitivity of the membrane-coated sensor to nitric oxide was 1.45 nA/µM (r^2=0.99).

Study of nitric oxide transport

To determine the transport characteristics of nitric oxide, the signal upon microinjection was compared between *in vitro* and *in vivo* preparations. The diffusion coefficient can be determined using equation 2 (Dayton et al. 1983):

$$\mathbf{D = r^2/6t_{max}}$$

Here D is the diffusion coefficient, r is the distance separating the syringe and sensor, and t_{max} is the time between injection and maximum amplitude. In both preparations the microsensor was affixed to a 2.5 µL syringe with a separation of 500 µm determined under a microscope. The size of the 1.9 mM nitric oxide droplets was determined under the microscope to be approximately 300 µm. Once the size of the droplets had been appropriately characterized, the syringe/sensor was placed into a block of 0.6% w/v agarose gel. The electrochemical signal in response to the 100 nL injection was approximately 6.5 nA, with a return to baseline time of approximately 50 s (Fig. 5.10a). The diffusion coefficient for nitric oxide in agarose determined from tmax was 1.0×10^{-4} cm^2/s. The syringe/sensor was then lowered into the CP of the rat brain where nitric oxide has been suspected to play an important role (Sammut et al. 2006; Ondracek et al. 2008). The electrochemical signal in response to the 100 nL injection was an order of magnitude lower than was found in the agarose gel, 0.65 nA (Fig. 5.10b). Additionally the return to baseline time was approximately 1.5 s. This discrepancy in response time is likely due to the natural degradation of nitric oxide *in vivo* due to its reaction with oxyhemoglobin and superoxide dismutase (Doyle and Hoekstra 1981; Goretski and Hollocher 1988; Beckman and Koppenol 1996). The diffusion coefficient for nitric oxide in the CP was 3.5×10^{-4} cm^2/s, which is different from the literature value of 3.8×10^{-5} cm^2/s (Meulemans 1994). This disagreement could be due to the slower temporal resolution of their sensor. The syringe/sensor was later lowered into the nucleus

accumbens (NAcc), a region that has not been implicated in nitric oxide signaling. The response in this region was nearly identical to that measured in the caudate-putamen, with a maximum amplitude of 0.5 nA and a return to baseline time of 2 s (Fig. 5.10b). The diffusion coefficient for nitric oxide in the NAcc was 4.6×10^{-4} cm^2/s. These results begin to describe the fate of nitric oxide upon its release in the brain, though more work is needed to fully understand its *in vivo* degradation.

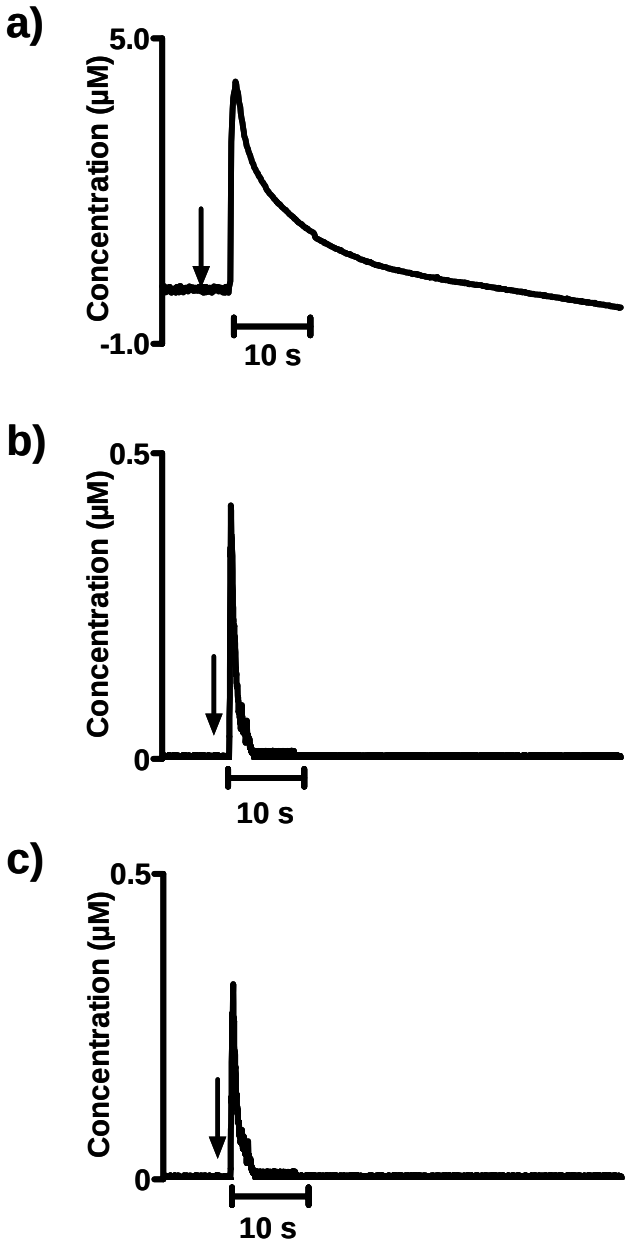

Figure 5.10. Detection of nitric oxide *in vitro* and *in vivo* following microinjection. A 200 nL of 1.9 mM injection of nitric oxide occurred at the time point indicated by the arrow. Micropressure injection in **(a)** 0.6% w/v agarose gel, t_{max} = 4.1 s, **(b)** caudate putamen, t_{max} = 1.2 s, **(c)** nucleus accumbens, t_{max} = 0.9 s..

SUMMARY

Desired characteristics for a selective nitric oxide sensor include ease of fabrication, reproducible responses, rapid temporal resolution, excellent sensitivity, and high selectivity. The fluorinated xerogel membrane microsensor provides an ideal combination of these attributes. The relatively simple platinum plating and electrochemical deposition of platinum black, as well as the simplicity of the dip coating, makes the electrode ideal for repetitive *in vivo* use. Additionally, the sensor is capable of maintaining at least 90% of initial signal for up to 2 months, which is significantly greater than current detection schemes. The 300 ms temporal resolution makes it possible to record subsecond fluctuations in nitric oxide in response to pharmacological or electrical stimulation, and its sensitivity makes it possible to record the nM signals often seen in the caudate-putamen. *In vivo* microinjections have verified the ability of the sensor to measure the diffusion of nitric oxide *in vivo*, furthering the likelihood of a successful in vivo implantation.

REFERENCES

Archer S. (1993) Measurement of nitric oxide in biological models. *Faseb J* **7,** 349-360.

Bard A. J. and Faulkner L. R. (2001) Electrochemical Methods: Fundamentals and applications, 2nd ed.**,** p 570.

Bath B. D., Michael B. J., Trafton B. J., Joseph J. D., Runnels P. L. and Wightman R. M. (2000) Subsecond adsorption and desorption of dopamine at carbon-fiber microelectrodes. *Analytical chemistry* **72,** 5994-6002.

Beckman J. S. and Koppenol W. H. (1996) Nitric oxide, superoxide, and peroxynitrite: the good, the bad, and ugly. *The American journal of physiology* **271,** C1424-1437.

Bedioui F. and Villeneuve N. (2003) Electrochemical nitric oxide sensors for biological samples - Principle, selected examples and applications. *Electroanalysis* **15,** 5-18.

Bryan N. S. and Grisham M. B. (2007) Methods to detect nitric oxide and its metabolites in biological samples. *Free radical biology & medicine* **43,** 645-657.

Dayton M. A., Ewing A. G. and Wightman R. M. (1983) Diffusion-Processes Measured at Microvoltammetric Electrodes in Brain-Tissue. *Journal of Electroanalytical Chemistry* **146,** 189-200.

de Vooys A. C. A., Beltramo G. L., van Riet B., van Veen J. A. R. and Koper M. T. M. (2004) Mechanisms of electrochemical reduction and oxidation of nitric oxide. *Electrochimica Acta* **49,** 1307-1314.

Diab N., Oni J. and Schuhmann W. (2005) Electrochemical nitric oxide sensor preparation: a comparison of two electrochemical methods of electrode surface modification. *Bioelectrochemistry (Amsterdam, Netherlands)* **66,** 105-110.

Doyle M. P. and Hoekstra J. W. (1981) Oxidation of nitrogen oxides by bound dioxygen in hemoproteins. *Journal of inorganic biochemistry* **14,** 351-358.

Friedemann M. N., Robinson S. W. and Gerhardt G. A. (1996) o-Phenylenediamine-modified carbon fiber electrodes for the detection of nitric oxide. *Analytical chemistry* **68,** 2621-2628.

Gally J. A., Montague P. R., Reeke G. N., Jr. and Edelman G. M. (1990) The NO hypothesis: possible effects of a short-lived, rapidly diffusible signal in the development and function of the nervous system. *Proc Natl Acad Sci U S A* **87,** 3547-3551.

Garthwaite J. and Boulton C. L. (1995) Nitric oxide signaling in the central nervous system. *Annu Rev Physiol* **57,** 683-706.

Garthwaite J., Charles S. L. and Chess-Williams R. (1988) Endothelium-derived relaxing factor release on activation of NMDA receptors suggests role as intercellular messenger in the brain. *Nature* **336,** 385-388.

Gomes A., Fernandes E. and Lima J. L. (2006) Use of fluorescence probes for detection

of reactive nitrogen species: a review. *Journal of fluorescence* **16,** 119-139.

Goretski J. and Hollocher T. C. (1988) Trapping of nitric oxide produced during denitrification by extracellular hemoglobin. *The Journal of biological chemistry* **263,** 2316-2323.

Griess P. (1879) Bemerkungen zu der Abhandlung der HH. Weselsky und Benedikt „Ueber einige Azoverbindungen&rdquor, pp 426-428.

Guthohrlein G. and Knappe J. (1968) Modified determination of citrulline. *Analytical biochemistry* **26,** 188-191.

Helmke S. M. and Duncan M. W. (2007) Measurement of the NO metabolites, nitrite and nitrate, in human biological fluids by GC-MS. *Journal of chromatography* **851,** 83-92.

Hermans A. and Wightman R. M. (2006) Conical tungsten tips as substrates for the preparation of ultramicroelectrodes. *Langmuir* **22,** 10348-10353.

Ignarro L. J., Buga G. M., Wood K. S., Byrns R. E. and Chaudhuri G. (1987) Endothelium-derived relaxing factor produced and released from artery and vein is nitric oxide. *Proc Natl Acad Sci U S A* **84,** 9265-9269.

Lee Y., Oh B. K. and Meyerhoff M. E. (2004) Improved planar amperometric nitric oxide sensor based on platinized platinum anode. 1. Experimental results and theory when applied for monitoring NO release from diazeniumdiolate-doped polymeric films. *Analytical chemistry* **76,** 536-544.

Lim M. H. and Lippard S. J. (2007) Metal-based turn-on fluorescent probes for sensing nitric oxide. *Accounts of chemical research* **40,** 41-51.

Malinski T. and Taha Z. (1992) Nitric oxide release from a single cell measured in situ by a porphyrinic-based microsensor. *Nature* **358,** 676-678.

Meulemans A. (1994) Diffusion coefficients and half-lives of nitric oxide and N-nitroso-L-arginine in rat cortex. *Neuroscience letters* **171,** 89-93.

Michael D. J., Joseph J. D., Kilpatrick M. R., Travis E. R. and Wightman R. M. (1999) Improving data acquisition for fast scan cyclic voltammetry. *Analytical Chemistry* **71,** 3941-3947.

Miki N., Kawabe Y. and Kuriyama K. (1977) Activation of cerebral guanylate cyclase by nitric oxide. *Biochemical and biophysical research communications* **75,** 851-856.

Moncada S. and Higgs A. (1993) The L-arginine-nitric oxide pathway. *The New England journal of medicine* **329,** 2002-2012.

Moncada S., Palmer R. M. and Higgs E. A. (1991) Nitric oxide: physiology, pathophysiology, and pharmacology. *Pharmacological reviews* **43,** 109-142.

Montague P. R., Gally J. A. and Edelman G. M. (1991) Spatial signaling in the development and function of neural connections. *Cereb Cortex* **1,** 199-220.

Ondracek J. M., Dec A., Hoque K. E., Lim S. A., Rasouli G., Indorkar R. P., Linardakis J., Klika B., Mukherji S. J., Burnazi M., Threlfell S., Sammut S. and West A. R. (2008) Feed-forward excitation of striatal neuron activity by frontal cortical activation of nitric oxide signaling in vivo. *The European journal of neuroscience* **27,** 1739-1754.

Pereira-Rodrigues N., Zurgil N., Chang S. C., Henderson J. R., Bedioui F., McNeil C. J. and Deutsch M. (2005) Combined system for the simultaneous optical and electrochemical monitoring of intra- and extracellular NO produced by glioblastoma cells. *Analytical chemistry* **77,** 2733-2738.

Piedrafita B., Cauli O., Montoliu C. and Felipo V. (2007) The function of the glutamate-nitric oxide-cGMP pathway in brain in vivo and learning ability decrease in parallel in mature compared with young rats. *Learning & memory (Cold Spring Harbor, N.Y* **14,** 254-258.

Robinson J. K., Bollinger M. J. and Birks J. W. (1999) Luminol/H2O2 chemiluminescence detector for the analysis of nitric oxide in exhaled breath. *Analytical chemistry* **71,** 5131-5136.

Sammut S., Dec A., Mitchell D., Linardakis J., Ortiguela M. and West A. R. (2006) Phasic dopaminergic transmission increases NO efflux in the rat dorsal striatum via a neuronal NOS and a dopamine D(1/5) receptor-dependent mechanism. *Neuropsychopharmacology* **31,** 493-505.

Shibuki K. (1990) An electrochemical microprobe for detecting nitric oxide release in brain tissue. *Neuroscience research* **9,** 69-76.

Shin J. H., Weinman S. W. and Schoenfisch M. H. (2005) Sol-Gel Derived Amperometric Nitric Oxide Microsensor. *Anal. Chem.* **77,** 3494-3501.

Tsikas D. (2007) Analysis of nitrite and nitrate in biological fluids by assays based on the Griess reaction: appraisal of the Griess reaction in the L-arginine/nitric oxide area of research. *Journal of chromatography* **851,** 51-70.

Venton B. J., Michael D. J. and Wightman R. M. (2003) Correlation of local changes in extracellular oxygen and pH that accompany dopaminergic terminal activity in the rat caudate-putamen. *Journal of neurochemistry* **84,** 373-381.

Zhang X. (2004) Real time and in vivo monitoring of nitric oxide by electrochemical sensors--from dream to reality. *Front Biosci* **9,** 3434-3446.